USNRDL-TR-1044
23 May 1966

c.7

EXPLOSION PRODUCT REDISTRIBUTION MECHANISMS FOR SCALED MIGRATING UNDERWATER EXPLOSION BUBBLES

by

J. W. Pritchett

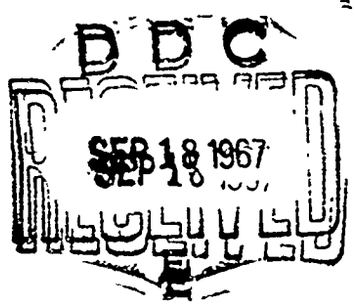

U.S. NAVAL RADIOLOGICAL DEFENSE LABORATORY

SAN FRANCISCO · CALIFORNIA · 94135

150

RADIOLOGICAL EFFECTS BRANCH
E. A. Schuert, Head

CHEMICAL TECHNOLOGY DIVISION
R. Cole, Head

ADMINISTRATIVE INFORMATION

The work reported is part of a project sponsored by the Defense Atomic Support Agency under NWER Program A-7, Subtask 10.061.

ACKNOWLEDGEMENT

Special appreciation is expressed to K. W. Kaulum for general contributions to all aspects of the project, to R. R. Buntzen for advice concerning the experimental facility, and to R. W. Caputi for active participation in the chemical phases of the experimental work.

DDC AVAILABILITY NOTICE

Distribution of this document is unlimited.

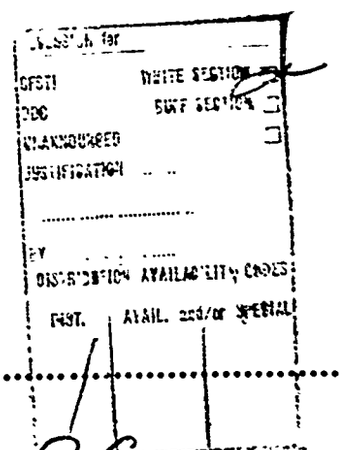

Eugene P. Cooper
Technical Director

D. C. Campbell, CAPT USN
Commanding Officer and Director

ABSTRACT

A submerged gold wire was electrically exploded to simulate a very deep underwater nuclear detonation. These small-scale tests were conducted in a test tank in which the air pressure may be varied to obtain various strengths of buoyant bubble migration.

The mechanics of explosion bubble formation, pulsation, and migration are discussed, and relevant relationships are derived for scaling large-yield bubble behavior in the laboratory by variation of environmental parameters. The mechanisms by which the explosion products, initially at the bubble center during the first cycle, are redistributed by bubble bottom collapse, compression, re-expansion, and migration, are investigated.

The experimental technique involved physically sampling the bubble and its environment at the second bubble maximum to define the extent and nature of explosion product re-distribution. Three different shot conditions were investigated, corresponding to a "rest-point" condition, a condition characterized by slight upward migration, and one characterized by strong upward migration.

In all cases, it was found that most (77 to 94%) of the explosion products are lost to the environment by the time of the second bubble maximum. The probable mechanisms for this loss are discussed, and rules are derived for application of these results to full-scale underwater bursts.

SUMMARY

The Problem

When a nuclear explosion occurs underwater, some of the radioactive fission products are lost to the liquid environment as the steam bubble pulsates and migrates upward. The remainder are ejected into the above-surface environment. In order to quantify the extent of this subsurface loss, it is first necessary to identify and evaluate in detail the mechanisms by which explosion product material is transferred from its initial location at the center of the bubble to the environmental water by the hydrodynamic processes occurring during bubble collapse, migration, and re-expansion. The objective of this study is to evaluate these phenomena as a function of the strength of bubble migration.

Findings

In the case of no migration, only about 18% of the explosion products were found within the bubble at its second maximum. If weak upward migration occurs, the retained fraction drops to about 6%, but, if migration strength is further increased, the underwater jet and decreased internal energy of the bubble at the minimum cause less material to be lost - the fraction remaining in the bubble at the second maximum for the "strong migration" case is about 23% of the total.

CONTENTS

CHAPTER 1

INTRODUCTION

With the development of nuclear weapons for use in antisubmarine warfare, contamination of the above-surface environment by the radioactive fission debris from the weapon has become a problem of some concern. Even if the burst is quite deep, some fraction of this residue will be carried to the surface by the migrating explosion bubble, and will become involved in the plumes and the radioactive base surge which may represent a serious hazard to surface vessels.

It has always been assumed that, if the depth of burst is sufficiently deep so that the explosion bubble will pulsate several times before reaching the water surface (the "very deep" burst classification),[1] a substantial fraction of the fission products will be transferred from the bubble to the water environment, thus reducing the above-surface hazard. Quantitative information concerning this loss, however, is not available. There has been only one full-scale nuclear detonation falling into the "very deep" category (Operation Wigwam), and the data obtained concerning post-shot fission product distribution was too fragmentary and incomplete to evaluate the relevant loss mechanisms. It is intrinsically quite difficult to estimate, for example, the fraction of the total activity present in the plumes, both because radiation field data is rather poor and the water density structure of the plume is not known. An attempt was made at Wigwam to determine the total amount of activity present in the subsurface, radioactive "pool", but measurements were not possible at early times, and by the time radioactivity was encountered, oceanographic processes had so distorted and diffused the debris that no reliable result was obtainable.[2,3,4] In any case, the vertical distribution of fission products in the water to

be found several days after burst is not necessarily characteristic of that prevailing at early times.

Furthermore, simulation of the radiological transfer processes for deep and very deep bursts by means of traced, relatively low yield high-explosive field tests is not desirable, for two reasons. First, the strength of bubble migration is yield dependent, and consequently approximations must be made. Second, the explosion bubble atmosphere in the high-explosive case consists of non-condensable gaseous reaction products, rather than steam as in the nuclear case. Developmental work is now in progress on high-explosive charges producing steam as a principal reaction product, but such explosives are not as yet available. The importance of a condensable bubble atmosphere to explosion product transfer processes will be discussed at length in later chapters.

The conceptually simple approach of firing a large explosion and then taking measurements after violent motion has subsided may not prove particularly fruitful in any case. In order to generalize results, more than an a posteriori distribution for some particular charge fired at some particular depth at some particular time after burst is required. That is, a prerequisite to any method of prediction of the distribution of activity is an understanding and evaluation of the processes by which material is lost to the environment by the bubble as it pulsates and migrates to the surface, as functions of yield and shot depth.

For this investigation, the experimental work was carried out in a vacuum tank using an electrically exploded gold wire, which is a good simulant to a nuclear explosion since it generates a steam bubble in which the explosion products are initially distributed in the appropriate manner.[5] In order to simulate large-yield bubble behavior (migration strength) the air pressure over the water was varied. Three shot conditions were investigated; one for which there was no migration,

one for which migration was upward but relatively weak, and one for which upward bubble migration was a dominant feature of the motion.

The initial distribution at the first bubble maximum has previously been documented.[5] In the present work, in order to identify and evaluate the hydrodynamic mechanisms by which the explosion products are re-distributed in, and ejected from, the bubble during bubble collapse, translation and re-expansion, the bubble and the fluid environment from each of these three conditions were physically sampled at the time of the second maximum. The samples were then analyzed for explosion product (gold) content by neutron activation techniques. From these distributions of explosion products, processes are postulated based on knowledge concerning the flow, both inside and outside the bubble, near the time of recompression.

A prerequisite to any understanding of the mechanisms of loss and re-distribution of explosion products is familiarity with the bubble phenomenon and the type of fluid motion to be expected after an underwater explosion. Consequently, Chapter 2 deals with the present state of the art concerning bubble mechanics and scaling of bubble behavior. Later chapters will discuss such matters as the experiment itself, data reduction, and quantitative results concerning the mechanisms of explosion product loss.

CHAPTER 2

PHENOMENOLOGY AND SCALING OF UNDERWATER EXPLOSION BUBBLES

FORMATION OF THE BUBBLE

The sequence of events following a deep underwater explosion depends to some extent on the nature of the explosive. Generally speaking, we may divide explosives into two major classes. First, we have conventional high-explosives which liberate energy by high-speed chemical reactions and have energy densities less than 3,000 calories/cm^3 or so. The "point-source" explosives, on the other hand, are characterized by energy densities at least an order of magnitude higher than those of most high-explosives, and therefore have non-chemical energy sources; these include high-energy electrical discharges, electrically exploded conductors, and nuclear devices.

Considering first the high-explosive case, when the detonation wave reaches the surface of the charge, it proceeds into the water, leaving behind it a sphere of gaseous reaction products at high temperature and pressure. After this time, the interaction between the shockwave and these residual gases may be considered negligible. It may be reasonably assumed that, at this stage, this "initial bubble" is relatively homogeneous as regards temperature and density. These gases, as a consequence of their high pressure, do work on the environment and expand adiabatically in a spherically symmetric fashion.

In the case of the point-source detonation with its much higher energy density, the materials constituting the device are immediately raised to extremely high temperature, and are, in general, ionized. The emission of high energy photons and the radiation of heat from the

device causes vaporization of the water in the vicinity. The resulting high pressure system expands as a shock front. As this shockwave passes through the adjacent water, the water is first raised to high pressure and temperature above the critical point, and then, as the shock front passes on, the pressure drops and the water goes into the vapor phase. At fairly early times, the shock front surface energy density drops below that value required to further vaporize water, and separation between the bubble front and the shock front occurs. As can be seen, the two mechanisms of steam generation (initial radiation and shock energy dissipation) both tend to deposit less energy per unit mass of water with increasing distance from the device. Consequently, in the point-source case, the gas temperature is highest and the density is lowest in the center of the initial bubble.[1]

The volume of the bubble at the time of separation is about the same as that of a high explosive charge of the same yield. Hence, after this time, the initial bubble motion should be similar for both cases. However, the fact that the high-explosive bubble atmosphere is identical with the explosion products, whereas the debris remaining of the point-source device is located at the center of a matrix of condensable steam, causes appreciable differences in behavior at later times. More will be said about this later. The best qualitative distinction between a point-source explosion and the usual high-explosive detonation may therefore be made in terms of the composition of the bubble atmosphere, which is in turn related to the energy density of the explosive. That is, high-explosive energy densities are typically in the range 1000-3000 calories/cm^3; it is probably safe to assume that behavior will be characteristically "point-source" (that is,the bubble atmosphere will be primarily steam) if the explosive energy is greater than 10,000 cal/cm^3.

THE NON-MIGRATING CASE

For the present, in order to simplify the initial development, the effects of gravity will be neglected, and, furthermore, it will be assumed that both the sea surface and bottom are far away from the explosion point. Under these circumstances, the bubble remains spherical and the problem is one-dimensional. The more general case will be taken up later in this chapter.

After the initial bubble has been formed, and the shock wave has separated from the bubble front, the motion for high-explosive and point-source bubbles is almost identical until much later times. By virtue of the high internal pressure, the system expands radially, initially with very high velocity. As the bubble does work on the environment, generating kinetic energy in the adjacent water, the internal energy of the adiabatically expanding gas drops rapidly. At a fairly early time, the internal pressure becomes equal to the external (hydrostatic) pressure.[6] At this time, most of the total energy resides as kinetic energy in the water environment. After this time, the environment begins to do work on the bubble (the net force is now inward), eventually bringing the expansion to a stop, much later. Then, the system begins to contract, and the process is reversed. The bubble internal pressure increases to some peak value, and the system re-expands. These cycles continue, with decreasing amplitude and period, until all the available energy has been lost.

The maximum radius and the period of the bubble for the first cycle are related to the total energy released and to the local hydrostatic pressure. In order to avoid ambiguities concerning explosive type, which lead to correction factors which must be carried throughout the development, the basic unit of explosive bubble energy will be taken as the "pound-TNT-equivalent-bubble". This transformation allows

the rest of the development to be done in terms of dimensionless quantities. If the weight of the charge (which is proportional to the total energy available, for a given explosive) is denoted by W', then we define the "TNT equivalent bubble yield" as follows:

$$W = 2W' \left[\epsilon/\epsilon_{TNT}\right] \left[1 - \frac{E_S}{E_T}\right]$$

where

W = TNT equivalent bubble yield - expressed in pounds
$\epsilon = \varphi/\rho_e$ for the explosive of interest
$\epsilon_{TNT} = \varphi/\rho_e$ for TNT
φ = energy density of the explosive
ρ_e = density of the explosive
E_T = total energy released
E_S = energy initially radiated in the shockwave

It can be seen that the term $(1 - (E_S/E_T))$ simply represents the fraction of the total energy released which remains available for bubble motion. This quantity does not change with yield, and is characteristic of the explosive used - the appropriate value for TNT is about 0.5. If the energy density of the explosive is high enough (as for a point-source explosion), losses may also occur through electromagnetic radiation, in which case the above term should be replaced by $(1-(\{E_S + E_R)/E_T))$. The value of ϵ_{TNT} may be taken as 1000 calories/gram. We may then simply say that

$$W = kW' \tag{2.1}$$

where k is characteristic of the explosive. Values of k for several common explosives are listed in Table 2.1.

TABLE 2-1

Values of the Bubble Yield Conversion Factor for
Various Explosives
(Compiled from various sources)
$k = W/W'$

Explosive	k
Amatol (cast)	1.1
HBX-1	1.5
Lead Azide	0.36
Minol-2 (cast)	1.4
Minol-2 (pressed)	1.7
Pentolite	1.0
PETN	1.6
RDX (loose mix)	1.2
RDX (pressed)	1.0
Tetryl (loose)	1.1
Tetryl (pressed)	1.0
TNT	1.0 (by definition)
Torpex	1.5
Exploding wire) Spark Gap)	0.6 - 1.0 (depends on circuit parameters, etc.)

The hydrostatic pressure at the shot point is denoted by Z and is expressed in feet of water. Hence, if the air over the water is at one atmosphere pressure,

$$Z_o = D_o + 33$$

Thus, the parameters describing the burst are W, (the bubble energy); Z, (the hydrostatic head); and ρ (the fluid density). Dimensionally, these are simply energy, energy density, and mass density, or rather:

W has dimensions $\frac{ML^2}{T^2}$ (Energy)

Z has dimensions $\frac{M}{LT^2}$ (Pressure)

and ρ has dimensions $\frac{M}{L^3}$ (Density)

To construct a "characteristic length" describing the explosion, we may combine:

$$\left(\left(\frac{ML^2}{T^2}\right)\left(\frac{LT^2}{M}\right)\right)^{1/3} = (W/Z)^{1/3} = \alpha \text{ (the characteristic length, feet)} \quad (2.3)$$

$$\left(\frac{ML^2}{T^2}\right)^{1/3}\left(\frac{LT^2}{M}\right)^{5/6}\left(\frac{M}{L^3}\right)^{1/2} = \frac{W^{1/3}\rho^{1/2}}{Z^{5/6}} = \tau \text{ (the characteristic time, seconds)} \quad (2.4)$$

Other characteristic units may then be formulated, for example:

Characteristic area = $\alpha^2 = (W/Z)^{2/3}$

Characteristic volume = $\alpha^3 = W/Z$

Characteristic mass = $\rho\alpha^3 = \rho\, W/Z$

Characteristic velocity = $\alpha/\tau = (Z/\rho)^{1/2}$

Characteristic acceleration = $\alpha/\tau^2 = (Z^{4/3}/W^{1/3}\rho)$

Characteristic momentum = $\rho\, \alpha^4/\tau = W(\rho/Z)^{1/2}$

Characteristic energy = $\rho\, \alpha^5/\tau^2 = W$

$$\text{Characteristic force} = \rho \alpha^4/\tau^2 = W^{2/3} Z^{1/3}$$

and so on.

It has been observed that, if the bubble is approximately spherical (that is, gravity and interface effects are small), the maximum radius for the first cycle is given by

$$R = 12.6 \alpha \text{ (feet)} \tag{2.5}$$

and the first oscillation period is:

$$T = 4.36 \tau \text{ (seconds)} \tag{2.6}$$

It might now be pointed out that W may be more simply defined as "that weight of TNT which would produce the 'equivalent bubble' as regards R and T" (or α and τ).

So far, we have considered all explosion bubbles, whether point-source or high-explosive, to be equivalent after the time of shockwave separation. This is a fairly good assumption, at least for gross behavior (the non-homogeneity of the steam bubble as regards temperature, density, and explosion product distribution should, nevertheless, be kept in mind). However, the fact that the high-explosive bubble atmosphere is composed of largely non-condensable reaction products, whereas the point source bubble contains steam, begins to have its effect at about the time of the first bubble minimum.

This "first minimum" is accompanied by instabilities of the bubble interface, and turbulence, both inside and outside the bubble. In general, energy losses occur at bubble minima as a consequence of these phenomena. In the high-explosive bubble case, the rise in the internal pressure causes the emission of a pressure pulse, which carries energy away from the system. Also (and more important) the turbulent, unstable flow near the bubble minimum causes transfer of heat from the bubble atmosphere to the water environment - also, the kinetic energy involved

in this turbulence is derived from the bubble energy and hence represents an additional loss. Consequently, the bubble energy available in the second cycle is noticeably less than that of the first, and in the HE case, is about 39% of the first cycle bubble energy.[7] In the case of a steam bubble, all the above losses occur, and in addition, energy is lost through another mechanism. As the bubble collapses and the interface becomes unstable, small jets of water penetrate the bubble, cooling the bubble atmosphere and causing condensation of steam, thus depositing the latent energy of condensation in the water as heat. This loss is quite significant, since in the point-source case, the bubble energy available for the second cycle is only about 8% of that originally available.[1]

The maximum radius and the period of oscillation for the second and subsequent cycles may be found simply by replacing the total bubble energy (W) by the reduced amount available for the next cycle. Both cases (HE and point-source) are compared in Fig. 2-1.

THE EFFECTS OF GRAVITY AND NEIGHBORING SURFACES - BUBBLE MIGRATION

In most cases of practical interest, the above model is not sufficient to completely describe the phenomena. So far, we have assumed that all fixed and free-surfaces are far away, and that the effect of gravity is negligible. An extreme case of the failure of the first of these assumptions is, for example, the nuclear test Crossroads Baker, in which the shot depth was a great deal less than the theoretical first maximum bubble radius. Also, as large yields become of interest, even for explosions at great depths, the effects of gravity are certainly not negligible.

In order to deal with the effects of gravity and nearby surfaces, various models have been advanced. These tend to divide themselves

into two types, which will be dealt with separately.

Spherical Models

Classically, the effects of gravity and surfaces have been treated as separable. The basic assumption involved is that the bubble remains spherical, and that gravity and surface effects may be treated as first-order perturbations of the non-migrating case discussed above. The effect of gravity is, of course, the buoyancy of the bubble. Qualitatively, it may be seen that the total amount of upward momentum generated by the bubble through its first cycle due to gravity is:

$$p = \int_0^T F_{buoyant}\, dt$$

The buoyant force is given by:

$$F = \frac{4}{3}\pi\rho g\,(R(t))^3$$

So that,

$$p = \frac{4}{3}\pi\rho g \int_0^T (R(t))^3\, dt$$

where,

p = upward momentum

T is the first bubble period

R(t) is the bubble radius (a function of time)

ρ is the fluid density

Now since

$$R \sim \alpha$$

$$T \sim \tau$$

we have

$$p \sim \rho g\, \alpha^3 \tau$$

If we normalize this momentum by dividing by the "characteristic momentum" given by $(\rho\alpha^3)(\alpha/\tau)$, where α and τ are our "characteristic length" and "characteristic time", we see that:

$$p_{reduced} \sim \frac{g\tau^2}{\alpha} = \frac{\rho g W^{1/3}}{Z^{4/3}}$$

That is, the effect of gravity increases with yield, and decreases with shot depth.

Now, this momentum is accumulated with time as the cycle proceeds. When the bubble is large, the "virtual mass" of the bubble is large, and consequently, the rate of migration is small. Near the bubble minima, however, the virtual mass of the bubble is small, and consequently the upward velocity of the bubble is large.

Superimposed upon this buoyant upward migration is the effect of adjacent surfaces. Intuitively, this is somewhat more difficult to grasp. An excellent discussion is to be found in Ref. 8. The effect of a free surface, such as the surface of the water, is to "repel" the bubble - that is, to cause it to migrate downward, whereas the effect of a rigid surface, such as the sea bottom, is to attract the bubble.

The effects of surfaces increase rapidly as the surface is approached. Thus, generally speaking, for a relatively shallow burst, the effect of the free surface will predominate, and the bubble will migrate downward. As shot depth is increased, the "repulsion" of the free surface drops off rapidly, so that the effect of gravity begins to predominate. At some intermediate shot depth called the "upper rest point" the effects of the free surface and the buoyancy of the bubble cancel; the bubble does not migrate, and behaves like the non-migrating bubble described previously. Below this depth, migration will be upward, until, as the sea bottom is approached, the "attraction" of the sea

bottom will again cancel the buoyancy: this is the "lower rest point". If shot depth is further increased, migration will be downward.

The amount of migration affects the amount of energy lost at the bubble minimum, and consequently it has been necessary to evaluate the loss as a function of the strength of migration. This has been done empirically in Ref. 7, for high-explosive bubbles, and in Ref. 1 for steam bubbles.

The qualitative picture for the spherical bubble model is, then, as follows. The bubble is assumed to remain stationary until the time of the first bubble maximum, and then, as the bubble contracts, it migrates more and more rapidly, with peak velocity being attained at the time of the bubble minimum. Upon re-expansion, the bubble slows down, becoming almost stationary at the time of the second maximum. Thus, the bubble continues to migrate in a series of "jerks", remaining spherical throughout, until it either erupts from the surface or dissipates all its energy.

Quantitatively, the migration between the first and second bubble maxima may be represented by the following[7] (considering the free surface only):

$$\frac{D_1 - D_2}{Z_1} = 3.5 \left(\frac{R_1}{Z_1}\right)^{3/2} \left(1 - S\frac{R_1 Z_1}{D_1^2}\right) \qquad (2.7)$$

where

D_1 = Shot depth (ft)
D_2 = Depth of second bubble maximum
Z_1 = Shot depth plus 33 feet
R_1 = First maximum bubble radius
S = The "surface correction coefficient"

The value of the "surface correction coefficient" is a matter of some debate. Estimates vary between 0.1 and 0.5. Perhaps, as suggested in Refs. 8, 9, the proper value of S is a function of the shot geometry. More will be said of this later.

In order to better define shot geometry, we will define β, the "geometrically scaled depth", as follows:

$$\beta = D \left(\frac{Z}{W}\right)^{1/3} = \frac{D}{\alpha} \qquad (2.8)$$

where $(Z = D + 33)$

Note that β is just equal to the shot depth, measured in first maximum bubble radii, times a factor of 12.6. That is, a charge fired at a depth such that $\beta = 12.6$, would produce a bubble that, at the first maximum, would presumably be tangent to the pre-shot surface: a shot at $\beta = 25.2$ would have a bubble with first maximum radius equal to one-half the shot depth, and so on.

Now, equation (2.7) may be transformed as follows:

$$M_S = \text{specific migration} = \frac{D_1 - D_2}{R_1} = 12.4 \left(\frac{W^{1/3}}{Z^{4/3}}\right)^{1/2} \left[1 - S \left(\frac{12.6}{\beta}\right) \frac{Z}{D}\right]$$

The specific migration is essentially the vertical displacement of the bubble center between the times of the first and second bubble maxima normalized to the first maximum bubble radius. The first factor in parenthesis represents the gravity migration, and the second is the so-called "free surface effect". If the specific migration is positive, the bubble migrates upward - if negative, downward. Fig, 2.2 presents specific migration as a function of β for $W = 10^{-4}$, 10^{-2}, 1, 100, 10^4, 10^6 and 10^8 pounds. Note that, as yield increases, the effect of gravity gets more and more important. It should be pointed out that for $\beta < \sim 15$, a "rest point" should not be expected even if predicted

by this theory, since the surface is too close for this model to apply.[8] In order to generate these curves, the "surface correction coefficient" was assumed to be a function of β which gets large near the surface, but approaches 0.1 at large depths as shown in Fig. 2-3. This information was derived from rest point data from various sources, as noted.

This kind of "spherical migration" model has several advantages and has many useful applications. First, it predicts with reasonable accuracy the locations and times of emission of "bubble pulses" - the pressure pulses emitted at bubble minima. The results derived from this model agree well with observations when migration is relatively weak, that is, for small yields fired at fair distances from surfaces, or for large yields fired at great depths. Also, it is analytic and readily applied, requiring no more than pencil and paper to obtain results.

On the other hand, there are many shortcomings to this sort of model. For example, it breaks down badly when surfaces are nearby, and when migration is strong. Clearly, in these kinds of situations, the assumption of a spherical form (particularly for the second and later maxima) is rather poor. Finally (and more important, at least as regards the subject matter of this report) the model says nothing whatever about the actual events occurring within the bubble near the minimum.

Non-Spherical Models

Essentially, the problems involved with the spherical bubble models arise from their basic assumption that the bubble retains its spherical form throughout all phases of its motion. In order to evaluate the effect of gravity and surfaces upon the bubble form, models have been constructed on the basis of the following set of assumptions:

1. Spherical symmetry is not assumed, but axial symmetry about the shot axis normal to the free surface plane is maintained.

2. All flow is radial about the shot point.

3. The position of the bubble interface is a function of both time and ϕ (the latitude).

There are two such models in use at present. The first[6,10] starts at zero time with a sphere of gas, the size of the initial bubble, with a specified internal energy. This system is divided into a number of segments with various values of ϕ. The equations of motion are then solved numerically for each segment (periodically re-evaluating the internal energy by averaging over all the segments), keeping in mind the variability of the hydrostatic pressure with depth. The results are as follows:

1. The bubble is non-spherical, in general, and an assumption of spherical form gets worse as the first cycle proceeds.

2. The maximum radius and the "period" are functions of ϕ. In particular, it is clear that, at $\phi = 90^{\circ}$, the maximum radius and "period" at that latitude will be the same as that predicted by a spherical model for the bubble as a whole, that is,

$$R\ (\pi/2) = 12.6\alpha$$

$$T\ (\pi/2) = 4.36\tau$$

However, at, say $\phi = 180^{\circ}$ (the bubble bottom), the period and radius will be reduced, due to the increase in hydrostatic pressure with depth. In the upper hemisphere (say, $\phi = 0^{\circ}$ - the bubble top) the maximum radius attained will in general be greater than that at any other value of ϕ. At shallow shot depths, however, the period of the bubble top may be quite short, due to the small mass of material between the bubble and the water surface. At great shot depths, on the

other hand, this effect becomes unimportant, until for sufficiently deep shots, the period at $\phi = 0^{\circ}$ may be the longest of all, due, once again, to the variation of hydrostatic pressure with depth.

The second non-spherical model[11] is essentially a simplification of the first; it considers only the bubble top and bottom ($\phi = 0^{\circ}, 180^{\circ}$) and neglects the internal energy of the bubble. The output consists of the maximum radii attained by the bubble top and bottom and the times at which these maxima occur. The results are essentially identical to those of the more general model, discussed above. Typical output for $W = 10^{4}$ pounds is presented in Fig. 2-4a and 2-4b.

Neither of these models deals with events occurring after the first minimum - in fact, the models terminate prior to the end of the first cycle. In the more general model, termination occurs when some segment of the bubble has returned to the explosion point. By this time, however, the important information about bubble behavior has been obtained. The fact is that explosion bubbles, in general, collapse asymmetrically. For shallow bursts, the "top period" is shorter than the "bottom period", whereas for deep bursts, the reverse is true. This asymmetric collapse gives rise to a jet of water which passes through the bubble[1,6,9,10,11], thus causing translation of the system as a whole.

A "characteristic number" describing this phenomenon, corresponding to the specific migration in the spherical model, is the "period ratio", r_T, where

$$r_T = T_{1/2}\ (\phi = 0)/T_{1/2}\ (\phi = 180^{\circ})$$

That is, if $r_T < 1.0$, the bubble will collapse from the top, and we have downward migration; if $r_T > 1.0$ we have "bottom collapse" and

the system translates upward. The magnitude of r_T should also correlate with the strength of the migration.

Actually, the two types of models (spherical and non-spherical) are describing the sane phenomenon. That is, for deep bursts, the driving force is bubble buoyancy, and this is the mechanism for the bottom collapse - the difference between the top and bottom periods in the non-spherical model is a consequence of the pressure gradient in the water, and buoyancy is simply the hydrostatic pressure integrated around the surface of the bubble. Note the similarity between Fig. 2-5, which shows r_T as a function of β for several values of W, and Fig. 2-2, which has ordinate M_S. When the spherical model indicates appreciable upward migration, r_T is quite a bit greater than 1, whereas when downward migration occurs, r_T is less than 1.

The most obvious shortcoming of these non-spherical models is, of course, that they do not deal with later phases of the event at all. In order to predict events after the first recompression, it is necessary to resort to a spherical model.

The radial-flow constraint, while an improvement over a spherical constraint, causes problems when free surfaces are nearby, and also, in general, just prior to the termination of the model. Under these circumstances, the flow has a tangential component, which is not accounted for in the model.[11] The simplified version of the model, by not dealing with times after maximum expansion and by treating only the bubble top and bottom, avoids some of these problems, but the imposition of a radial-flow velocity potential may account for the model's failure to predict rest points and other observable data precisely. For example, unpublished Hydra series film data indicates that a 1-pound charge has a rest point at 8 feet, but the model yields $r_T = 0.9$ for this yield and depth, which would indicate

downward migration. For greater scaled depths, however, these "free-surface" problems should not be so significant.

Furthermore, the non-spherical models, in contrast to the spherical models, require a substantial amount of computer time to solve a single yield-depth configuration. If these models are further refined in the future, however, some improvement may be possible. Nevertheless, the elimination of the spherical constraint represents a considerable improvement over classical models from a conceptual standpoint. That is, the radial-flow bubble model provides insight into the processes actually occurring within the bubble, rather than simply idealizing the system as a pulsating, translating sphere. Although not perfect, in terms of explaining observed phenomena, it is a much better model when surface interactions or strong migration are dominant modes of behavior. Intuitively, it is much more satisfying also - it explains more clearly the reason for the so-called "surface repulsion" for example, and suggests reasons for the observed non-spherical form of the second and later maxima when the migration is strong.

THE SCALING OF EXPLOSION BUBBLES IN THE VACUUM TEST TANK

Having discussed at some length the phenomenology of underwater bursts, we will now address ourselves to the problem of studying these phenomena. For practical reasons, it is simply not feasible to study the bubble from a large explosion. As we have seen, however, small explosions, which are more amenable to investigation, produce bubbles which behave differently from those of large ones. That is, the specific migration M_S, for example, is yield dependent and never reaches large values for small charges. The problem is, then, to discover what environmental parameters must be varied in order to reproduce the behavior of bubbles from large explosions in the labor-

atory. The relevant governing equations are derived and discussed in appendix A.

Briefly, it may be shown that the behavior of the bubble (pulsation, migration, etc) from a large explosion may be reproduced on a small scale by appropriate adjustment of any or all of P_A (the air pressure over the water, in atmospheres), g(the force of gravity), or ρ (the density of the fluid medium). The effect of a condensable bubble atmosphere does not scale well near the bubble maxima, but error may be minimized by requiring that the hydrostatic pressure at the shot point be sufficiently great so that the bubble interface does not "boil" near maxima. Near minima, on the other hand (where the phase-change process becomes important), evaporative and condensive effects should scale well. The effects of viscosity and compressibility of the fluid are not properly reproduced, but it may be shown that they are not important to the bubble motion. (See Appendix A).

If a model explosion is to occur underwater in a laboratory environment, in a fixed test tank, the only environmental parameters which may be varied are the yield of the model explosion (W_m), the shot depth (D_m), the water temperature, and the pressure over the water (P_A). Hereafter, any difference in density between, say, sea water and fresh water will be neglected. Under these circumstances, the scaling equations as derived in appendix A become:

$$\text{Yield scale factor} = \frac{W_p}{W_m} = P_A^{-4} \tag{2.9}$$

$$\text{Linear scale factor} = \frac{D_p}{D_m} = \frac{\alpha_p}{\alpha_m} = P_A^{-1} \tag{2.10}$$

$$\text{Time scale factor} = \frac{\tau_p}{\tau_m} = P_A^{-1/2} \tag{2.11}$$

where P_A is in atmospheres

As can be seen, a given set of the parameters W_m, D_m, and P_A define a unique prototype, of yield (W_m/P_A^4) and depth (D_m/P_A).

The problem is that there is a lower limit on P_A; the vapor pressure of water even at the freezing point is 0.006 atmospheres. In general practice, even this limit is difficult to attain - a more reasonable value might be 0.010 atmospheres. As a consequence, a linear scale factor of 100, and a yield scale factor of 10^8, represent the upper limit on the scaling capability of the system. This may not seem a serious limitation, and indeed it is not, for many applications. In a laboratory environment, however, it is not practical to use model yields much greater than about 10^{-4} lb. Thus, using water as a test fluid, the largest prototype yield which may be scaled is about 5 tons of TNT; however, if simulation of the behavior of the bubbles formed by an underwater nuclear detonation is of interest, required prototype yields fall into the kiloton, or even the low megaton ranges.

In order to simulate the migration of explosion bubbles caused by detonations of this size, it is necessary to have recourse to approximations. In particular, if explosions in the "very deep" category are of interest ($\beta > \sim 50$), the effect of the free surface is not terribly important. Thus, it is not unreasonable to forfeit geometric scaling (equality of β) in favor of scaling of gravitational effects. One approach is as follows. If the model and prototype bursts are sufficiently deep that the effect of the free surface is small, then scaling of bubble behavior will be accomplished if the Froude numbers for both shots are equal (Appendix A, equation A.8).

$$\frac{Z_m^{4/3}}{W_m^{1/3}} = \frac{Z_p^{4/3}}{W_p^{1/3}} \quad \text{or,} \quad \frac{Z_m}{W_m^{1/4}} = \frac{Z_p}{W_p^{1/4}} \tag{2.12}$$

This is the so-called "fourth-root scaling rule" for very deep bursts, that is often applied in high-yield high-explosive field tests[1,9,12] The procedure is simply to compute the fourth-root scaled depth for the model explosion, and then to assume that a full-scale explosion which has the same value of this parameter will generate a bubble that [illegible] in the same way as the model bubble does. The distance and [illegible]ale factors are then simply the ratio of the α's and τ's for [illegible]odel and prototype.

The problem that may arise with this rather simple approach is that although the effect of the free surface may be negligible for the prototype, it will in general be more important for the model. A better approximation to actual behavior (particularly if free-surface effects are important for either model or prototype) is to determine the prototype shot depth for which bubble behavior will be the same as the model by appeal to one or another of the bubble migration theories discussed previously.

One approach might be to specify the specific migration, M_S, as a scaling criterion; that is, scaling is accomplished if:

$$\left(\frac{W_m^{1/3}}{Z_m^{4/3}}\right)^{1/2} \left(1 - S\left(\frac{12.6}{\beta_m}\right)\frac{Z_m}{D_m}\right) = \left(\frac{W_p^{1/3}}{Z_p^{4/3}}\right)^{1/2} \left(1 - S\left(\frac{12.6}{\beta_p}\right)\frac{Z_p}{D_p}\right) \tag{2.13}$$

The same procedure may be followed using r_T, the period ratio, as a scaling criterion. These approximations are not precise, for, as we have seen, neither of them is entirely trustworthy as regards the actual effect of the free surface on the bubble motion. Nevertheless,

they should not lead to serious discrepancies for deep bursts. The judgment of the user must be applied to determine which method is best for the particular configuration of interest.

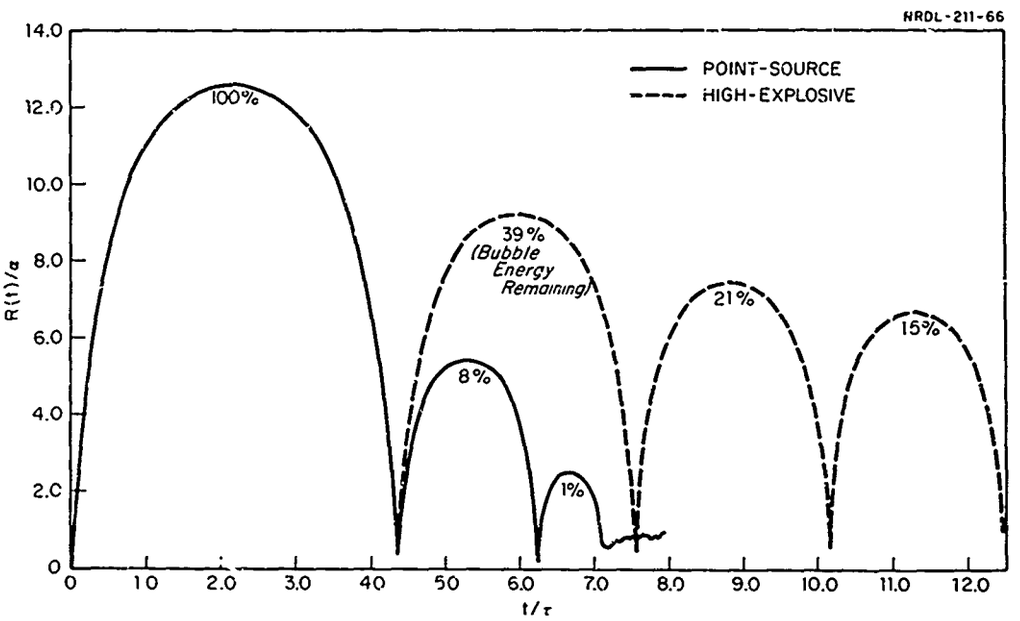

Fig. 2-1 Reduced Radius vs. Reduced Time - The Non-Migrating Case.

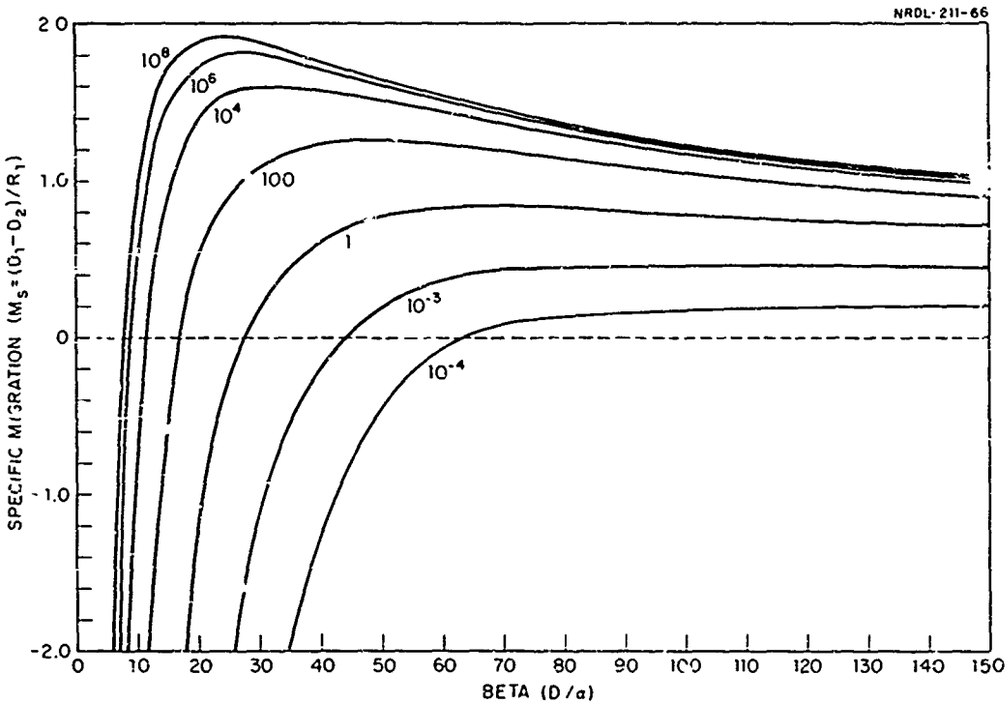

Fig. 2-2 The Specific Migration $((D_1-D_2)/R_1)$ as a Function of Beta (D/α) for $W = 10^{-4}$, 10^{-2}, 1, 10^2, 10^4, 10^6, and 10^8 Pounds.

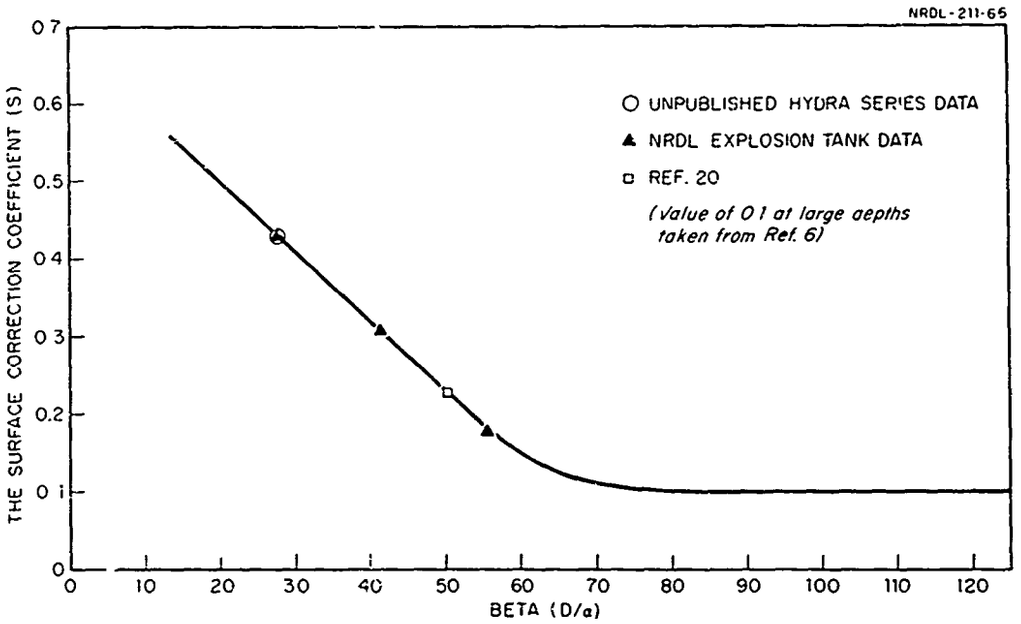

Fig. 2-3 The Surface Correction Coefficient, S, As a Function of Beta (L/α).

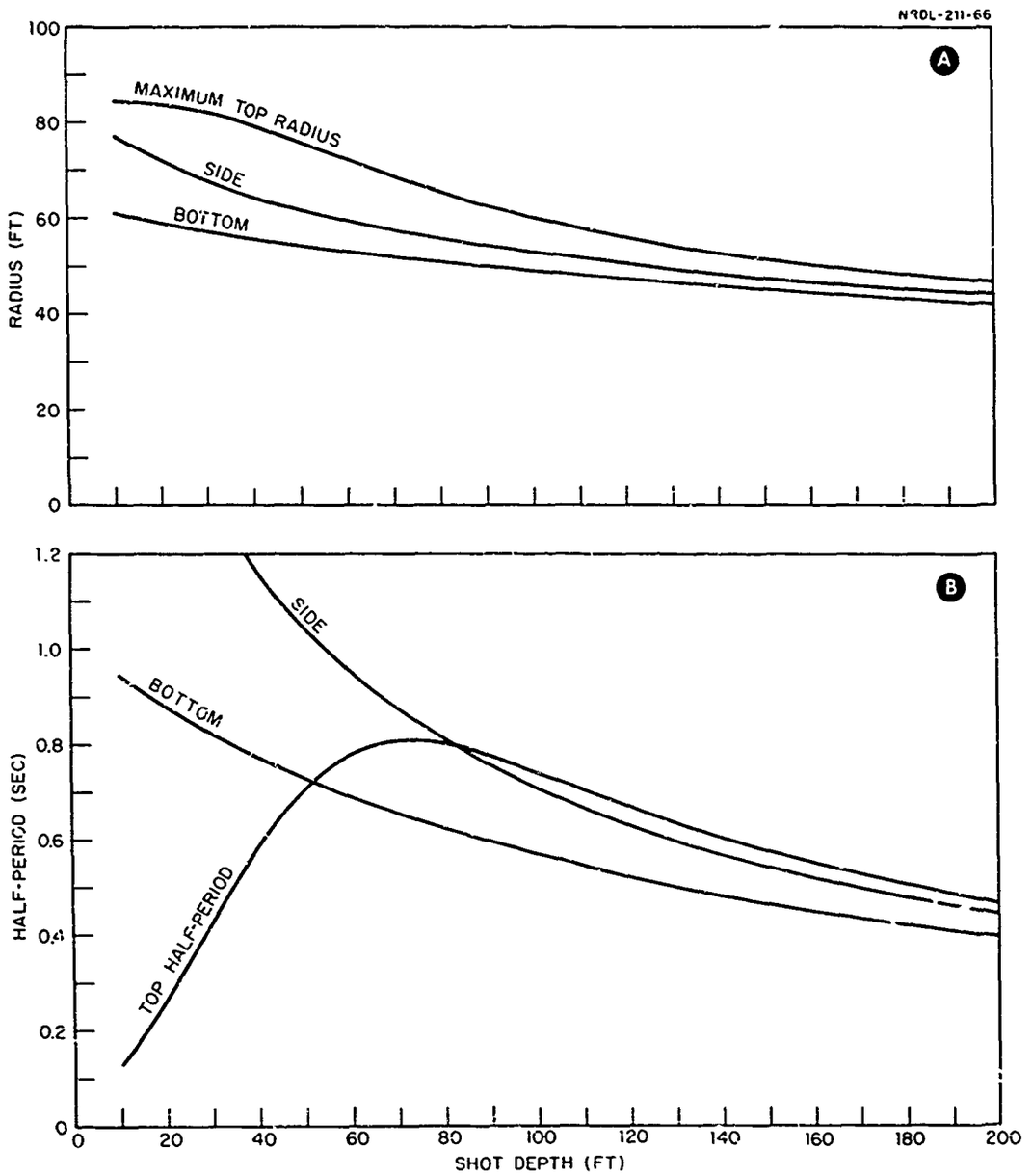

Fig. 2-4a Maximum Radii for the Bubble Top, Bottom, and Side for W = 10,000 Pounds as Functions of Depth of Burst.

Fig. 2-4b Bubble Top, Bottom, and Side "Half Periods" for W = 10,000 Pounds as Functions of Depth of Burst.

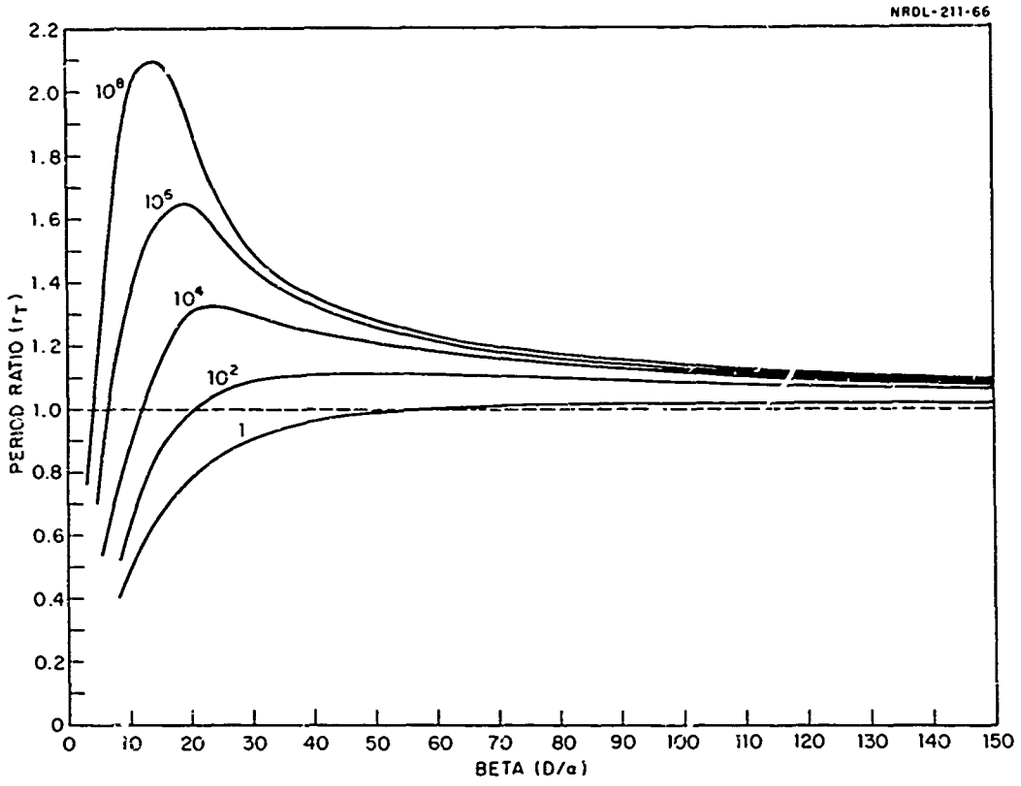

Fig. 2-5 The "Period Ratio" (r_m) as a Function of Beta (D/α) For W = 1, 10^2, 10^4, 10^6 and 10^8 Pounds.

CHAPTER 3

EXPERIMENTAL APPROACH

CONCEPT

The problem involved is that of the identification and evaluation of the processes by which the explosion products are redistributed in, and ejected from, the explosion bubble as a consequence of bubble pulsation and migration. In this study, point-source explosions are of interest since the results will eventually be applied to the effects of deep underwater nuclear explosions. Previous work[5] has indicated that, at the first bubble maximum, all of the explosion products are contained within the bubble, and that most of them reside within a concentrated central core. The objective in the present work, then, is to examine the distribution after migration, recompression and reexpansion of the bubble have occurred. It is apparent that the extent and nature of the redistribution of explosion products will depend on the behavior of the bubble, that is, the strength of the bubble migration. Therefore, the method adopted was as follows.

Explosion tests were carried out in the NRDL low-yield underwater explosion tank. Three scaled shot configurations were selected, including a rest-point condition, a condition characterized by weak upward bubble migration, and a strong upward migration condition. Scaling was accomplished by reduction of the air pressure within the tank, as discussed in Chapter 2. The explosive source used was an electrically exploded gold wire suspended between electrodes in the center of the tank. The energy densities of these explosions were quite high,

so that they may be considered point-source.

The investigation was carried out by physically sampling the bubble and its environment at the time of the second bubble maximum. The samples were then analyzed for gold content by neutron activation. In order to avoid perturbation of the bubble behavior by the sampling system, the sampling device was small and only one sample was taken for each explosion. Consequently, a large number of shots were fired at each condition in order to build up an array of explosion products concentration data, which could then be viewed as a whole.

THE EXPERIMENTAL FACILITY

The apparatus used in this study was basically the same as that used in the work reported in Ref. 5 and much of the basic equipment has been described at some length in Ref. 13. Therefore, the facility will be described only briefly here, with emphasis upon those features which have been significantly changed.

The Test Tank

The explosion tank itself is essentially an upright circular cylinder, of height 12 feet and inside diameter of 5 feet (See Fig. 3-1). Three viewing windows are provided, each 60 inches high and 18 inches wide. These are of 1-inch tempered glass, and are mounted in heavy rectangular steel frames. The firing electrodes are mounted in ports 5 1 2 feet above the tank bottom. Other ports provide access for electrical power, pneumtaic lines, etc. for auxiliary instrumentation, and also for a thermometer for measuring water temperature. Since the explosion point is fixed in the tank, the shot depth is varied by adjustment of the water level.

Access to the tank interior is through the front viewing window. Therefore, it is necessary to lower the water level in the tank after each shot in order to reset the sampler and replace the exploding wire. This window, as well as all other apertures, is sealed to maintain vacuum when the pressure is lowered prior to a shot. The explosion tank walls tend to collapse inward slightly under vacuum - the total change in tank diameter being about 1/16" under full vacuum. This deflection was found to vary linearly with the pressure differential, and to be reproducible within 10%.

The capacitors used to store the explosion energy are the same as were used previously.[13] These are six General Electric Type 14F756, 50 kilovolt clam shell type, low-inductance, high capacitance discharge condensers arranged co-axially in parallel just outside the tank, providing a total capacitance of 5.76 μf.[13] Switching is accomplished by a three-ball gap which is pneumatically operated and actuated by a solenoid valve. The capacitor bank is charged by a Sorenson Model 2060-50 high voltage DC power supply.

Ordinary tap water was used for this work, as its background level of gold is far below the range of interest. An auxiliary holding tank, located outside the building, was used to store the water when the water level in the explosion tank was to be lowered. When not is use, the water was constantly recirculated through a sand filter and a thermostatically controlled refrigeration unit in order to prevent the growth of algae in the system and to keep the vapor pressure low.

A fresh tank of water was introduced periodically (every 10-20 shots), in order to avoid buildup of the gold background level. The background was monitored by taking samples of the water in the tank at various times during the series.

The Sampling Device

The sampler used to investigate the explosion product concentration was similar to the device used in earlier work.[5] Essentially, it consists of two basic parts - a sampler body made of two co-axial metal tubes, open on both ends, and a rod with three attached pistons; a large piston on one end, and two smaller ones at the other (Figs. 3-2, 3-3). When high pressure air is released by the solenoid valve (A) it passes into the rear chamber (B) and exerts force on the large rear piston (C), thus causing the entire piston assembly to move backward. This draws the forward pistons (D,E) into the forward part of the smaller tube, thus trapping the material inside. The motion continues until piston (E) strikes the bumper ring (F). The excess pressure in the rear chamber is relieved by a pin-hole size port in the side of the chamber, and also by blow-by past the rear piston (C).

The pistons are fitted with O-rings, so that the sample, once taken, is vacuum sealed in the sampling chamber. In practice, leakage did occasionally occur (about 20% of the time) but it is quite likely that this leakage occurred fairly slowly. In general, if leakage occurred, the flow would be expected to be into, rather than out of, the sample chamber; unless the leakage occurred within the first second or so, the explosion products in the adjacent water would be quite dilute because of mixing.

The volume of the sample chamber is 1.05 cubic centimeters, this relatively small volume being necessary to avoid excessive perturbation of bubble behavior. This is less than 0.1% of the volume of the bubbles under study. The possibility existed that the "effective" sample volume may vary with the hydrostatic pressure because of the high speed of the sampler pistons. In preliminary tests, the sampler was therefore operated underwater at hydrostatic pressures as low as

0.03 atmospheres and the captured water weighed. In no case was the derived effective sample volume significantly different from 1.05 cm^3.

Monitoring of the sample operation time was accomplished in two ways. A small microswitch (See Fig. 3-2, 3-3) is mounted in the sampler body in such a way that its actuating pin rides on a cam that is attached to the piston shaft. Thus, prior to operation, the switch is open, during operation it is closed, and when the sampling operation is completed, the switch is again open. A 6V battery is connected in series with the switch, and the voltage is monitored on a Textronix 545A oscilloscope. Thus, both the sample time and sample duration may be determined. The sample duration - full open to full close - with a driving pressure of 100 psi, was about 4 msec, which is quite short compared to the bubble periods of interest. The sample time - the time between the explosion and the operation of the sampler - was taken as the time midway between the beginning and end of sampler operation. Sample times determined in this way could be read within about 1%. The sample time could also be determined from the high-speed motion-picture records. When the sampler closes, the excess pressure in the rear chamber causes a large bubble of air to be energetically expelled from the relief port in the side of the sampler body. This occurs at about the end of sampler operation, and is clearly visible in the motion pictures. Sample times determined in this way agree within 2 milliseconds with those measured by the microswitch circuit.

The electrical pulse that opens the solenoid valve and initiates sampler operation was obtained from the sawtooth output of a Textronix 535A oscilloscope. The scope was triggered by the explosion discharge, and the sweep delay was adjusted so as to obtain the desired sample time. Sample times could be reproduced within about 3 ms in this way.

The sampler was pre-positioned in the tank prior to the shot in such a way that the sampler axis was parallel to the electrodes and perpendicular to a radius joining the vertical explosion axis and the mid-point of the sampling volume. This was done for two reasons. First, it is assumed that the explosion product distribution is axially symmetric, and hence this orientation would minimize uncertainties due to finite sampler size, as the sample chamber diameter is less than its length. Also, this approach eliminates ambiguity concerning "effective" sample position, since all motion of the sample pistons is then tangential. Second, since there is no fluid circulation around the explosion axis, this orientation tends to eliminate "masking" of the sample by the front piston.

Photography

High speed motion pictures were taken of each event to determine the position of the sample relative to the bubble, and to make direct measurements of bubble phenomena. Three cameras were available, and at least two were used for each shot. Pertinent camera information is included in Table 3-1 and Fig. 3-4.

The primary function of cameras 1 and 2 was to provide three-dimensional coverage of the sample position relative to the bubble. Each of these also provided additional data as well. Ideally, camera 1 should have been located further from the tank, but this was prevented by space limitations. Therefore, the camera 2 records were used for precise distance measurements (bubble radii and the like) to avoid parallax. As can be seen in Fig. 3-4, from the camera 2 position, the bubble was backlighted. Consequently, details of the internal bubble structure could be discerned, whereas from the camera 1 position, the bubble was front- and sidelighted, and therefore the bubble appeared opaque. On the other hand, the camera 1 records proved

TABLE 3-1

Camera Data

Camera Number	Make	Type	Film	Frame Rate	Lens Focal Length	Distance from Axis to Film Plane	Angular Position
1	Milliken DBM 4A 16 mm	Pin-register	Ektachrine ER (color)	400 $\frac{\text{frames}}{\text{sec.}}$	25 mm	11.50 feet	90°
2	Milliken DBM 4A 16 mm	Pin-register	Ektachrome ER (color)	400 $\frac{\text{frames}}{\text{sec.}}$	Variable-usually 61 mm	28.91 feet	0°
3	Fairchild HS 100 16 mm	Rotating prism	TRI-X Negative (B & W)	~ 1700 $\frac{\text{frames}}{\text{sec.}}$	102 mm	28.95 feet	2°

valuable in that regions of high explosion product concentration were visible. The explosion products consist principally of small particles of black gold oxide, and these are distinguishable from the white background and from the many tiny bubbles that appear during the explosion which also appear white. From the backlighted camera 2 position, both these small bubbles and the explosion products appear black, and cannot be resolved.

Camera 3 was not used for all the shots. The nature of the camera mechanism and the graininess of the Tri-X film used resulted in poor photographic resolution, and therefore the records were not as useful for quantitative measurements. The high speed at which the camera was operated, however, allowed much better time resolution than was obtainable from cameras 1 and 2.

Distance scaling for all photographic records was accomplished by means of marks placed on the viewing windows. These were located in such a way that their separations corresponded to 6-inch intervals at the explosion axis from the vantage points of the various cameras.

Air Pressure

The required reduction of air pressure in the tank was obtained by means of a vacuum pump, and was measured with a Wallace and Tiernan model 1464 mercury manometer which incorporates a barometer for determination of ambient pressure. This equipment made it possible to obtain the required pressure within 0.0001 atmospheres. Generally speaking, it was found that in the time between the final setting of the pressure and the explosion (about one minute) the change in pressure due to leakage and de-gassing of the water was never more than about 0.0004 atm. This pressure uncertainty corresponds to about 4 mm of water, which is about the same as the uncertainty in total shot depth measurement.

Explosion Yield Determination

To determine the total energy yield of the explosion, the same system was used as in the work reported in Ref. 13. Essentially, the method involves measurement of the total released energy through knowledge of the discharge circuit resistance with the explosion gap shorted, the inductance and capacitance of the circuit, the voltage on the condensers, and the logarithmic decrement of the underdamped sinuscidal discharge current waveform. This current waveform was determined by integration through an RC network of the voltage induced in a coil placed adjacent to the discharge circuit, and the resultant voltage was monitored on a Tektronix 551 oscilloscope.[13]

The yield measurements were attempted for each explosion, but instrumentation problems were frequently encountered so that traces were obtained for only 2/3 of the shots. The results for those shots for which data was obtained showed wide scatter in the derived yields for identical shot conditions. This scatter resulted from at least three sources. First, the traces indicated that polarization may have occurred in the capacitor bank for some of the shots. Also, apparently some shift occurred in the vertical amplitude calibration of the oscilloscope, which was not detected until sampling was nearly complete. Finally (and most important) the method in its present form is intrinsically imprecise because the derived yield is extremely sensitive to small errors in measurement of the values of the current peaks in the discharge waveform; these can be determined from the oscilloscope camera records only with limited accuracy.

The parameter of real interest in this study, however, was not the total yield (W') but the TNT equivalent bubble yield (W), as was discussed in Chapter 2. The bubble yield is readily determined by measurement of the first maximum side bubble radius, according to equa-

tion 2.5. These measurements were made from the camera 2 films for all shots which provided explosion product concentration data. The derived yields showed much less scatter than the total yields obtained from the discharge decay rates. As a matter of academic interest, the value of k (W/W'; equation 2.1) was calculated for each shot, and the mean value was

$$k = 0.9 \pm 0.2$$

This may be compared with the value of 0.62 obtained in Ref. 14 for a different wire geometry.

Pressure-Time Measurements

A Crystal Research 1/8" tourmaline gauge was installed in the tank approximately one-foot directly below the explosion point. In order to obtain an overall pressure-time history of the explosion, the output was recorded on a Tektronix 535A oscilloscope, so that the bubble pulses provided immediate-readout estimates of the bubble periods and hence the explosion yield. More important, the same output was recorded on a much shorter time base on a Tektronix 545A with the sweep delay adjusted to obtain a detailed record of the first bubble pulse. Several such records were obtained, and results are presented in the next section.

The tourmaline gauge was removed from the tank about half-way through the test series, since an adequate number of bubble-pulse waveform had been obtained, and also since it was found that the photographic records yielded bubble periods with greater precision.

EXPERIMENTAL PROCEDURE (TYPICAL RUN)

The nature of the experiment involved reproduction of essentially the same explosion many times. Consequently, it was quite important thet the firing conditions for each shot be made as identical as possible.

The firing electrodes were installed in the tank, and the gap set at 0.50 inches. The wire segment was then mounted in the holes in the electrodes in such a way that no stress was placed on the wire when the tank deformed under vacuum. The wire simply slid freely further into the electrode to accommodate the deflection. (Fig. 4-1).

The sampler was first disassembled and cleaned with a dilute HCl solution, and then was lubricated with a silicone grease and reassembled. It was installed in the tank in the "open" position, the tank was sealed, and the water level was raised. The electrodes, exploding wire, and sampler installed in the tank are shown in Fig. 3-5. If the shot conditions required particularly low air pressures, the tank had to be filled very slowly, since any great surface turbulence would have caused air to go into solution in the water. When vacuum was subsequently drawn, this air had then to be pumped out of solution, which might take several hours to accomplish.

The water level was adjusted to approximately the correct shot depth, and vacuum was drawn. Once the desired vacuum was attained, the water level was re-adjusted (the deflection in the tank walls caused the water to rise slightly). The system was allowed to stand for about 15 minutes to allow outgassing. The vacuum was re-adjusted, and the shot was fired.

Immediately after the shot, the vacuum was released, the water was pumped into the auxiliary tank, and the sampler was removed. The outside of the sampler was cleaned with HCl, and the sample was released into a 7 ml polyethylene vial which had been previously weighed. The sample was then weighed, and the sample chamber was subsequently flushed into the sample vial with 1N HCl. The sample vial was then heat-sealed with a soldering pencil to prevent leakage.

After about 30 or 40 samples had been collected, they were shipped to General Atomic, San Diego, for neutron activation analysis. Without further manipulation, the sample vials and a gold comparator standard were placed in the General Atomic TRIGA Mark I nuclear reactor and irradiated for 30 minutes at a thermal neutron flux of 1.8×10^{12} n/cm^2-sec. The samples were then permitted to decay for at least one day to eliminate shortlived interferences, and then were counted on a multi-channel gamma-ray spectrometer for Au^{198}, with gamma energy = 411 Kev and half-life = 2.7 days.

Typically, results from the analysis procedure were available about a month after sample shipment, and consequently the sampling schedule was divided into only two separate series. The first was exploratory in nature, being designed primarily to determine the distribution in a gross fashion. The second was planned after the results of the first were obtained, to provide sufficient data to make quantitative estimates of the explosion product distributions in the three shot conditions of interest.

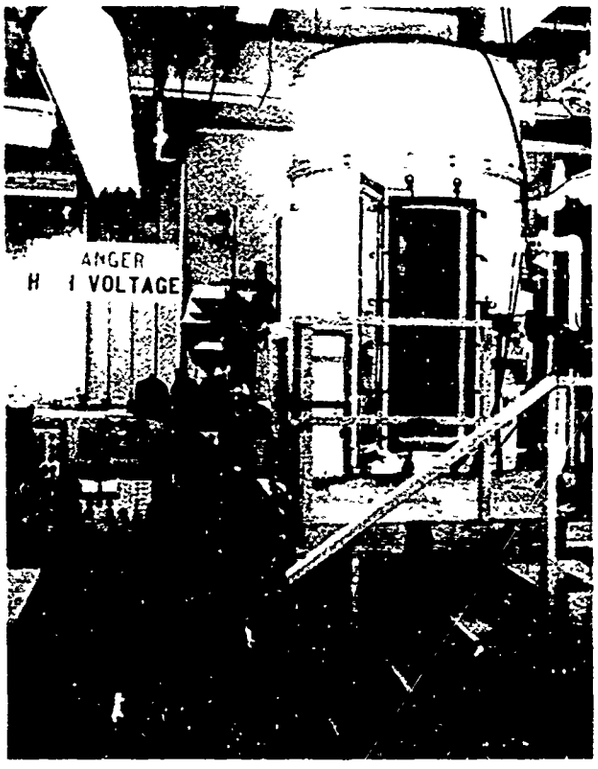

Fig. 3-1 General View of Test Facility

NRDL-211-66

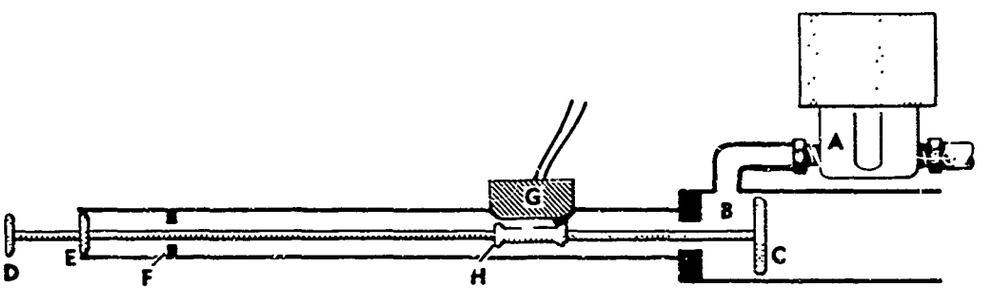

A	SOLENOID VALVE	**E**	REAR SAMPLE CHAMBER PISTON
B	REAR CHAMBER	**F**	BUMPER RING
C	REAR PISTON	**G**	MICROSWITCH
D	FORWARD SAMPLE CHAMBER PISTON	**H**	CAM

Fig. 3-2 Cutaway View of Sampler

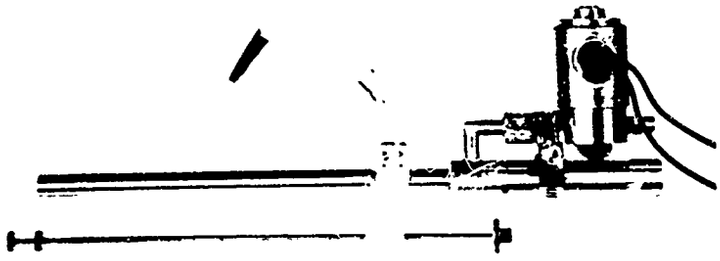

Disassembled

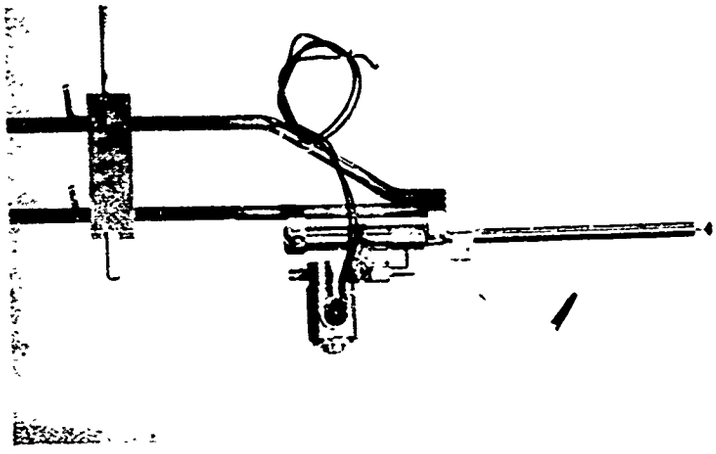

Mounted on Support Bracket

Fig. 3-3 The Sampling Device

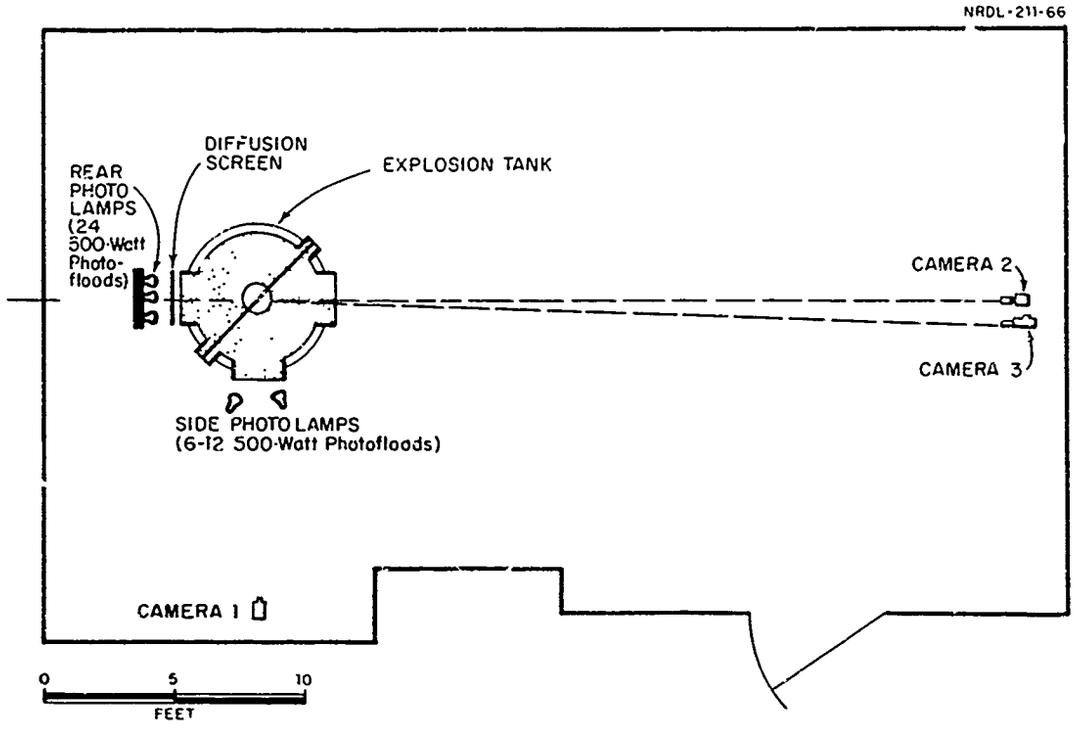

Fig. 3-4 The Explosion Tank Facility Showing Photographic Layout.

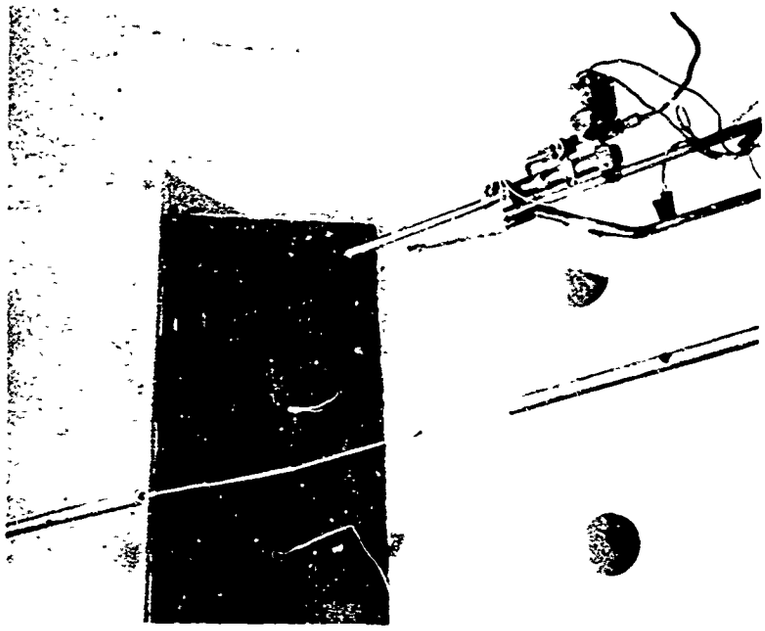

Fig. 3-5 General View of Explosion Tank Interior Prior to Shot

CHAPTER 4

DETAILS OF EXPERIMENTAL CONDITIONS, DATA REDUCTION, AND ANALYSIS

THE SHOT CONDITIONS

The three shot configurations under study were selected to provide three distinctly different sorts of bubble behavior. The defining parameters for these shot conditions are summarized in Table 4-1.

Since the independent variable involved is the strength of bubble migration, it is clear that a shot configuration in which the bubble does not migrate at all is of interest. As was discussed in Chapter 2, there are, in practice, two ways to generate a non-migrating explosion bubble. First, the non-migrating situation is approached as a limit as shot depth is increased to very large values (assuming that the sea bottom is always very far away). The problem involved in this approach, however, is that there will always be some migration, even though it may be extremely weak, and that very great shot depths are required. This means, of necessity, that the bubble will be quite small, and that the bubble period will be very short. In the experimental situation, sufficiently great shot depths are simply not available in the explosion tank, and, in any case, the bubbles would be far too small and would pulsate too rapidly to make study feasible.

The alternative to this method of avoiding bubble migration is to take advantage of boundary effects - in particular, the "repulsion" of the free surface. An explosion fired at such a depth that the surface correction term in equation 2.7 is zero, i.e.,

TABLE 4-1

The Shot Conditions

Shot Condition	Environmental Parameters		Discharge Parameters		Primary Shot Parameters			Secondary Shot Parameters				Scaled Prototype Shot Parameters	
	Air Pressure (atm.)	Water Temp. (°C)	Firing Voltage (kv)	Wire Length (in.)	W (mg TNT)	First Max Side Bub. Rad. (in.)	Shot Depth (in.)	Alpha (in.)	Beta (D/α)	M_s $\Delta D/R_s$	R_T T_t/T_b	W (lb. TNT)	Shot Depth (ft.)
A	0.1467	4.6	30	0.446	209	6.42	14.10	0.510	27.6	0.00	0.90*	0.994	8.01
B	0.1467	5.3	30	0.446	173	5.75	25.16	0.456	55.2	0.79	0.99**	0.825	14.3
C	0.0150	4.2	23	0.438	134	7.05	29.00	0.560	51.9	1.47	1.20	5830	161

*This is a "rest point" shot configuration - the failure of the radial flow model for situations of [illegible] or no migration is apparent. See Chapter 3.

**In this case, the bubble migrates upward slightly - the same remarks apply.

$$S(\beta)\ \frac{R_1 Z_1}{D_1^2} = 1$$

will generate a bubble at the "upper rest point", and the bubble will not migrate. Consequently, the following shot parameters were chosen for Condition A.

The air pressure over the water was set at 0.1467 atmosphere, and the water depth was adjusted to 14.10 inches. The explosion yield was originally intended to be 210 mg TNT and was determined precisely a posteriori by taking the mean yield of all data shots - the result was that the TNT equivalent bubble yield was 209 ± 12 mg TNT. These particular shot conditions were chosen since they scale the upper rest-point of a one-pound charge, which has been previously documented. The actual prototype conditions obtained were W = 0.994 ± 0.057 lb, and D = 8.01 ft.

The second shot configuration (Condition B) used in this study was chosen to be characterized by upward migration, but this migration was to be relatively weak ($M_s \simeq 0.8$). The air pressure was again 0.1467 atmospheres, and the shot depth was 25.15 inches. The explosion yield was again intended to be 210 mg, but the yield obtained by averaging all data shots of this series was 173 ± 11 mg TNT equivalent bubble, so that the specific migration (M_s) was 0.79. This discrepancy in yield will be discussed later in the chapter. It was hoped that this choice of shot conditions would allow correlation of results with the exploratory work done at the second bubble maximum reported in Ref. 5 for which M_s was about 0.75. More will be said about this later. The scaled prototype for these shot conditions is a charge of bubble yield 0.825 ± 0.05 pounds fired at a depth of 14.3 feet.

For the third shot configuration (Condition C), it was desired to maximize the migration strength, and consequently the air pressure was set at the lowest value which could be readily reproduced, to obtain the largest possible prototype yield. On the other hand, the burst must be kept fairly deep (which tends to repress migration) for three reasons. First, as shot depth is decreased, the bubble gets quite large, and it is desirable that the bubble radius remain small relative to the radius of the explosion tank to minimize wall effects. Second, as discussed in Chapter 2, excessive boiling of water into the bubble may occur near maxima if the hydrostatic head at the shot point is too low. Finally, if the depth of burst is too shallow, since the migration is upward, the second bubble maximum may be perturbed by the proximity of the free surface.

The shot conditions selected for condition C were $P_A = 0.0150$ atmospheres and D = 29.00 inches. The designed yield was 138 mg TNT. and the mean bubble yield was determined to be 134 $\pm$ 13 mg TNT. The derived specific migration was 1.47, and r_T, the ratio of the top and bottom bubble half-periods, was 1.20. These shot conditions correspond to a prototype yield of 5830 $\pm$ 560 pounds fired at a depth of 161 feet.

Explosion bubble yields for individual shots were determined, as discussed in Chapter 3, by measurement of the first maximum side bubble radius. The TNT equivalent bubble yield is then given by $R_S = 12.6\ \alpha$, or in this case,

$$W = 0.01095\ (R^3)\ (D + 396\ P_A)$$

where

W = TNT equivalent bubble yield in milligrams TNT
R = First maximum side bubble radius (inches)
D = Shot depth (inches)
P_A = Air pressure (atmospheres)

The variation from shot to shot in the total hydrostatic head was less than 0.5%, which is quite negligible compared to the variation in yield. Typically, the standard deviation in yield for all three conditions was 11-13 mg TNT, which amounted to a variation of about ± 6% for conditions A and B, and about 10% for condition C. This variation in yield was a result of several different sources of error. First, the firing voltage could be reproduced only within about ± 500 volts. This alone would tend to cause a variation of about ± 6 mg in the bubble yields. Also, the three-ball-gap trigger resistance depends on the breakdown distance in air, which is a function not only of applied voltage, but also of ambient air density and absolute humidity. Finally, as mentioned in Ref. 5, the length of the exploding wire may have varied from shot to shot, but it is felt that this variation was not very significant in the present work - one standard deviation in wire length is only about ± 1.5%.

Although the firing voltages for conditions A and B were identical (30 kv), a systematic difference between the yields of the shots was observed, the difference between the mean yields being about three standard deviations of the individual yields for either shot condition alone. The reason for this difference is not known, since the only difference in the nominal shot conditions was the water depth in the tank. One possibility is that the additional mass of water in the tank for condition B may have caused slight mechanical deformation of the tank structure, or elastic settling of the tank as a whole, causing a change in the geometry of the three-ball-gap trigger, or even a change in the basic circuit parameters. However, an understanding of the mechanism for the variation in yield is not critical to this study, and hence the matter was not pursued further.

DETERMINATION OF TOTAL AMOUNT OF GOLD PRESENT

From data collected concerning the effect of vacuum on the tank diameter, it is known that the gap length (separation between the tips of the firing electrodes) was 0.446 ± 0.006 inches for conditions A and B and 0.438 ± 0.006 inches for conditions C. The exploding gold wire was of 0.020 inch diameter, with a linear density of 99.6 mg/inch. Therefore, if the total mass of gold involved in the event is taken as that of a segment of the wire of length equal to the gap length, the "total device" or total input gold quantity becomes 44.4 ± 0.6 mg for conditions A and B and 43.6 ± 0.6 mg for conditions C. However, there are at least two mechanisms which tend to change this amount. First, the "effective" wire length is somewhat greater then the gap length - erosion of the electrode tips is observed, which suggests that some wire material which was originally within the electrode was involved in the explosion. On the other hand, the exterior portion of the electrode is observed to be coated with a thin film of material after the shot, of which some portion is undoubtedly gold. (See Fig. 4-1).

In order to evaluate the net effect of these mechanisms, a segment of wire was carefully weighed and exploded at shot conditions corresponding to condition B. The electrode tips (containing the unaffected ends of the original wire) were then dissolved in aqua regia and analyzed for gold content. The net amount of gold involved in the explosion (the total initial amount less that present in the tips) was found to be the 45.4 mg, which agrees remarkably well with the above value. This indicates that, for the wire geometry under study, the effects of erosion and plating tend to counteract each other. Hence, the amount of gold involved in the explosion for all three conditions was taken as 45 mg, and this value is probably good within a few percent.

SAMPLING DATA

Sampling Position

The position of the sample with respect to the bubble was determined from the camera 1 and 2 film records. Because the explosion bubble motion is turbulent and the initial conditions cannot be reproduced exactly, the bubble shape at the second maximum varies slightly from shot to shot. Consequently, an outline of the 'mean' second bubble maximum was drawn, and then the position of each sample collected, with respect to this 'mean' bubble, was determined.

The vertical coordinate (z) of the sample with respect to the actual bubble was readily found, and then the horizontal cross-section of the actual bubble at that altitude (z) above the explosion point was defined by the four interface positions provided by cameras 1 and 2 - this cross-section was, in general, slightly elliptical. The distance of the sample from the explosion axis, and the sample's angular position, were then determined and the sample placed with respect to the horizontal bubble cross-section. Finally, the ratio of the sample radius (relative to the center of the cross-section) to the bubble radius at that altitude and angle was determined. The sample position in the 'mean' bubble was defined to be the relevant altitude (z) and a radius that was the same fraction of the 'mean' bubble radius at z as was found in the actual bubble.

Density Measurements

As was mentioned in Chapter 3, the mass of water trapped in the sampler was measured after each shot. This was done for two reasons. First, the amount of water in the sample determines the contribution of the gold background level in the tank to the gross quantity of

gold in the sample - this will be discussed later. Furthermore, this measurement is valuable in itself, as it provides information concerning the internal structure of the bubble.

The density of the sample was taken simply as the mass of the sample divided by the sample chamber volume (1.05 cm^3). Since the bubble atmosphere is steam, condensed steam would tend to add mass to the sample. In general, however, the mass of the steam is negligible - that is, if the internal bubble pressure is taken as 0.2 atmospheres, the hydrostatic pressure at condition B shot depth (which over-estimates the pressure by about an order of magnitude or so), then the mass of saturated steam in the sampler volume would be only about 10^{-4} grams, which is about the lower limit of the measurement capability of the balance used. Consequently, any measurable density detected must be ascribed to the presence of liquid water, or spray.

It should be pointed out that density results will be preferentially low since, in general, it is not possible to remove all of the material from the sample chamber without flushing the sampler. Also, since spray is composed of droplets of finite size, the results will not be reproducible - a droplet of radius 1 mm weighs 4 mg, and a region of mean density 0.1 grams/cm^3 would have only 25 droplets of this size per ml. Nevertheless, in terms of identifying gross phenomena, these measurements proved quite valuable, as will be seen later.

Measurements of Explosion Product Concentration

The amount of gold (in micrograms) present in each sample as reported by General Atomic was initially divided by 1.05 cubic centimeters (the sample chamber volume) to obtain gross gold concentration. Several corrections to these results were considered, as outlined below. Relevant data for all samples are included in Tables

4-2, 4-3, 4-4, and 4-5.

The Effect of Sample Timing: The times of the second bubble maxima were 39 msec, 87 msec, and 220 msec for conditions A, B and C respectively, and the time of sampler operation was usually within about ± msec of these maxima. Of course, the times of the maxima also varied slightly, due to the variation in yield from shot to shot. In general, if sample time was appreciably different from the time of the second maximum for a particular shot, the sample was not used for analysis. Therefore, it is felt that no sample timing correction to the explosion product concentration is necessary.

The Effects of Yield Variation: The appropriate correction factor to be applied to take into account the effect of shot-to-shot variation in yield depends on the mechanism which causes the variation. For instance, if it is assumed that the only sources of yield variability are such things as variation in firing voltage and trigger resistance - that is, that the gap length is constant from shot to shot, we find a "characteristic concentration"

$$C = M/\alpha^3$$

where M is the mass of the exploding wire and α^3 is W/Z. We assume that Z and M are constant, so

$$C' = C(W/W')$$

where C and W are measured values and C' and W' are, respectively, the corrected gold concentration and the mean bubble yield for the shot condition. If we assume, on the other hand, that all variation in yield is due to gap length variation, then, approximately

TABLE 4-2

Sampling Data - Condition A

Shot	First Max Side Bub. Rad. (in.)	W (mg TNT)	Sample Water Content (mg)	Sample Density (g/cm^3)	Uncorrected Gold Quantity (μg)	Corrected Gold Concentration ($\mu g/cm^3$)	Location z(in)	Location r(in)	Sample Rad. / Bubble Rad.
A-1	6.42	210	Full	-	9.34	8.90	0.0	0.75	0.30
A-2	6.34	201	Full	-	7.62	7.25	0.0	1.0	0.40
A-3	6.34	201	87.4	0.08	4.61	4.39	-2.0	0.0	0.57
A-4	6.26	195	43.1	0.04	4.35	4.14	0.0	1.5	0.60
A-5	6.61	229	140.0	0.13	4.05	3.86	0.0	2.0	0.80
A-6	-	-	286.8	0.27	-	-	0.0	2.2	0.88
A-7	6.38	207	343.8	0.33	5.76	5.49	0.0	2.3	0.92
A-8	6.42	210	Full	-	5.73	5.46	0.0	3.1	1.24
A-9	6.54	222	559.2	0.53	2.49	2.37	0.0	3.7	1.48
A-10	-	-	593.9	0.56	-	-	0.0	3.6	1.44

TABLE 4-3

Sampling Data - Condition B

Shot	First Max Side Bub. Rad. (in.)	W (mg TNT)	Sample Water Content (mg)	Sample Density (g/cm^3)	Uncorrected Gold Quantity (μg)	Corrected Gold Concentration ($\mu g/cm^3$)	Location z(in.)	Location r(in.)
B-1	5.62	160	702.9	0.67	0.024	0.020	10.3	0.0
B-2	5.63	161	Full	-	7.87	7.49	9.4	0.0
B-3	5.70	168	91.4	0.09	3.76	3.58	8.7	0.0
B-4	5.90	187	657.1	0.63	0.091	0.081	8.6	1.2
B-5	5.69	168	31.6	0.03	4.62	4.40	7.8	0.0
B-6	5.69	168	33.3	0.03	1.94	1.85	5.0	0.9
B-7	5.78	176	20.7	0.02	3.86	3.68	4.0	0.0
B-8	5.69	168	57.9	0.06	0.94	0.90	4.0	1.7
B-9	5.76	174	88.3	0.08	0.754	0.718	3.7	2.5
B-10	5.70	169	Full	-	1.39	1.32	3.7	2.8
B-11	5.71	170	57.8	0.06	3.89	3.70	2.7	2.8
B-12	5.98	195	739.3	0.70	34.4	32.8	1.0	1.5
B-13	5.90	187	534.6	0.51	26.7	25.4	1.0	2.0

TABLE 4-4

Sampling Data - Condition C

Shot	First Max Side Bub. Rad. (in.)	W (mg TNT)	Sample Water Content (mg)	Sample Density (g/cm^3)	Uncorrected Gold Quantity (μg)	Corrected Gold Concentration ($\mu g/cm^3$)	Location z(in.)	Location r(in.)
C-1	6.94	128	575.7	0.55	0.632	0.600	17.6	0.0
C-2	6.58	109	607.2	0.58	1.67	1.59	16.7	0.0
C-3	6.85	123	Full	-	1.73	1.64	16.0	2.0
C-4	7.01	132	301.5	0.29	1.18	1.12	15.5	0.0
C-5	6.89	125	489.1	0.47	2.64	2.50	15.5	2.0
C-6	7.03	133	551.8	0.53	0.0005	0.000	15.5	4.5
C-7	7.07	135	247.9	0.24	0.806	0.767	15.0	3.4
C-8	7.12	137	249.2	0.24	0.859	0.817	14.5	0.0
C-9	7.01	132	341.9	0.33	1.28	1.22	14.5	3.2
C-10	6.98	130	156.6*	0.15*	1 37	1.30	13.7	0.0
C-11	6.65	112	269.5	0.26	1.33	1.27	13.0	0.0
C-12	7.01	132	184.9	0.18	0.681	0.648	13.0	2.1
C-13	7.18	141	407.1	0.39	0.188	0.178	13.0	5.1
C-14	7.12	137	115.9	0.11	0.496	0.471	12.8	3.5
C-15	7.07	135	8.9	0.26	0.516	0.490	12.5	5.0
C-16	7.00	131	285.4	0.27	0.754	0.717	11.0	0.8
C-17	7.0	136	522.0	0.50	1.17	1.10	11.0	2.0
C-18	7.24	145	67.2	0.06	0.312	0.296	11.0	3.0
C-19	7.02	132	71.3	0.07	0.365	0.347	11.0	5.0
C-20	7.26	146	606.1	0.58	0.534	0.507	11.0	5.8
C-21	7.01	132	461.7	0.44*	0.0177	0.0151	11.0	7.0
C-22	6.64	112	Full	-	1.69	1.61	9.5	0.0
C-23	6.64	112	246.8	0.23	1.59	1.51	9.5	0.0
C-24	6.70	115	425.7	0.41	0.120	0.113	9.5	1.4
C-25	6.97	130	103.0	0.10	0.375	0.357	9.5	2.9
C-26	7.12	137	Full	-	3.35	3.21	8.4	0.0
C-27	7.20	143	Full	-	0.874	0.827	8.4	4.0
C-28	6.76	118	Full	-	0.629	0.595	8.2	5.7
C-29	6.97	130	320.6	0.30	1.89	1.80	7.0	0.0
C-30	7.38	147	55.5	0.05	0.950	0.905	7.0	4.2
C-31	7.26	146	599.2	0.57*	1.38	1.31	4.5	0.0
C-32	6.95	128	718.0	0.68*	1.11	1.06	4.5	2.0
C-33	7.32	150	1032.9	0.98	0.498	0.466	2.0	0.0
C-34	7.33	151	Full	1.0	0.465	0.438	2.0	3.0

*Lower limit

TABLE 4-5

Late-Time Condition C Sampling Data

Shot	First Max Side Bub. Rad. (in.)	W (mg TNT)	Uncorrected Gold Quantity (μg)	Corrected Gold Concentration (μg/cm^3)	Location z(in.)	Location r(in.)
			Taken 415 msec after burst			
C-101	7.09	136	0.242	0.229	20.0	0.0
C-102	7.30	149	2.05	1.94	15.0	0.0
C-103	7.12	137	3.26	3.09	9.0	0.0
C-104	7.24	145	0.502	0.448	3.0	0.0
			Taken 630 msec after burst			
C-201	6.88	124	0.481	0.454	20.0	0.0
C-202	7.49	161	0.788	0.737	15.0	0.0
C-203	7.39	154	1.36	1.27	9.0	0.0
C-204	7.38	153	0.600	0.536	3.0	0.0

$M \sim W$

and we find that no correction is necessary.

The fact is that variation in gap length is responsible for some fraction of the yield variation, but the importance of gap length variation relative to other sources has not been quantitatively determined. In any case, the variation in yield itself was small (at worst, about $\pm$ 10% for condition C), and consequently the correction, if applied, would be even smaller. Therefore, no correction of concentrations for individual shot yield was used.

The Effect of Background: The choice of gold as the exploding wire material was made for two reasons. First, quantities of gold may be determined by neutron activation analysis with great precision even in trace concentrations. Second, as a consequence of gold's relative scarcity in nature, the problems of contamination in sample handling and background are minimized.

In order to prevent the buildup of a high background level in the tank due to deposition in the water of the explosion products after each shot, a new tank of water was periodically introduced, as discussed in Chapter 3. If it is assumed that all the explosion products are uniformly mixed after each shot, in the total amount of water in the system (1500 gallons), then the upper limit on the rate of background buildup is about 8 nanograms of gold per cubic centimeter per shot. Consequently, in the first sampling series, a 7 ml sample of the water was taken after introduction of the fresh tank before any shots were fired, and another such sample was taken just prior to emptying the tank. It was found that the background level of gold in fresh tap water was quite low and fairly constant - 0.0037 μg/ml $\pm$ 31%. Therefore, for the second shot series, no samples were

taken of the fresh tanks; the concentration was assumed to be initially about 0.004 μg/ml.

The intended procedure was to assume a linear buildup of the background for each tank of water of the form

$$C_{bg} = C_{BG_o} + An$$

where C_{BG_o} is the concentration in fresh tank water, and n is the number of shots fired in that tank of water. The value of A (the buildup rate) is obtained from the sample taken just prior to emptying the contaminated tank of water. Thus, the background concentration of gold in the water is defined for each shot, and consequently the contribution of this background to the gross amount of gold in the sample is just the background concentration times the volume of water found in the sample chamber.

Upon examination of the background data, however, it became apparent that the background concentration was being affected not only by the rate at which explosions were contributing gold to the water, but also by mechanisms that were extracting the material. The gold explosion products were not in solution, but were in the form of an extremely finely divided particulate. Continuous recirculation of the water through the filter over long periods of time apparently extracted a significant amount of material from the water; gold particles may also have adhered to irregularities in the pipe walls, and so on. Since sufficient data were not available to permit evaluation of the effects of these transfer processes, the background concentrations derived from the linear fits to the data discussed above were used, with some reservation.

Fortunately, the contribution of the background to the total amount of gold in most of the samples was negligible. If the fraction

of the gross concentration represented by background is computed for the samples, the following table results:

Fractional Background Contribution (percent)	Percentage of Samples With Fractional Background Contribution Less than that Value.
0.01	9.5
0.1	38.1
1	84.1
10	95.2

The three samples with the background concentrations equal to or greater than 10% of the total were samples C-21 (10%), B-1 (14%), and C-6 (330%). Fortunately, C-21 and B-1 were each fired as the first shot in a fresh tank of water, and the background is well known under these conditions. As can be seen, in Table 4-4, shot C-6 provided a sample containing less gold than would be predicted for a sample of water containing only the calculated background level. The only reasonable conclusion is that the region in which this sample was taken was virtually uncontaminated, except for background.

Sources of Error in Explosion Product Concentration Data: Errors in the analysis of the samples were of great concern, since Ref. 5 reports variations of as much as a factor of 2 in standard samples sent to check precision of the neutron activation analysis. In order to minimize these errors, the sample handling procedure was simplified, as described in Chapter 3, and it appears that this solved most of the problems. General Atomics Inc. reported standard deviations in their reported values of gold content which were generally under $\pm$ 1%. These deviations were determined from counting statistics only, however. In order to evaluate overall analysis errors, such as variations in neutron flux, etc., a series of standard samples were prepared and included with test samples, the gold contents varying over the range

0.01 μg - 80 μg. The reported values were within 10% of the correct values for these standards, indicating that analysis problems need be of little concern.

Another source of error and non-reproducibility is intrinsic in the explosion products themselves. The explosion products are not all in solution, but are, at least in part, in the form of small gold oxide particles. This introduces the possibility of "particle counting error" - that is, at low levels of concentration, the sample may contain only a few particles, and the addition or subtraction of even one particle may make a noticeable difference in the derived gold concentration. In general, with a uniform particle size, the uncertainity (1 σ) associated with a measurement of n particles is $\sqrt{n}$. If we assume that all the explosion products are associated with identical spherical gold oxide particles of diameter D microns, that the density of the particles of Au_2O_3 is 3.6 grams/cm^3, and that the sample volume is 1.05 cm^3, then the density of the gold in the particles is 3.2 grams/cm^3, and it may be shown that the percentage uncertainty in the gold concentration is:

$$\frac{\Delta C}{C} \times 100\% = \pm 0.13 \frac{D^{3/2}}{C^{1/2}}$$

where the concentration is in micrograms per cubic centimeter.

As can be seen, the uncertainty is strongly dependent on particle size. To investigate the problem, a sample was taken of the particles, the sample was passed through a 10 mμ millipore filter, and the particles were photographed (see Fig. 4-2). Virtually all of the particles are below 1 μ in size. Even if 1 μ is taken as the mean particle size, the uncertainty over the concentration range of interest is under ± 1%, and consequently the problem of particle size is not relevant.

Another source of error arises from the use of the sampling technique. First, the sample position must be determined, and it is estimated that this may be done within 0.1 inch. Second, although the sampler size is small relative to the bubble, the sample is of finite extent - the diameter of the sample chamber is 0.435 inch. This tends to cause an "averaging" of the gold concentration data across the region in which the sample was taken. This effect will not be important except where concentration gradients are very large, and may indeed have the beneficial effect of masking turbulent microstructure which would otherwise tend to obscure the general distribution. Nevertheless, it may be safely stated that the average concentration found in the sample will reflect the exact concentration at some point along the sampler diameter, in all likelihood fairly close to the center. Somewhat arbitrarily therefore, the total uncertainty in "effective" sample position, reflecting both uncertainty in actual position and the effect of finite size was taken as $\pm$ 0.2 inches.

It should be pointed out that intrinsic uncertainty is introduced by the nature of the experiment, That is, the hydrodynamic processes occurring in the underwater explosion bubble phenomenon are turbulent in nature, and consequently small differences in initial conditions tend to generate larger differences from shot to shot as the event proceeds. The effects of the inability to reproduce the phenomenon exactly are extremely difficult to estimate a priori. Ideally under these circumstances the best procedure would be to accumulate many data for each sampling position within the bubble, and then to construct an a posteriori estimate of uncertainty. Quite aside from the difficulty of reproducing a sample position, however, this procedure would involve the taking of such a large number of samples as to render the project impossible, from the standpoints of both cost and time. The choice involved was essentially between having relatively few data positions for which the uncertainty is well

known quantitatively, or having a larger number of data with the uncertainty not so well defined; this investigator chose the latter approach, and the results appear to justify this choice. At one of the sample positions, where two samples (C-22 and C-23) were taken, the gold concentration results were 1.61 and 1.51 μgrams/cm^3 respectively. Although this close agreement may be somewhat fortuitous, it does indicate that the uncertainty caused by irreproducibility is probably no more important than the total caused by the sources of error already discussed. Furthermore, although the rigorous procedure of obtaining numerous data for each sampling position was not followed, a large number of samples was obtained at various positions, such that the sample density in the bubble was fairly high. It seems reasonable to assume that the effect of irreproducitility is not terribly important if the sample data give rise to meaningful, continuous concentration gradients and contours, which indeed they do. The judgment of the user must then be employed to evaluate the significance of deviations in the data. It should also be pointed out that too large a value at one sample position may be accompanied by too small a value at an adjacent position, so that when the concentration data is integrated over many sample positions to obtain a total gold content in some region, the error in the total will in general be less than the error in the individual sample data.

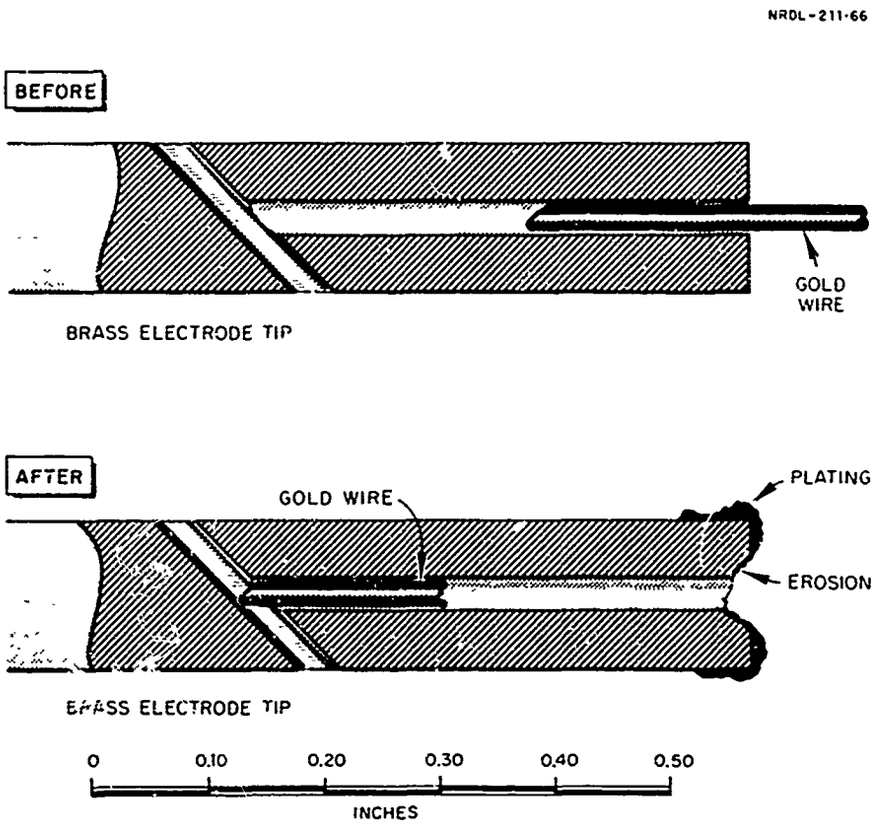

Fig. 4-1 The Electrode Tips and Exploding Gold Wire Before and After Explosion

Fig. 4-2 Explosion Product Particles From The Submerged Exploding Wire

CHAPTER 5

RESULTS AND CONCLUSIONS

DISTRIBUTION AND TRANSPORT MECHANISMS

The problem involved in this study is to determine how the central distribution of explosion products found in Ref. 5 for the first bubble maximum is changed by the hydrodynamic mechanisms of bubble collapse, re-expansion, and migration. For the initial discussion, we will consider the three shot conditions separately.

The Non-Migrating Case - Condition A

The Distribution of Explosion Products: Ideally, a non-migrating explosion bubble should remain spherical even after several cycles. The condition A bubbles, however, at the second maximum took the form of an ellipsoid of revolution centered at the shot point with the vertical radius ($\sim$ 3.5 inches) being greater than the horizontal radius ($\sim$2.5 inches) as shown in Fig. 5-1. This sort of behavior has been observed also at the prototype shot conditions (Unpublished HYDRA I film data), and is probably a consequence of the fact that the non-migrating situation was obtained by "balancing" the effects of the free surface and gravity rather than by firing at so great a shot depth that the pressure differential across the vertical bubble diameter was negligible relative to the total head. It was hoped that this departure from spherical form would not seriously affect the distribution.

Sampling was attempted along both the vertical and the horizontal bubble radii. Unfortunately, it was found that sample positions above

or below the shot point would generally induce upward or downward migration toward the sampler. After numerous attempts, one sample (A-3) was obtained along the vertical radius of a non-migrating bubble. If sample radii were normalized to the bubble radius at the appropriate latitude, it was found that this sample concentration agreed quite nicely with data taken along the horizontal radius. It was therefore concluded that the contours of equal concentration were ellipsoids of revolution of the same eccentricity as the bubble itself. The sample positions and corrected concentration data are shown in Fig. 5-2, and the reduced radial concentration is presented in Fig. 5-3.

In order to more easily compare results of shots at one condition to those at another, as well as to simplify integration for total content, the position and concentration data may be readily transformed to "reduced" values. That is, we may take α (i.e.$(W.Z)^{1/3}$) as our basic unit of length; the unit of volume then becomes α^3(i.e. W/Z). Rather than use units of mass (in this case, μg of gold) as a measure of the total quantity, we may use simply fractions of the "total device", or, as a basic unit of concentration $\mu d/\alpha^3$ (micro-devices per cubic alpha). If these transformations are made, using 1 d = 45 mg gold and α = 0.510 inches, we obtain:

$$1\ \mu g/cm^3 = 48.49\ \mu d/\alpha^3$$

Now, we may refer our ellipsoidal bubble to a spherical bubble of the same volume. If this is done, we obtain that the equivalent spherical radius at the second maximum is:

$$R_2 = 5.48\ \alpha$$

(Recall that the radius at the first maximum is 12.6α). Earlier work concerning the distribution of explosion products within the bubble at

the first maximum indicated that at this time, most of the explosion products reside in a concentrated central core.[5] This result corroborates earlier theoretical work which indicated the same sort of behavior for deep underwater nuclear explosion bubbles.[1] The study of the first bubble maximum was done in a manner similar to that of the present work, using an exploding gold wire, physically sampling the bubble, and analyzing for gold by neutron activation. The central concentration was found to be more than three orders of magnitude higher than the concentration near the periphery, the concentration away from the center dropping off approximately with $1/r^3$. Therefore, the distributions in reduced units for the first and second bubble maxima are as in Fig. 5-4. If this distribution is integrated, the fraction of the total device lying within a given reduced radius as a function of reduced radius may be obtained - this may then be compared with the situation at the first bubble maximum, as shown in Fig. 5-5.

As can be seen, whereas all of the explosion products reside within the bubble at the first bubble maximum for the non-migrating case, only about 18% are inside the bubble at the second maximum. Most of the remainder lie within a fairly short distance from the interface, but are outside the bubble. Just adjacent to the interface, concentrations are sufficiently high so that the explosion products are clearly visible on the camera 1 film records. The contaminated "patches" at the interface are shown in Fig. 5-6.

The Mechanisms of Explosion Product Transport: As was discussed in Chapter 2, as the explosion bubble collapses from its first maximum expansion, the internal pressure rises rapidly. Shortly before the bubble minimum, the gaseous bubble atmosphere begins to change phase near the interface - mass is lost to the liquid medium. Essentially, the interface begins to move with respect to coordinates fixed in the fluid. Consequently, the explosion products which were

embedded in the atmosphere are transferred through the bubble interface into the liquid environment. This transfer is visible on the camera 1 film records as a "blackening" of the originally white bubble interface just prior to the minimum.

As the contraction proceeds to the minimum, more and more material is lost. It should be pointed out that the minimum bubble radius is rather poorly defined, since the internal pressure and temperature are well above the critical point for water at and near the minimum. Also, at the bubble minimum the bubble is irregular and "spiky" in appearance due to Taylor instability.[9] This irregularity is reflected in the "blotchiness" of the explosion products visible near the interface at the second maximum.

At the bubble minimum, the quantity of explosion products within the bubble may be very small. As the bubble rebounds, however, the adjacent water begins to vaporize due to the drop in internal pressure, and material is thus transported back into the bubble; the interface is now moving outward with respect to the fluid. Most of the explosion product material remains outside the bubble, however, even after the phase change process is complete. The total bubble energy remaining in the bubble for the second cycle is a great deal less ($\sim$ 8%) than that which was available in the first, and consequently the total amount of water re-vaporized upon the second expansion is appreciably less than that which was condensed prior to the minimum. Also, near the bubble minimum, considerable turbulence is generated, resulting in both internal and external mixing. The result is that, at the second bubble maximum, there still remains a high central concentration, but concentration gradients are not nearly so large as at the first maximum. The bulk of the explosion products ($\sim$ 82%) now reside just outside the bubble interface. These transport mechanisms are illustrated in Fig. 5-7 for Condition A.

Weak Migration - Condition B

The Explosion Product Distribution: In many respects, condition B may be treated as a perturbation of condition A (the non-migrating case). At the second maximum the bubble is roughly pear-shaped as shown in Fig. 5-8. The protuberance at the top is a consequence of the bottom collapse which occurs just prior to the time of maximum recompression, as will be discussed later.

The sampling data is presented in Fig. 5-9. In order to convert this data to "reduced" units (as was done for condition A) the appropriate conversion factors are:

$$\alpha = 0.456 \text{ inches}$$

$$1\ \mu g/cm^3 = 34.51\ \mu d/\alpha^3$$

The concentration along the vertical centerline axis within the bubble is shown in Fig. 5-10. If the off-axis concentrations are plotted as a function of (cylindrical) sample radius normalized to cylindrical local bubble radius, all the values below $z/\alpha = 1.5$ and $z/\alpha = 5$ fall on a smooth curve, as shown in Fig. 5-11. A few relevant values obtained from Ref. 5 for a similar second maximum (see Chapter 4) also fall on the same curve. The similarity in form of Fig. 5-11 for condition B and Fig. 5-3 for condition A should be noted.

The region above $z/\alpha = 15$ (see Fig. 5-9) may be considered as relatively homogeneous in concentration - the sampler size is fairly large relative to this protuberance, so that the data would tend to be "average" values. If the mean concentration is taken as 200 $\mu d/\alpha^3$, the total content within the bubble below $z/\alpha = 15$ is 4-6% of the device, leaving 93 to 95% unaccounted for. The location of this excluded fraction is not difficult to determine, however. Although no

sampling data is available outside the bubble in the "blotchy" region along the sides visible in Fig. 5-12, this blotchiness is in all likelihood similar to that observed in condition A, and denotes a high concentration of explosion products just outside the interface. Even more important, the heavily contaminated region visible in Fig. 5-12 just below the bubble was sampled at two positions; the mean concentration in this region is well above 1000 $\mu d/\alpha^3$. Although sufficient data is not available to obtain a detailed distribution in these regions, concentrations of this magnitude indicate that the remainder of the device is to be found there. The distribution of the explosion products in the various zones of interest is summarized in Fig. 5-13.

The Mechanisms of Explosion Product Redistribution: The differences between conditions A and B arise from the collapse of the bottom of the bubble near the first recompression and the translation of the system as a whole in the latter case. As has been seen (Chapter 2), just prior to the recompression, after much of the explosion product material has been lost to the environment due to phase changes, the bubble bottom passes through the explosion point and impinges upon the top. The upward jet of water thus formed scavenges some of the contained explosion products and penetrates the water above the bubble. At this time, the gaseous portion of the bubble is translating upwards with high velocity through the water, leaving behind it much of the explosion products which were lost due to phase change of the bubble atmosphere. Thus, as the bubble re-expands and adjacent water is vaporized, much of the water that passes into the bubble atmosphere is uncontaminated and hence returns no explosion products to the bubble. Early in the re-expansion the narrow central vertical water jet breaks up into spray, is dispersed, and is in all likelihood in large part vaporized, since at the second maximum no central column was detected by the sample density measurements. As a conse-

quence, the internal distribution at the second maximum is similar to that in the non-migrating case except as follows: The central core has been smeared vertically through the bubble by the upward water jet, moving the region of highest internal concentrations up into the residual protuberance at the top. The total internal content of explosion products is only about 1/3 that found in the non-migrating case, since the system, upon re-expanding, has translated into relatively uncontaminated water. Thus, although some of the lost material is to be found in a degenerate form of the external irregular "shell" of condition A around the lower half of the bubble, much of the material remains in a relatively small, highly concentrated patch below the bubble, centered at about the position at which the bubble minimum occurred. These transport mechanisms for condition B are illustrated in Fig. 5-14.

Strong Migration - Condition C

Much more data was accumulated at this shot condition than at any other, for two reasons. First, the bubble at the second maximum is physically much larger than was true for condition A and B, and the flow is more complicated, requiring more samples for adequate definition of the distribution. Second, the bubble behavior (migration strength) is characteristic of nuclear explosions fired at nominal depths of burst.

The motion picture sequence in Fig. 5-15 shows general features of the bubble phenomena; relevant sample information at the second maxinum is presented in Fig. 5-16. The data obtained concerning the internal density is shown in Fig. 5-17 and indicates the existence of a central column or jet of extremely heavy spray (density $\sim$ 0.25 grams/cm^3) which passes vertically through the bubble. This column of spray is also faintly visible on the backlighted camera 2 film records

in Fig. 5-15. Clearly, the bubble may no longer be considered as a gaseous sphere, but is actually toroidal in form.

As was done previously, position and concentration data may be transformed to reduce quantities by application of the conversion factors:

$$\alpha = 0.560 \text{ inches}$$

$$1 \ \mu g/cm^3 = 63.76 \ \mu d/\alpha^3$$

The data may then be plotted, and contours drawn as shown in Fig. 5-18. Several features of the explosion product distribution may now be distinguished as illustrated in Fig. 5-19. Near the top of the bubble and extending slightly into the adjacent water above is a region (I) of relatively high explosion product concentration ($\sim$ 100 $\mu d/\alpha^3$) which is more or less homogeneous. This region corresponds to the top of the central spray jet shown in Fig. 5-17. The total content of this region is about 7% of the device. Continuous with region I is a vertical hollow cylinder of high concentration which corresponds in position with the edge of the central water jet, extending all the way to the bottom of the bubble (region II). The concentration in this region varies between 60 and 90 $\mu d/\alpha^3$, and the total contained quantity of explosion product is about 3% of the total device. Outside regions I and II but within the bubble is a torus-shaped zone (region III) wherein the spray content is quite low, and where the explosion product concentration varies from about 30-50 $\mu d/\alpha^3$ around the perimeter to about 20 $\mu d/\alpha^3$ at the center. This region accounts for about 10% of the total amount of explosion products present. Below region I and inside region II is a relatively thin shell (region IV) where the concentration is lower than in the adjacent water, varying from $\sim$ 50 $\mu d/\alpha^3$ near the top to values below 10 $\mu d/\alpha^3$ near the lower bubble interface. The total amount of material present in this

region is only about 0.4% of the device. Contained within region IV and continuous with the black "skirt" of debris visible below the bubble in Fig. 5-20, is region V, where concentrations are again high, reaching a peak of 200 $\mu d/\alpha^3$ near the lower bubble interface, and declining slowly below the bubble. Due to the small volume involved in that portion actually within the visible bubble interface (region Va) the total content involved there is only about 3% of the total device, but in the region below the bubble (Vb) the total volume is quite large due to the spreading of the region as the explosion point is approached. It is therefore assumed that the remaining amount of the device (77%) is distributed within this region. Although insufficient data is available to integrate a total content, the large volume involved and the relatively high concentrations present certainly indicate that this conclusion is not unreasonable.

The Redistribution Mechanisms: In condition C the bottom collapse and upward translation are dominant modes of behavior. The upward jet of water passes through the bubble and strikes the top at a time when the internal bubble pressure is not yet particularly high. Consequently, only a small fraction of the explosion products have been lost to the environment when the jet rushes through the highly contaminated center of the bubble. This effect can be seen in the pressure-time records shown in Fig. 5-21 taken near the bubble minima. The "bubble pulse" from condition A shots is merely a single sharp peak, whereas for conditions B and C a second, lower peak is observed just prior to the main (gas recompression) peak. This early pulse is a consequence of the impact of the upward jet against the upper bubble interface, and has also been observed at full-scale field tests[15]. The time-separation between the peaks was about 0.15 msec for condition B and about 1.2 msec for condition C, reflecting the earlier collapse at the strong migration shot configuration.

Therefore, a substantial portion of the explosion products becomes mixed into the top and sides of the jet prior to the time of maximum recompression. Physically, the "visible" bubble minimum is relatively large, but most of its volume consists of the water in the upward jet, the gaseous portion of the bubble being a relatively small annulus. Events occurring near the minimum are shown in Fig. 5-22. Once again, as the bubble recompresses, most of the remaining material is lost to the environment, and is swept into a skirt-shaped wake behind the bubble as it translates upward. The motion after the first recompression is observed to be somewhat similar to that of a ring, or spherical vortex, with the strong upward flow of the central jet continuing and spreading out along the top of the bubble. This circulating flow causes mixing of explosion products from the jet into the toroidal gaseous part of the bubble, and, furthermore, causes a small portion of the material which was initially lost near the minimum to be drawn back up into the center. In contrast to the behavior in condition B, the jet does not degenerate, but remains a dominant feature throughout the motion.

DISCUSSION

In general, as should be expected, the distribution at the second bubble maximum is more dispersed than that of the first. Furthermore, as migration strength is increased, the explosion products are not only translated upwards to a greater and greater extent but are more and more widely distributed, as can be seen in Fig. 5-23, where the distribution at the second maximum for all three conditions is compared with that at the first bubble maximum. The total amount retained in the bubble at the second maximum is fairly large when no migration occurs, but drops off as migration strength is increased, due to bubble re-expansion into uncontaminated water. As migration strength is further increased, however, the upward jet becomes a dominant

feature of the system, and the retained explosion product fraction again increases. Furthermore, as migration strength increases, the kinetic energy of migration becomes a significant term in the bubble's energy budget. Thus, the internal energy at the minimum decreases, recompression becomes less extreme, and less material is lost through the phase change process.

Two earlier studies have been made concerning the distribution of explosion products from a submerged exploding wire. One of thes concerned itself with the distribution at the first bubble maximum, and has already been discussed.[5] More recently, work was undertaken at Malaker Laboratories, Inc., in which an electrically exploded silver ribbon submerged in light mineral oil was used as an explosive source.[16,17] The system could be evacuated to obtain various migration strengths. Essentially, the procedure involved was that of taking high-speed motion pictures of the explosion and attempting to track the "debris cloud." It is suggested in Ref. 17 that the debris resided in a thin shell near the interface at the first bubble maximum. It is also concluded that little or no explosion product debris is transported by the bubble and released only after oscillation has ceased. These conclusions are at variance, both with the present study and with the work at the 1st bubble maximum presented in Ref. 5. There are several possible reasons for this disagreement, as follows.

First, the energies involved in the explosions were extremely low-in the range 0.1 - 1 calorie or about 0.1 - 1 mg TNT (as compared to $\sim$ 150 mg TNT for the present work). At these low yields, the fraction of the energy required merely to vaporize the wire material may well become a substantial fraction of the total. The explosion will, in any case, be of fairly low energy density so that the "point-source" approximation may not hold, and the explosion product particles may be fairly large.[18] These problems would in all likelihood serious-

ly affect the initial distribution of explosion products in the bubble. Also, the explosion bubbles were strongly perturbed by the small size of the container relative to the bubble size, and the large firing electrodes, as shown in the photographs of the bubbles in References 16 and 17.

Furthermore, the use of photography as a method of quantitative determination of explosion product distribution can be misleading. This is particularly true if backlighting is used (see Chapter 3). If, for example, the explosion products are fairly dilute over a large region, they may be invisible on film, but the integrated total explosion product content over the region may still be large. On the other hand, if explosion products are concentrated in a shell outside the interface, they may be indistinguishable from the interface itself.

In order to apply the present results to possible full-scale situations, one or another of the scaling criteria discussed in Chapter 2 may be applied. Strictly speaking, the prototype shot yields and depths for conditions A, B, and C respectively are 0.99 lb at 8.01 feet, 0.83 lb at 14.3 feet and 5830 lb at 161 feet. As was pointed out in Chapter 2, however, approximate scaling may be accomplished by resorting to one or another of the bubble models.

In free-field, condition A, the non-migrating case, does not correspond to any full scale shot conditions for large yields; it is only approached as a limit as shot depth is increased to very large values, except for yields of less than 100 lb or so, for which an upper rest point is possible. If the sea bottom is nearby, a lower rest point may be attainable and, if the bubble is not excessively distorted by proximity to the bottom, condition A may be a good model for bubble behavior and explosion product distribution.

Conditions B and C may be referred to other yields and shot depths by means of the bubble models. That is, condition B is characterized by $M_s = 0.79$ (that is, $\Delta D_{12} = 0.79R$) so that any yield-depth combination for which $M_s = 0.79$ should involve bubble behavior and explosion product loss mechanisms similar to those of condition B. The radial-flow model fails for condition B ($r_T = 0.99$; implied downward migration) so that the use of equality of r_T as a scaling criterion is not justified in this case. For conditions C, we obtain $M_s = 1.47$ and $r_T = 1.20$; both of these criteria give virtually identical results for yields greater than about 3,000 lb. Results of these approximate scaling calculations are shown in Fig. 5-24. For example, if we consider a nuclear explosion of TNT equivalent bubble yield 1.7 lb. (5 KT TNT) the relevant behavior of the bubble and the loss mechanisms should be similar to those of condition B for a depth of burst of 3450 feet, and to those of condition C for a burst depth of 1300 feet.

It should be pointed out that the distributions of explosion products found at the second bubble maxima for these three shot conditions are not necessarily the distributions to be expected at later times. For example, in the non-migrating case, the visible contaminated patch is observed to grow after this time by turbulent and particulate diffusion, as can be seen in Figs. 5-25 and 5-26. When migration occurs, further vertical re-distribution will take place due to "afterflow" in the water caused by the passage of the bubble. For condition B this can be seen qualitatively from the camera 1 film records in Fig. 5-27 as a vertical "smearing" of the contaminated region originally just below the bubble at the second maximum. In an attempt to qualitatively evaluate this mechanism for condition C, four samples were taken at intervals along the vertical explosion axis at each of two later times - one shortly after the time of the third bubble maximum which occurs just below the surface (415 msec) and one after the final collapse has occurred, and the resultant

above surface "plumes" are rising (630 msec). Results are presented in Table 4-5 and Figs. 5-28 and 5-29. As can be seen, this "afterflow" apparently does cause substantial upward translation of the lost explosion products even at these relatively early times.

CONCLUSIONS

In general, the most significant result of this study is that substantial quantities of explosion products are transferred to the water environment during the bubble migration phase of the underwater explosion event. Over the range of migration strengths studied (which covers most of the "very deep" explosion category), at least 3/4 of this debris has been lost from the bubble by the middle of the second cycle. For sufficiently deep bursts, ($D \approx 60W^{1/4}$ in the kiloton range) as much as 95% of the material may be ejected by this time. It is certainly not unreasonable to assume that additional material will be lost at subsequent minima. Consequently, it appears that considerable suppression of the radiological effects encountered at the surface may be obtained through these mechanisms. The reservation must always be made, however, that material deposited in the water may eventually appear at the water surface at later times through diffusion and afterflow of fluid generated by the upward motion of the bubble.

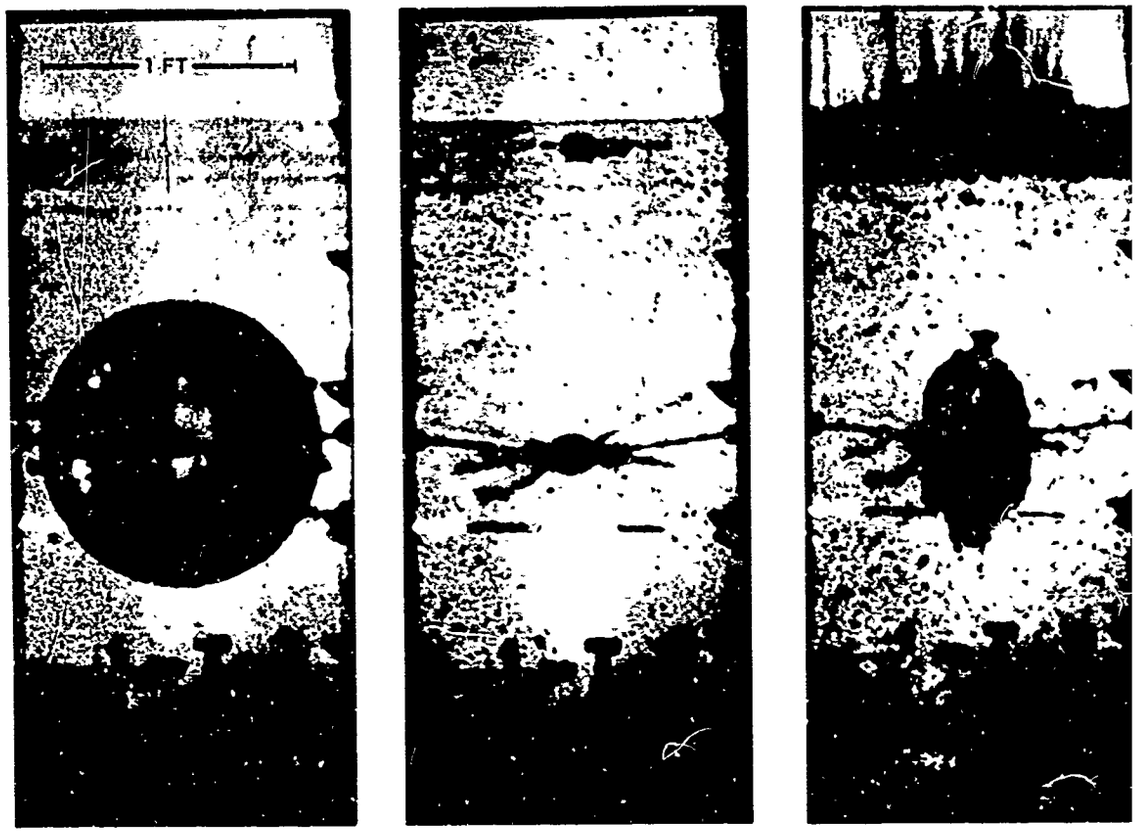

35 msec - First Maximum

72.5 msec - First Minimum

90 msec - Second Maximum

Fig. 5-1 Bubble Motion - Condit
(Camera 2 record)

A

90 msec - Second Maximum

107.5 msec - Second Minimum

117.5 msec - Third Maximum

Bubble Motion - Condition A
(Camera 2 record)

B

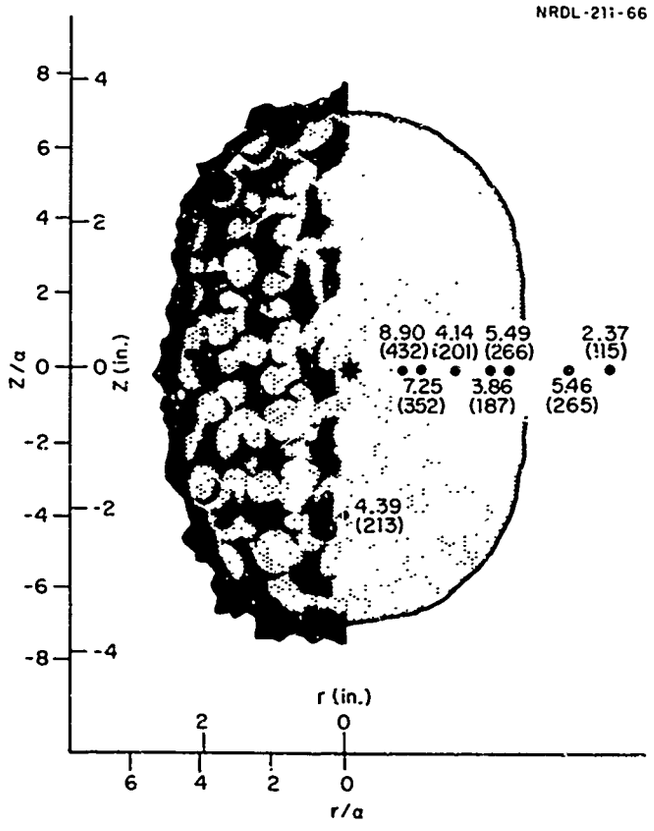

Fig. 5-2 Sampling Positions and Corrected Data - Condition A. Concentrations in $\mu g/cm^3$. Values in parenthesis are reduced concentrations - $\mu d/\alpha^3$.

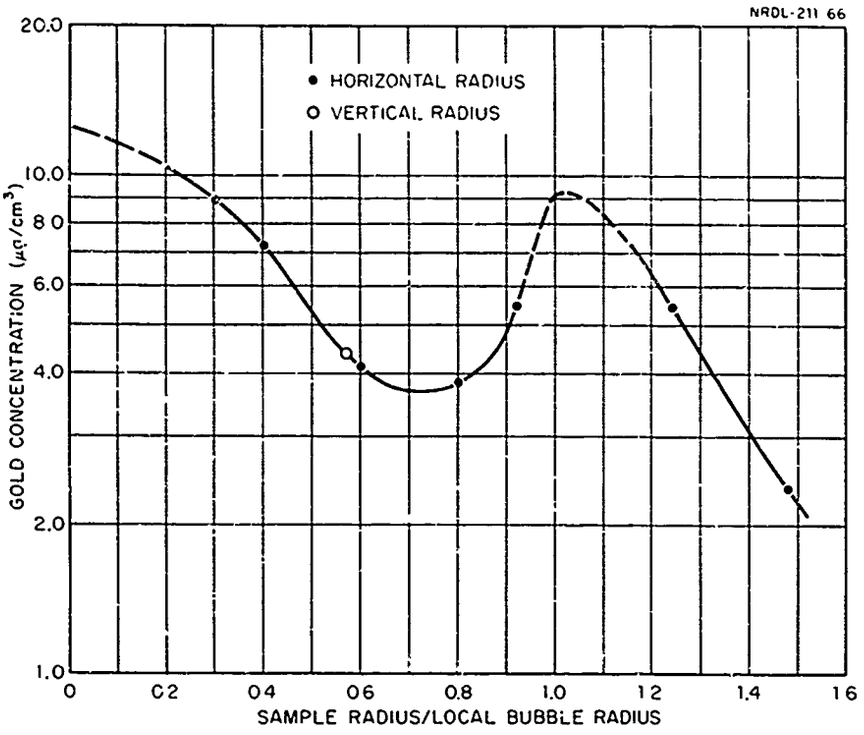

Fig. 5-3 Explosion Product Concentration as a Function of Sample Radius/Bubble Radius - Condition A.

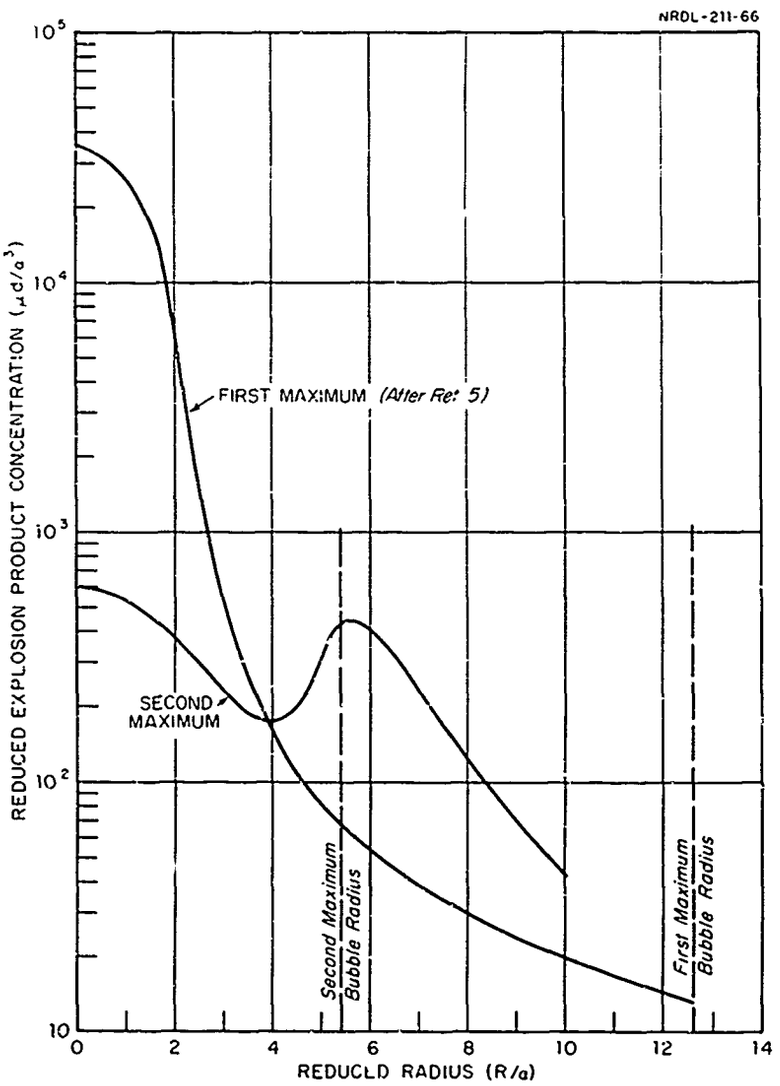

Fig. 5-4 Reduced Explosion Product Concentration vs. Reduced Radius at the First and "Equivalent Spherical" Second Bubble Maxima - Condition A

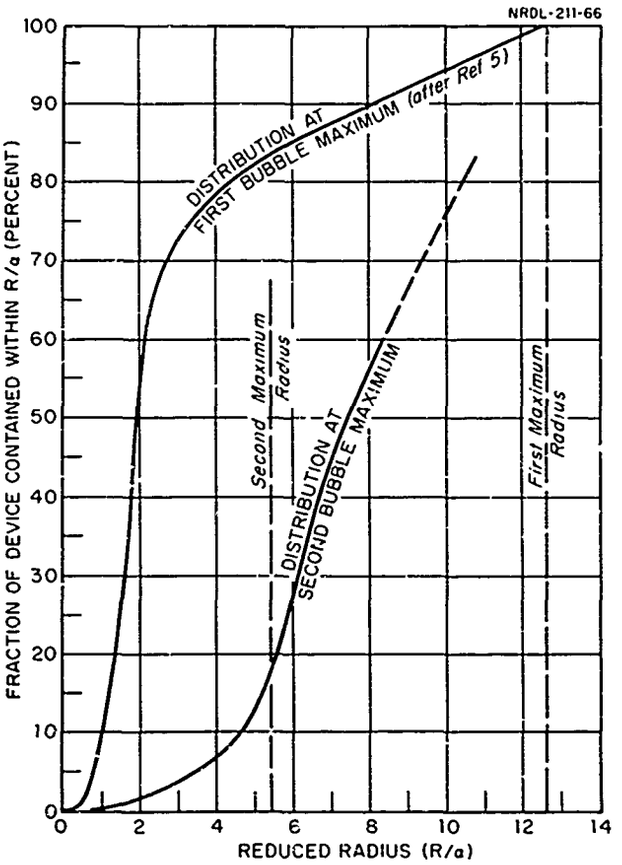

Fig. 5-5 Fraction of the Total Device Lying Within a Reduced Radius (R/α) of the Explosion Point as a Function of Reduced Radius for the First and Second Bubble Maxima - Condition A

Fig. 5-6 The Bubble at the Second Maximum - Condition A
(Camera 1 record)

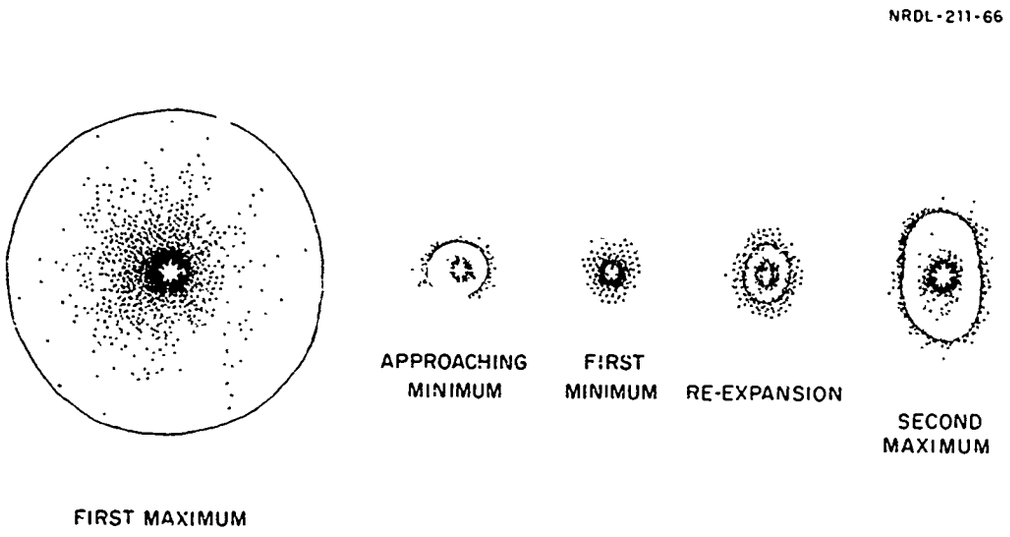

Fig. 5-7 Transport Mechanisms - Condition A

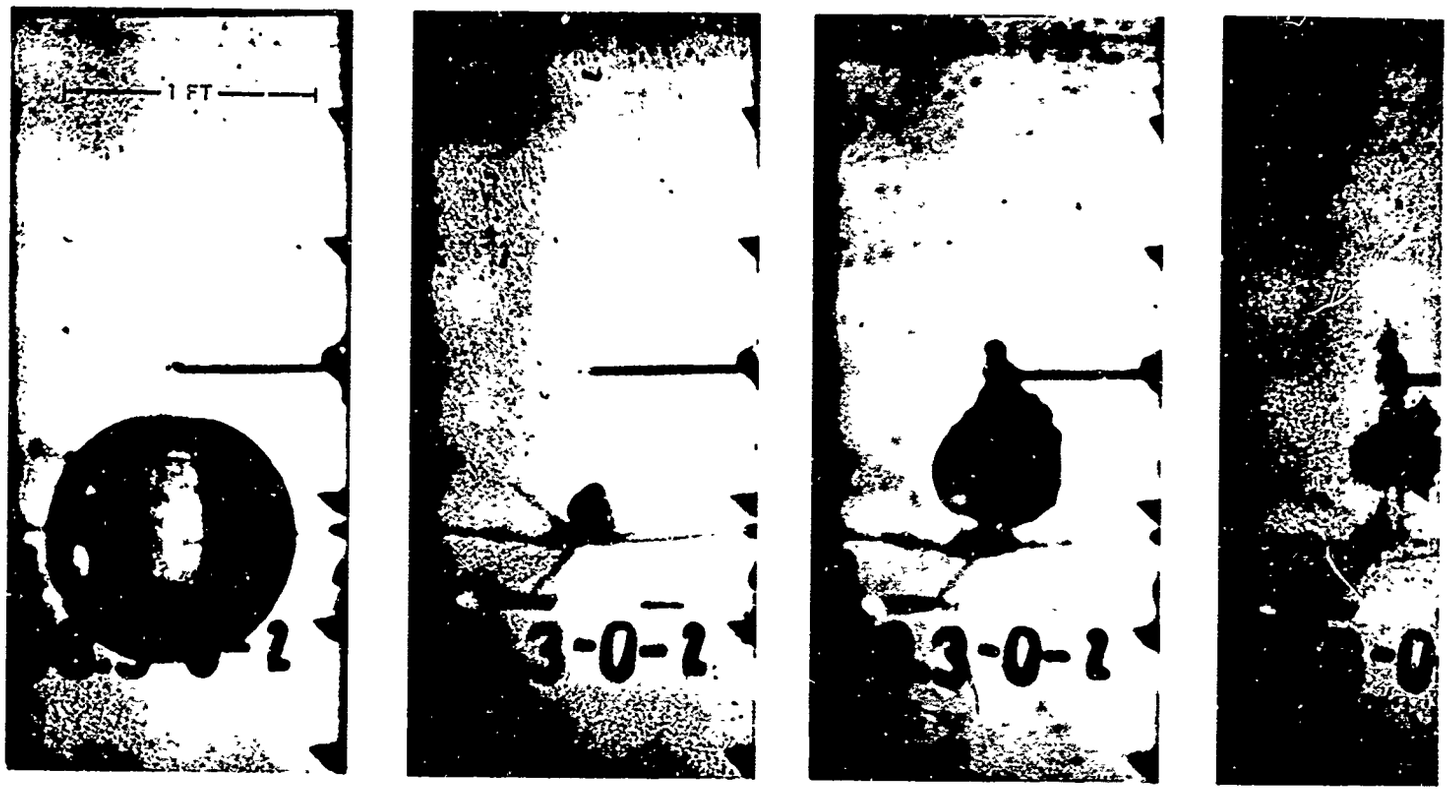

35 msec - First Maximum

70 msec - First Minimum

87.5 msec - Second Maximum

105 msec - Minimu

Fig. 5-8 Bubble Motion - Condition B
(Camera 2 record)

A

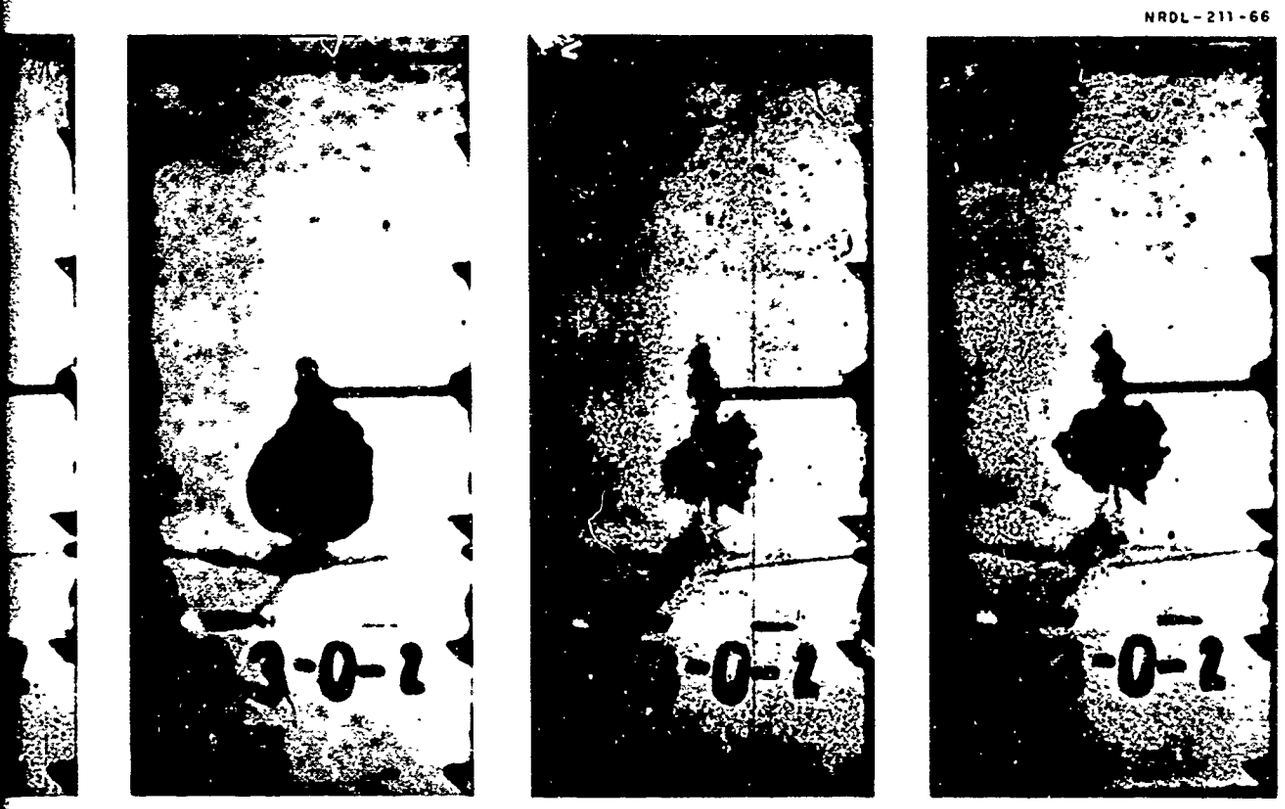

87.5 msec - Second Maximum

105 msec - Second Minimum

115 msec - Third Maximum

Fig. 5-8 Bubble Motion - Condition B
(Camera 2 record)

B

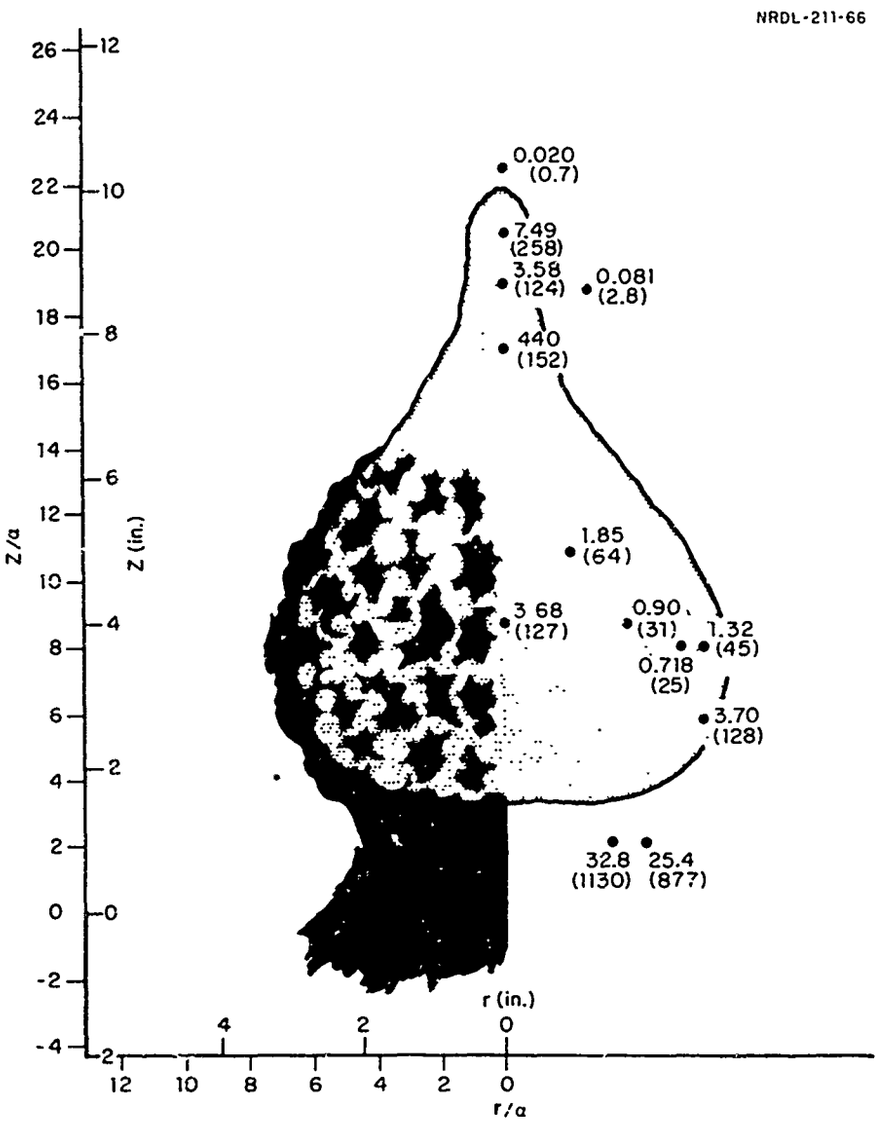

Fig. 5-9 Sampling Positions and Corrected Data - Condition B. Gold Concentrations in $\mu g/cm^3$. Values in Parenthesis are Reduced Concentrations - $\mu d/a^3$.

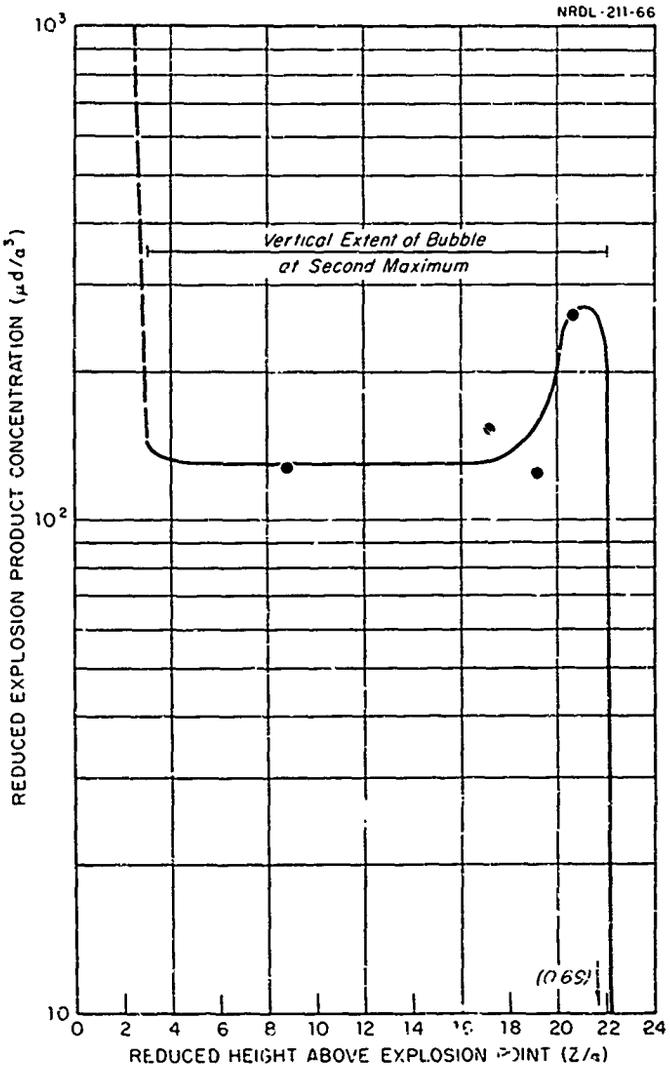

Fig. 5-10 Reduced Explosion Product Concentration Along Vertical Axis - Condition B

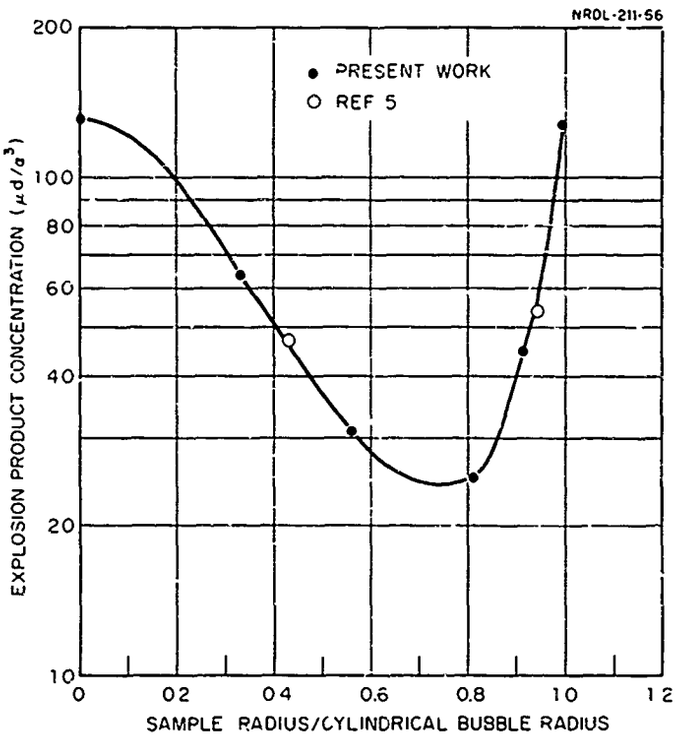

Fig. 5-11 Reduced Concentration vs. Reduced Horizontal Radius - Condition B ($5 \leq Z/\alpha \leq 15$)

Fig. 5-12 The Bubble at the Second Maximum - Condition B
(Camera 1 record)

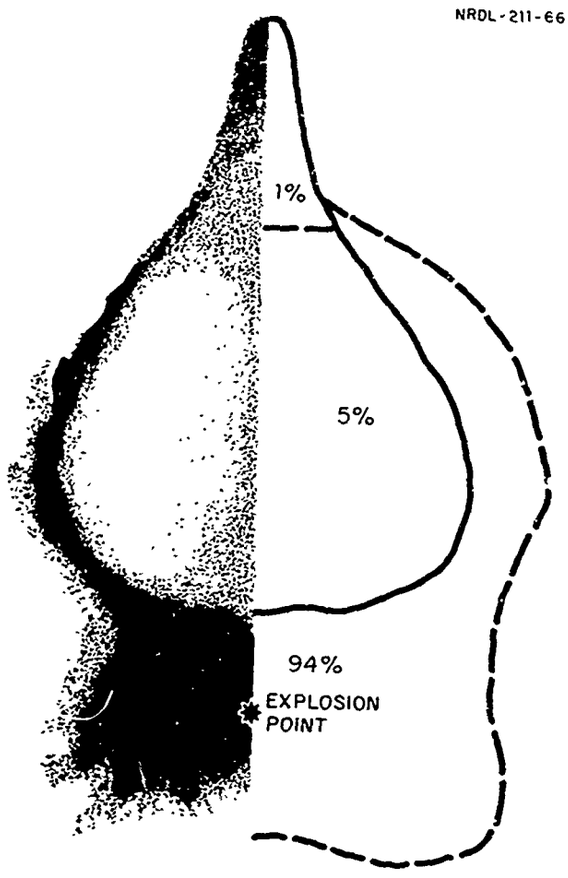

Fig. 5-13 Distribution of the Explosion Products at the Second Bubble Maximum - Condition B

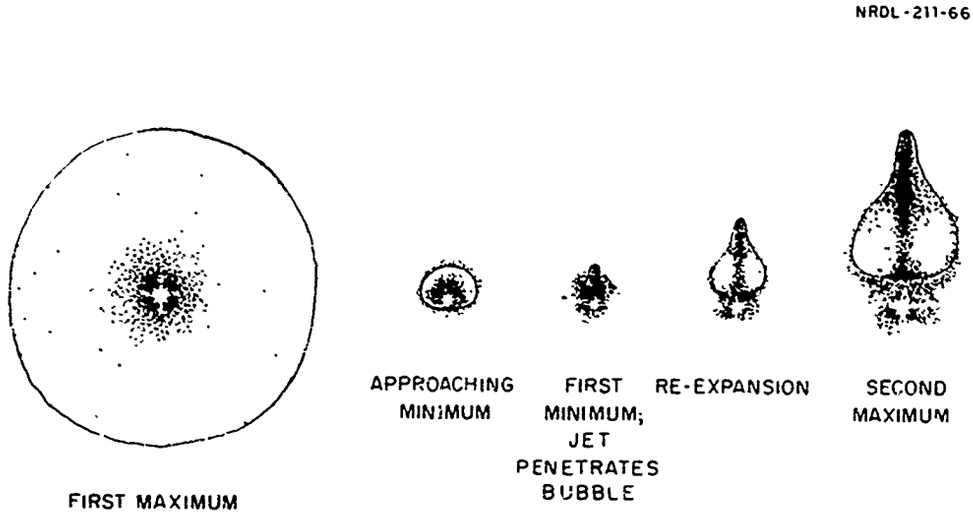

Fig. 5-14 Transport Mechanisms - Condition B

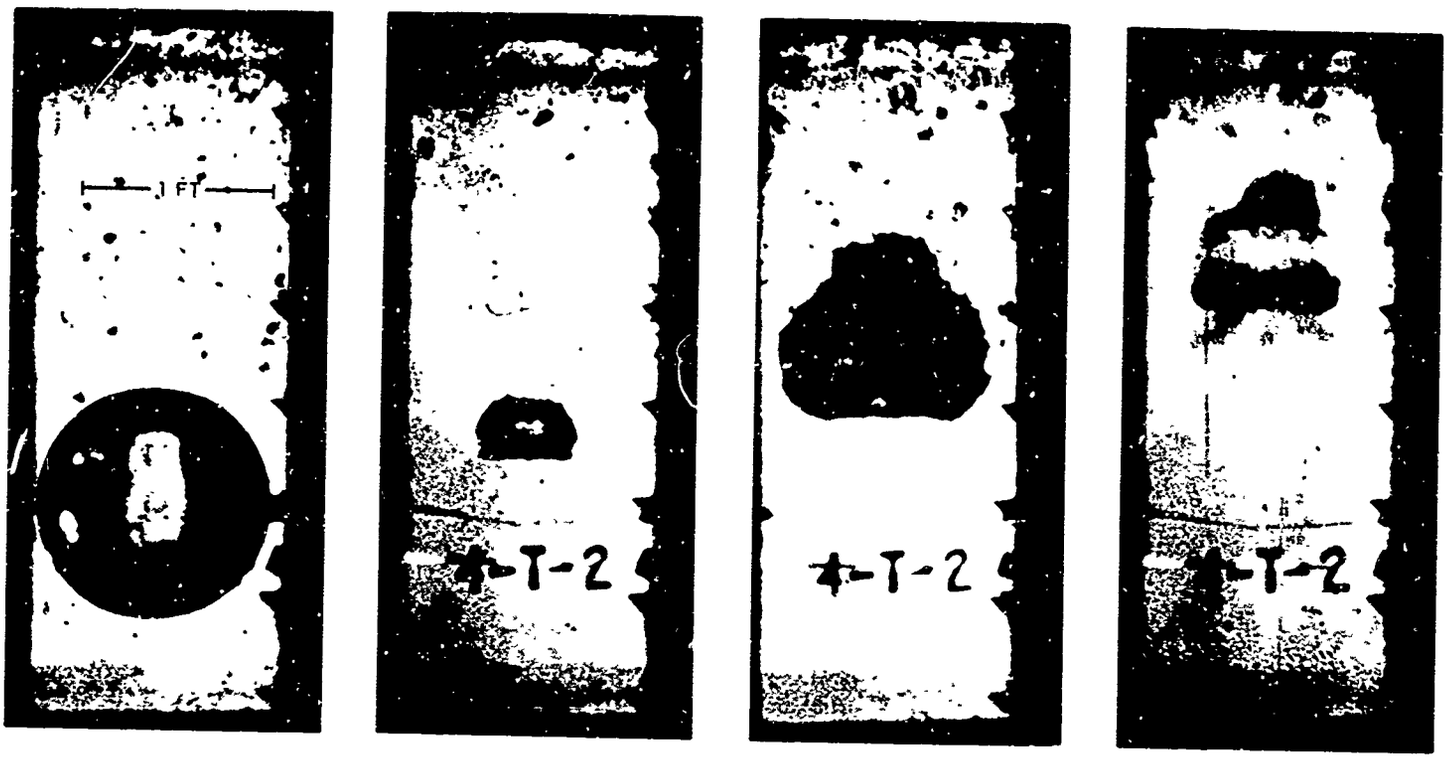

75 msec
First Maximum

152.5 msec
First Minimum

225 msec
Second Maximum

302 msec
Second Minimum

Fig. 5-15 Bubble Motion - Condition C
(Camera 2 Record)

A

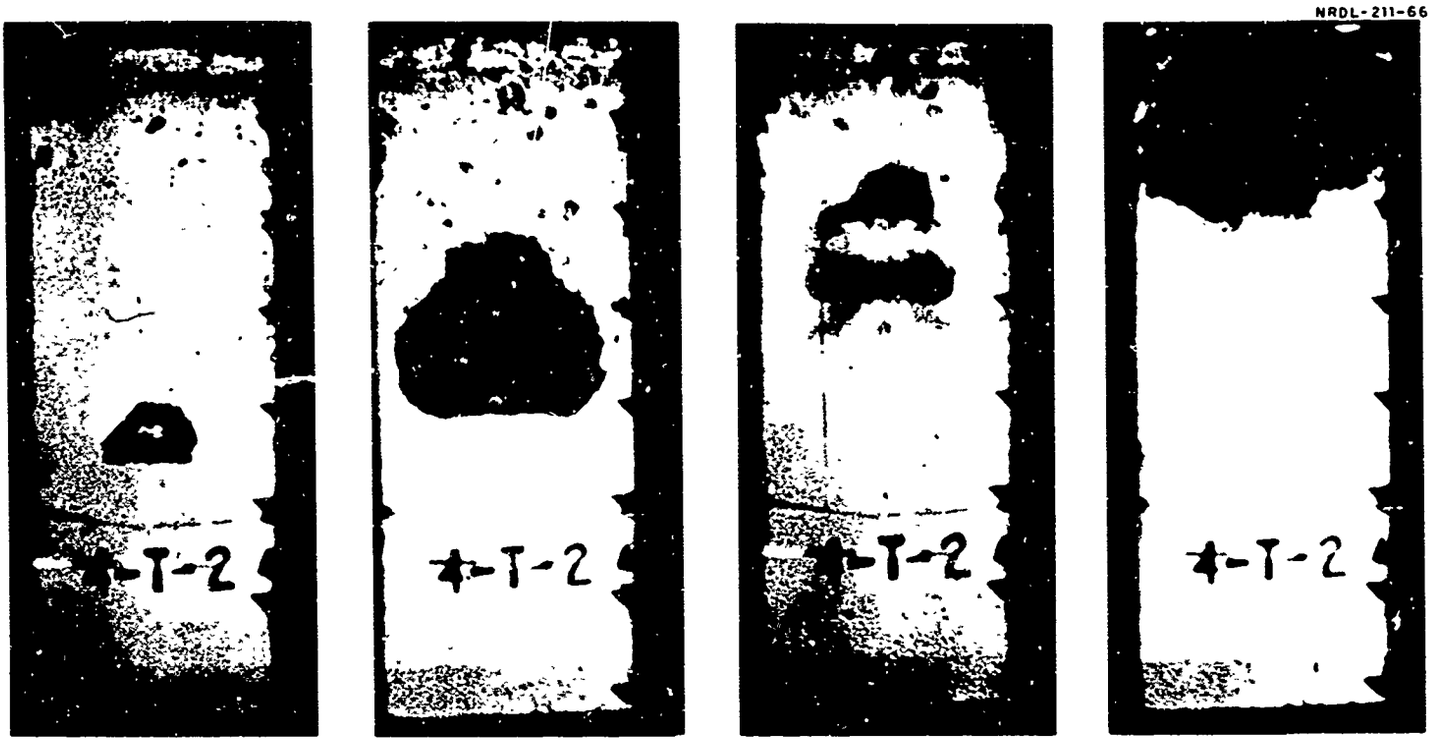

152.5 msec
First Minimum

225 msec
Second Maximum

302 msec
Second Minimum

415 msec
Third Maximum

Fig. 5-15 Bubble Motion - Condition C
(Camera 2 Record)

B

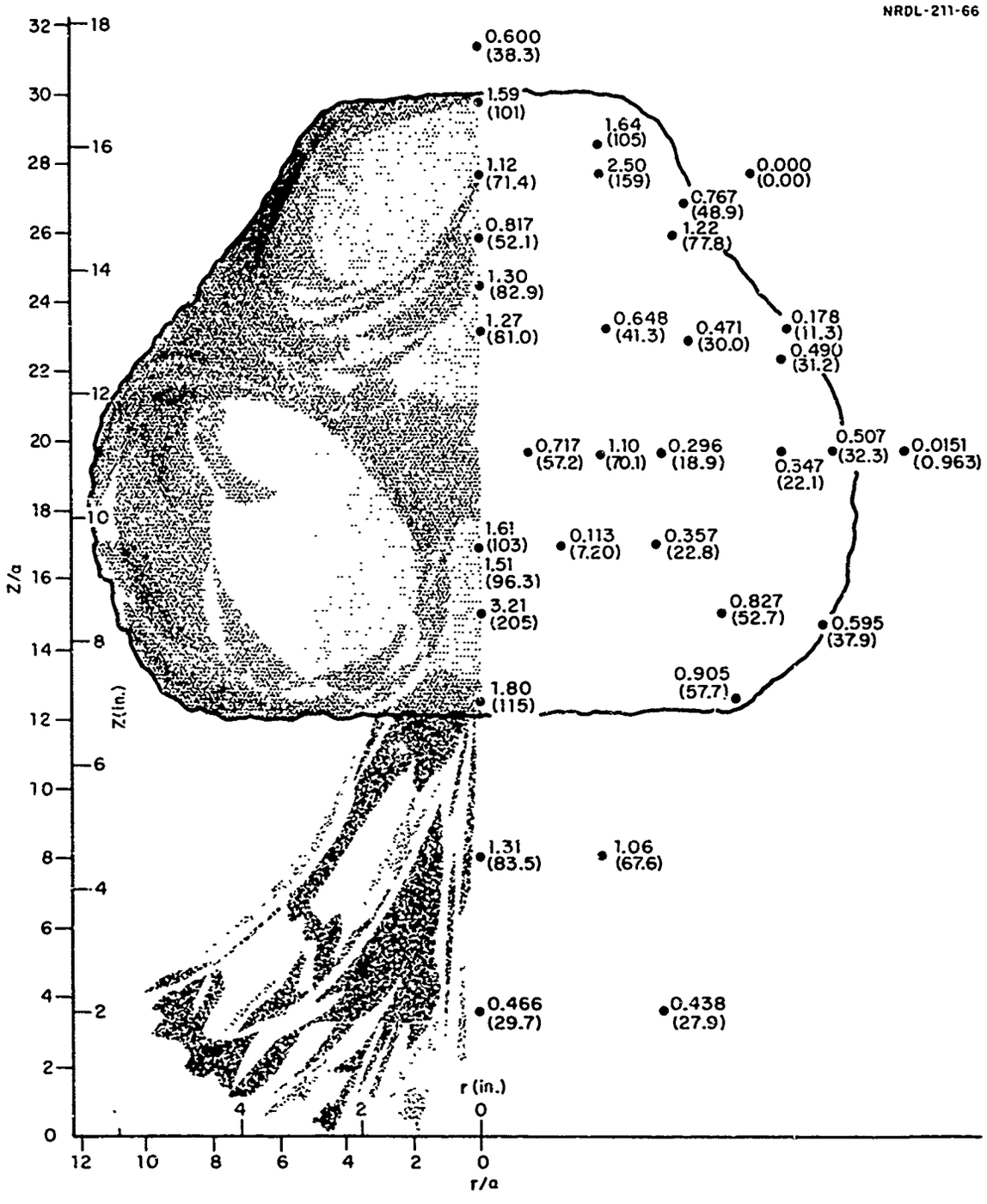

Fig. 5-16 Sampling Positions and Corrected Data - Condition C
Gold Concentrations in $\mu g/cm^3$. Values in Parenthesis are "Reduced" Concentrations, in $\mu d/a^3$.

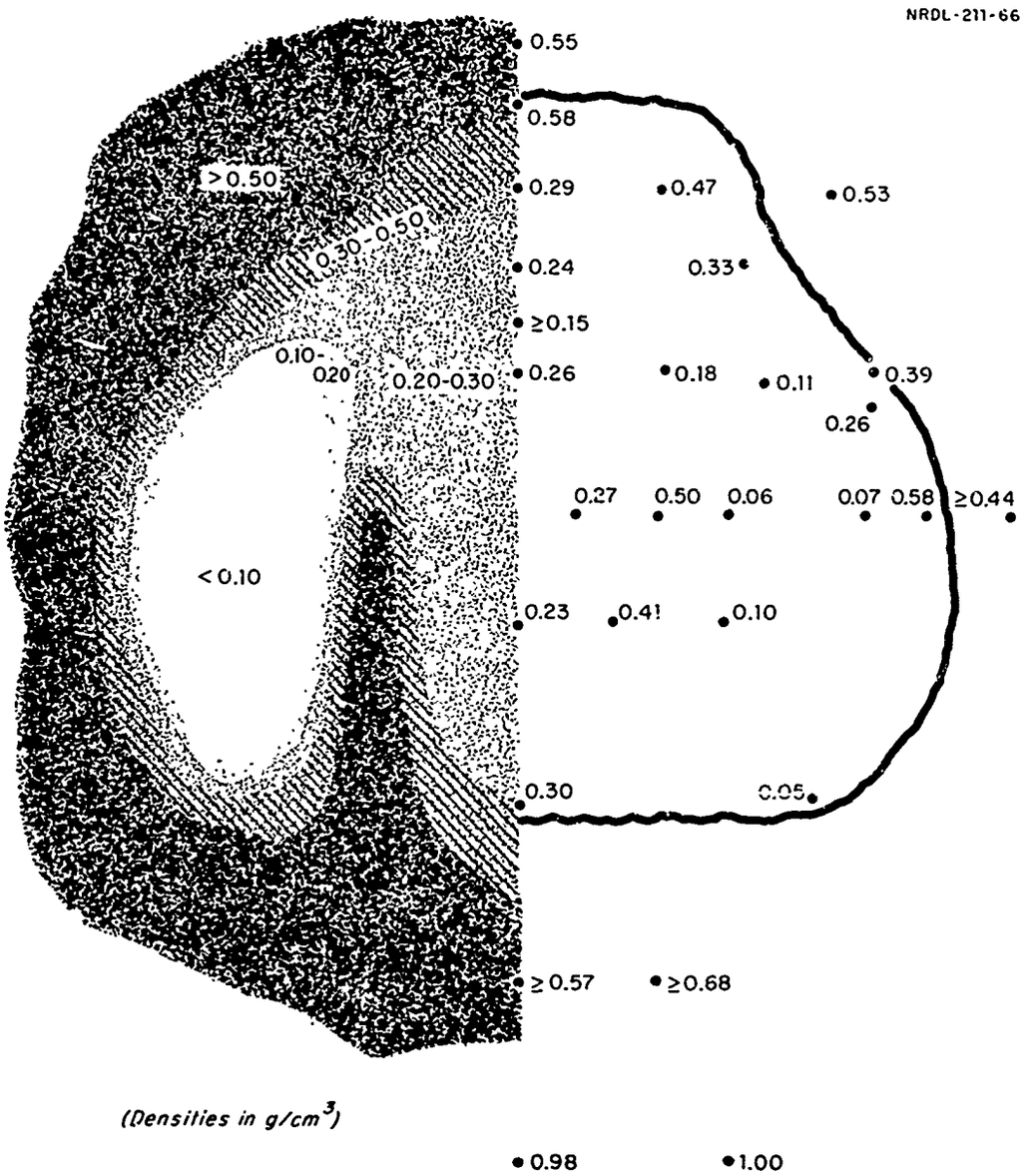

Fig. 5-17 The Internal Density Structure of the Bubble at the Second Maximum - Condition C

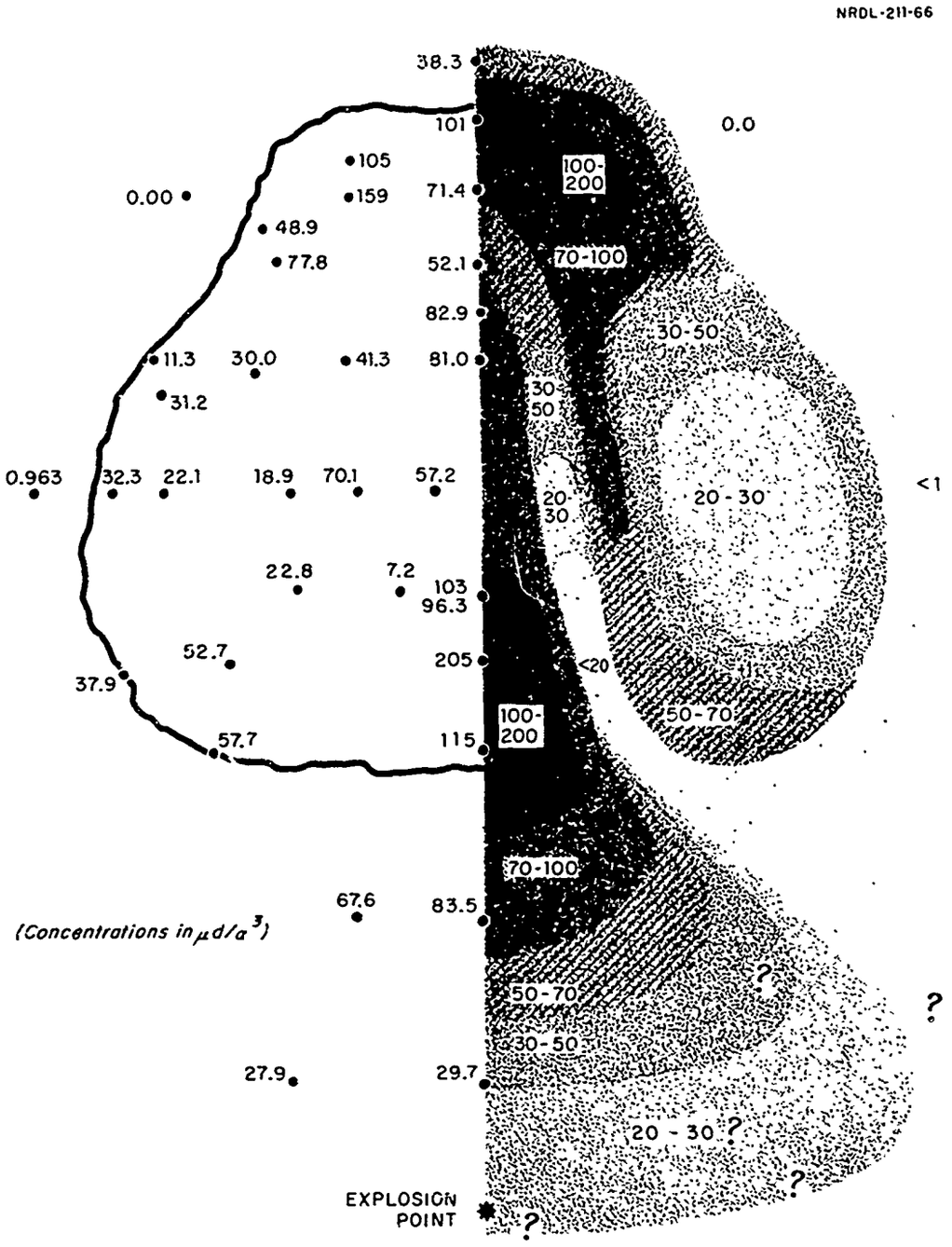

Fig. 5-18 Explosion Product Concentration - Condition C

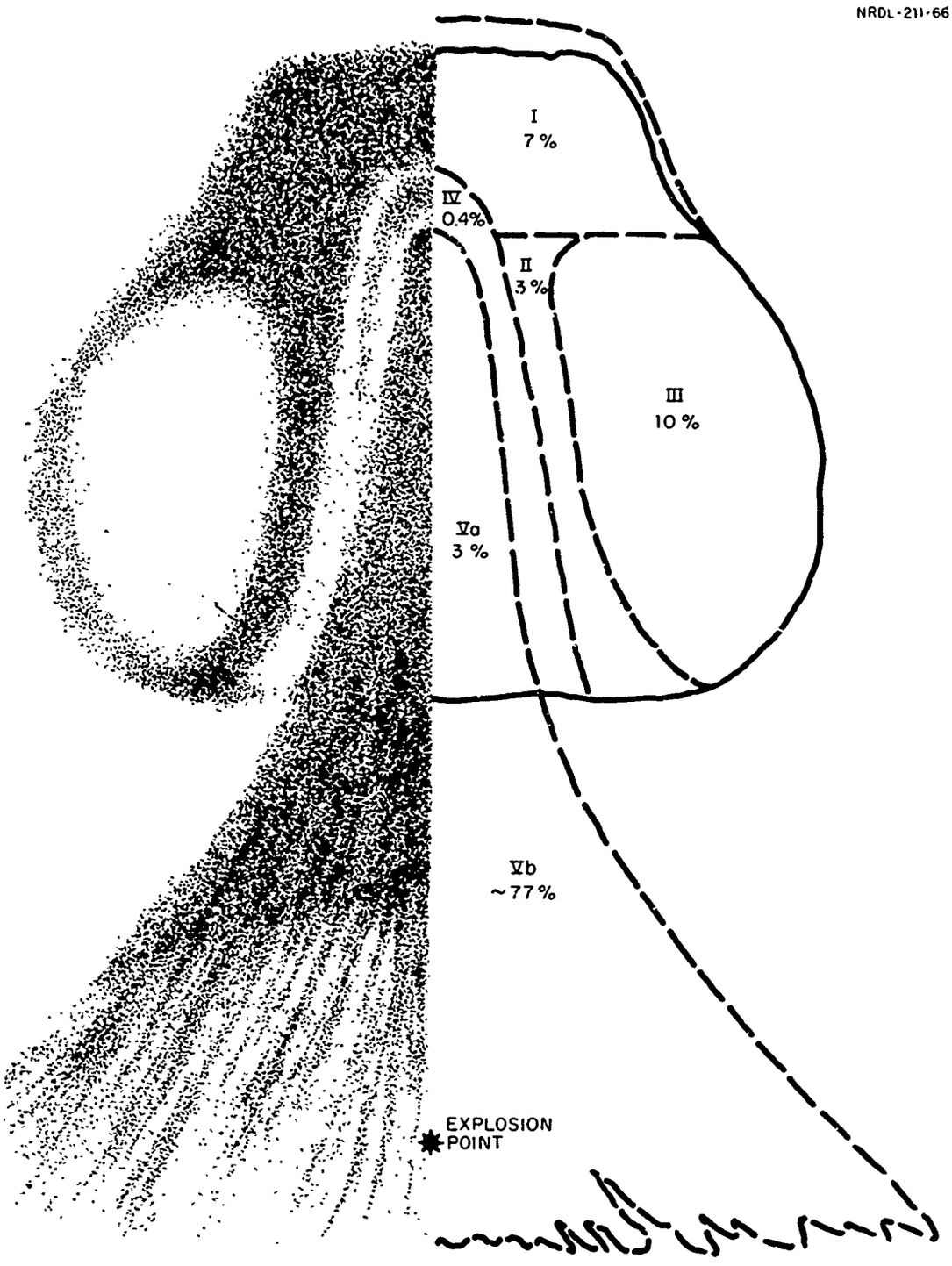

Fig. 5-19 Distribution of Explosion Products at the Second Bubble Maximum - Conditions C

Fig. 5-20 The Bubble at the Second Maximum - Condition C
(Camera 1 record)

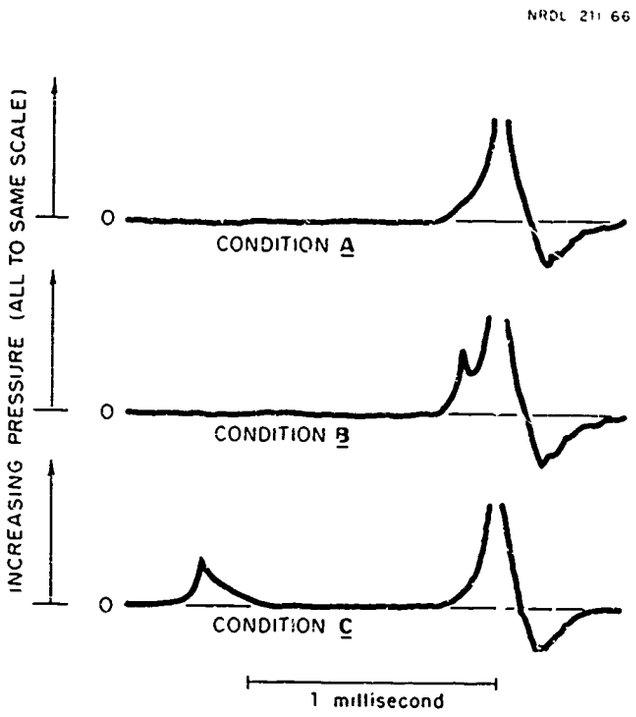

Fig. 5-21 Typical Bubble Pulse Waveforms

1. Upward Jet Visible Within Bubble

2. Jet Strikes Bubble Top

3. Jet has Penetrat Bubble

4. Gaseous Toroid Contracting

5. Maximum Recompression

6. Re-expansion Begi

Fig. 5-22 The First Bubble Minimum - Condition C
Camera 3 Record - Time Between Successive Frames is 0.645 msec

A

ard Jet Visible Within Bubble

2. Jet Strikes Bubble Top

3. Jet has Penetrated The Bubble

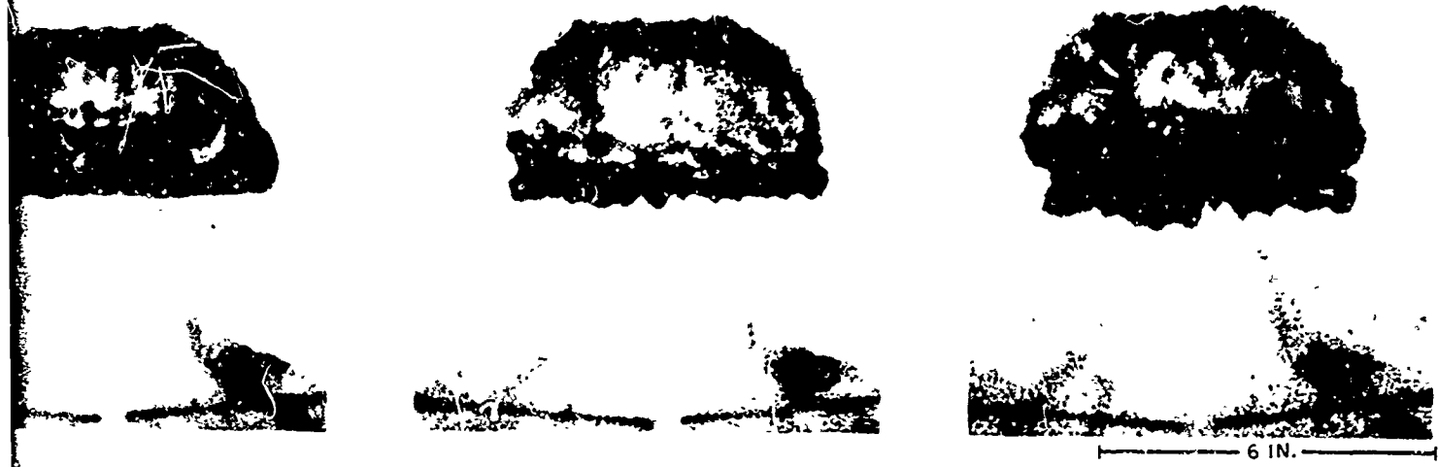

ecus Toroid Con-acting

5. Maximum Recompression

6. Re-expansion Begins

Fig. 5-22 The First Bubble Minimum - Condition C
Camera 3 Record - Time Between Successive Frames is 0.645 msec

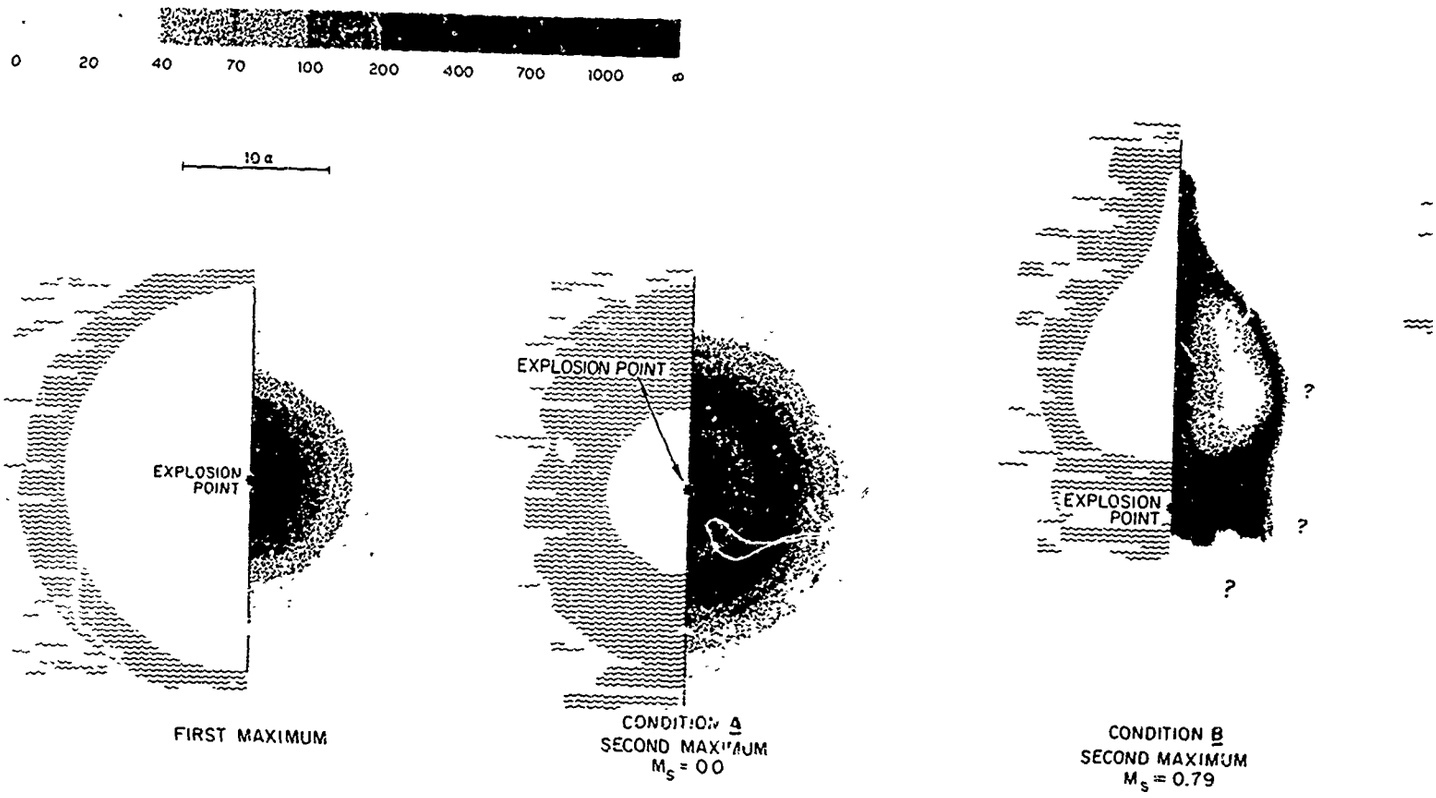

Fig. 5-23 The Distribution of Expl
and at the Second Maxi

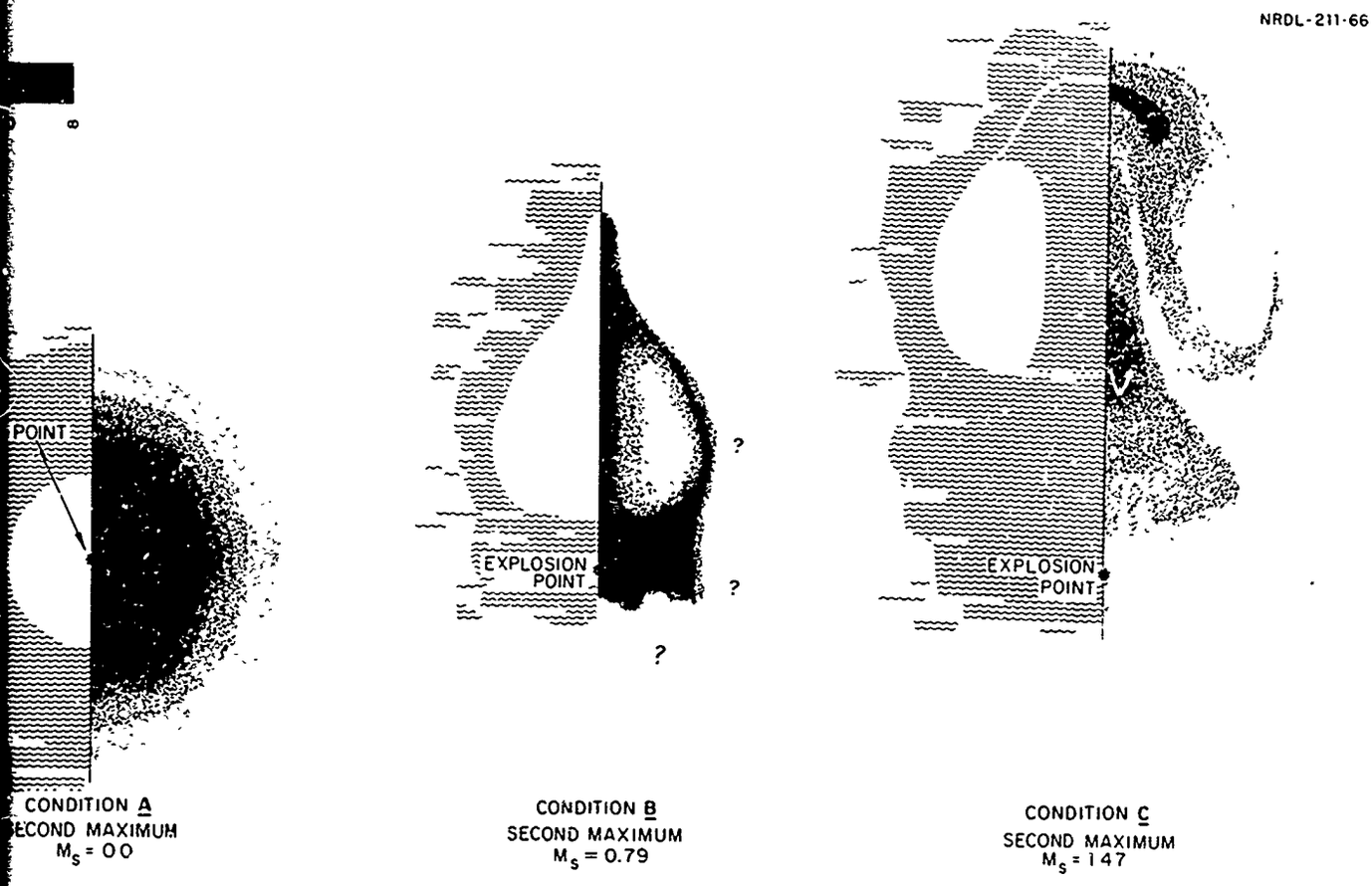

Fig. 5-23 The Distribution of Explosion Products at the First Maximum and at the Second Maxima for Conditions A, B, and C

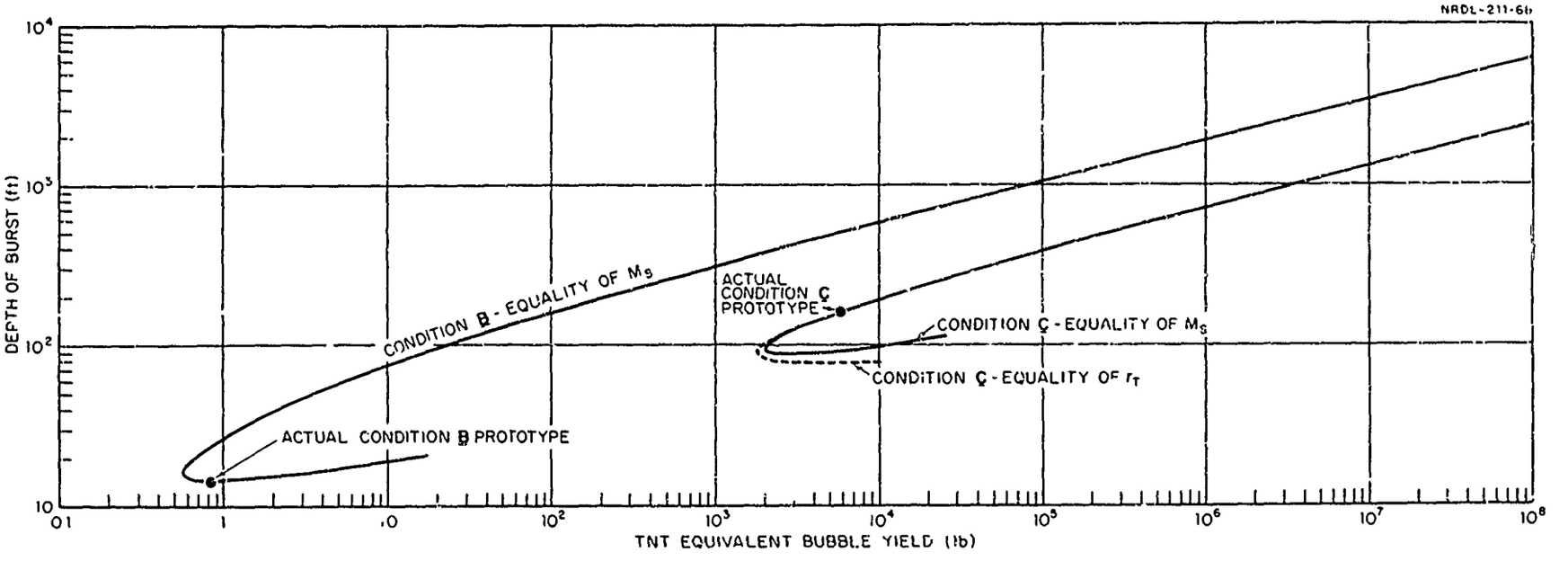

Fig. 5-24 Shot Configurations Characterized by Bubble Behavior Similar to that of Conditions B and C (Criteria as Noted)

150 msec
(About 25 msec After
Third Minimum)

300 msec

Fig. 5-25 Growth of The Contaminated Patch After Bubbl..
Condition A
(Camera 1 Record)

A

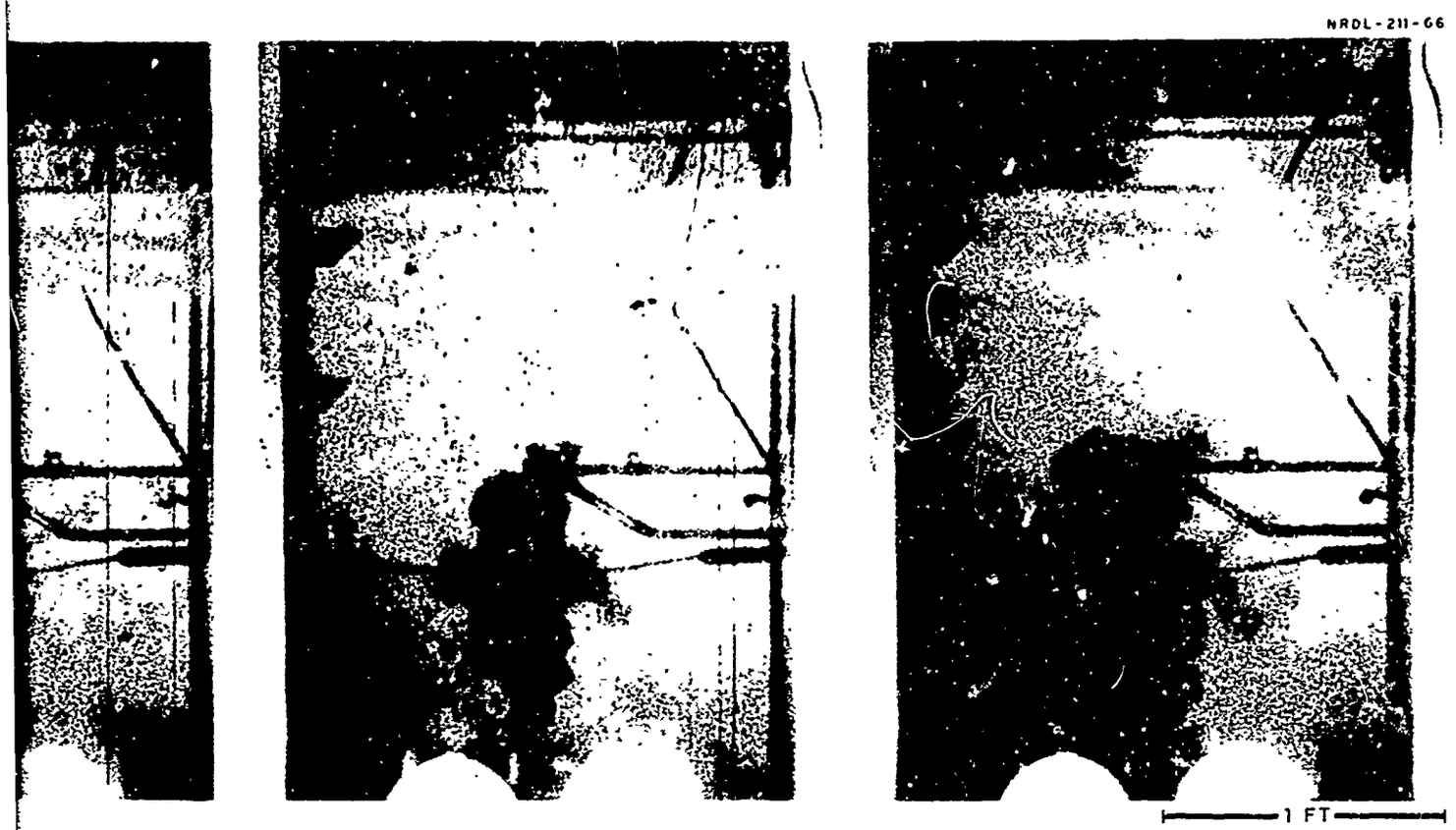

300 msec

600 msec

fter
um)

g. 5-25 Growth of The Contaminated Patch After Bubble Motion Has Ceased -
Condition A
(Camera 1 Record)

B

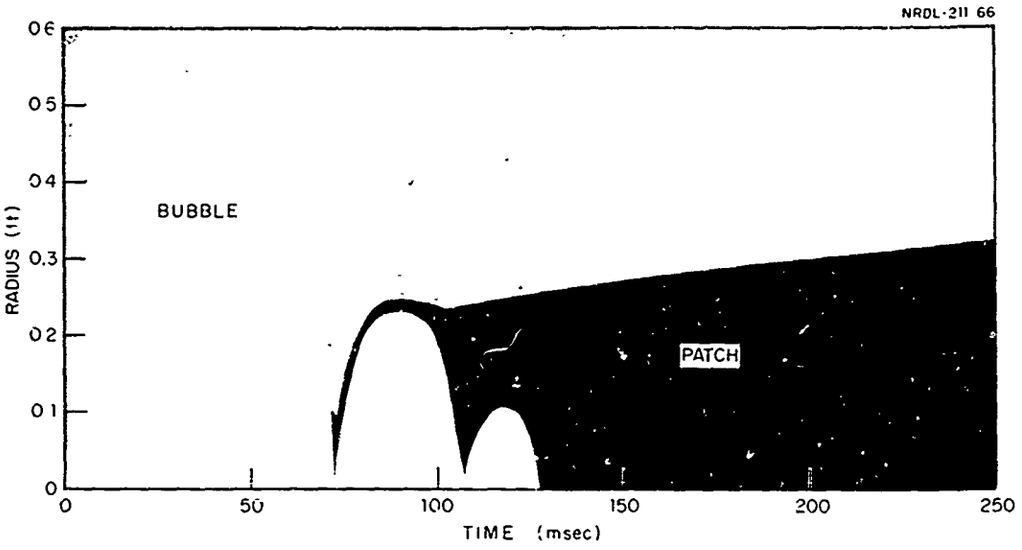

Fig. 5-26 Equivalent Spherical Radii vs Time for The Bubble and the Visible Patch of Explosion Debris - Condition A

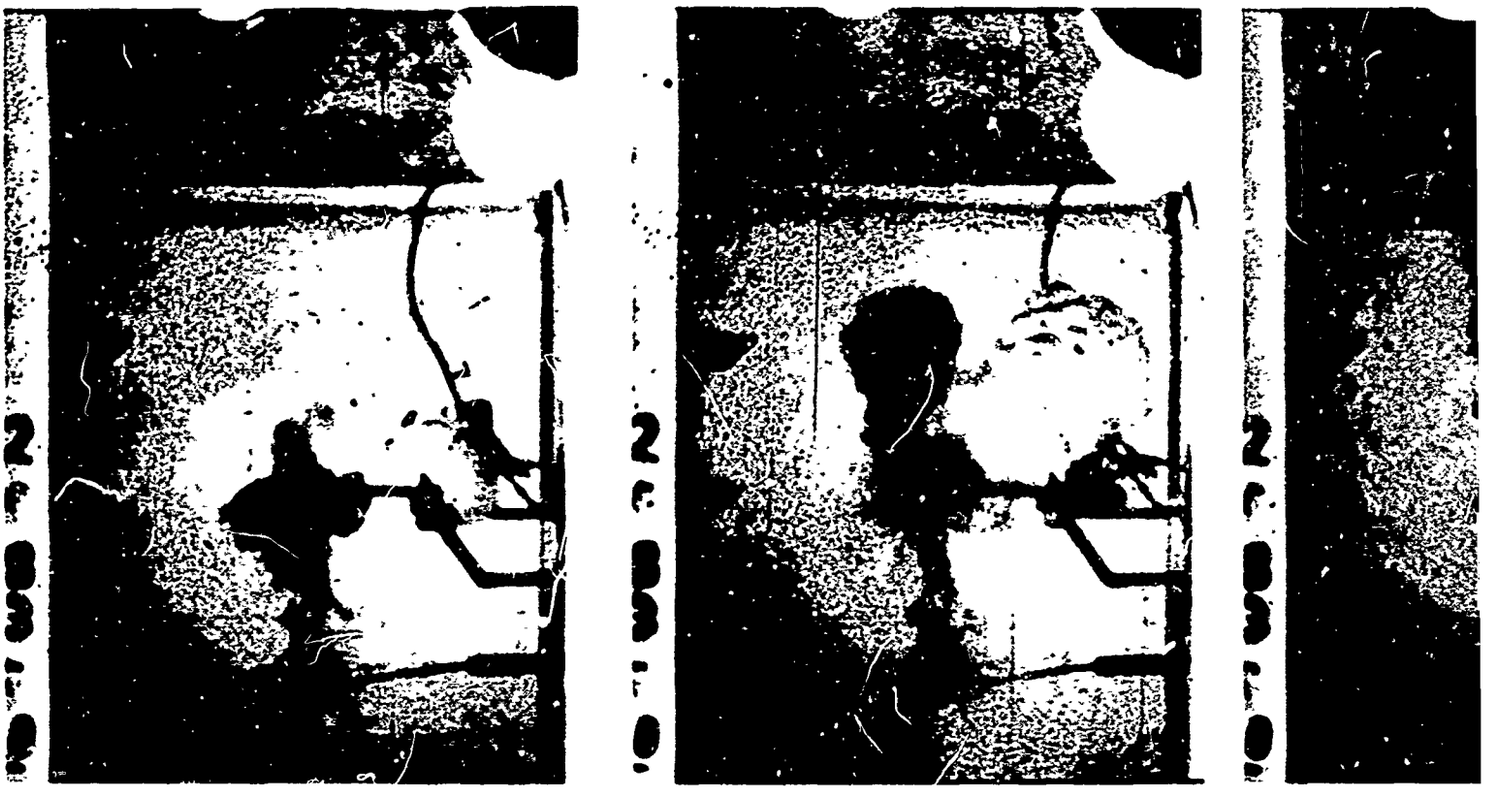

150 msec
(25 msec After Third Minimum)
Vortex Ring has Formed

300 msec
Vortex Ring Rising

Vortex R

Fig. 5-27 The Effect of Afterflow on the Explosion Product Distribution - Condition B
(Camera 1 Record)

Minimum)
rmed

300 msec
Vortex Ring Rising

600 msec
Vortex Ring Arrives at Water Surface

Effect of Afterflow on the Explosion Product Distribution - Condition B
(Camera 1 Record)

B

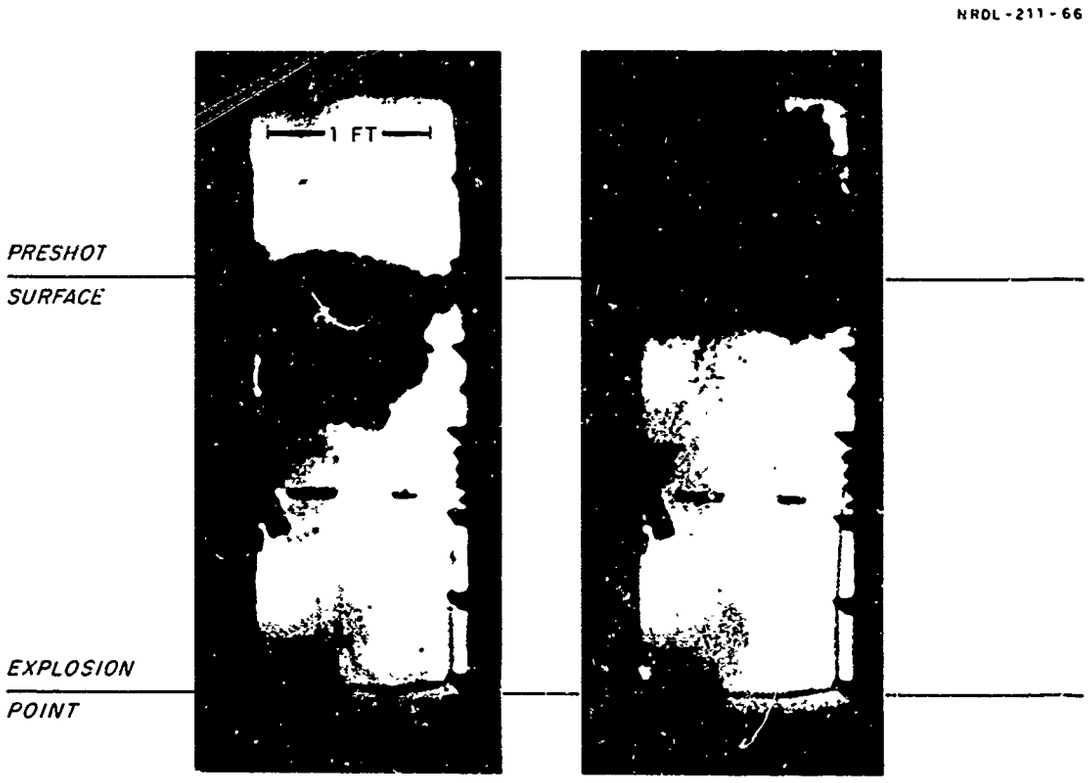

Fig. 5-28 Late-Time Effects - Condition C
(Camera 2 Record)

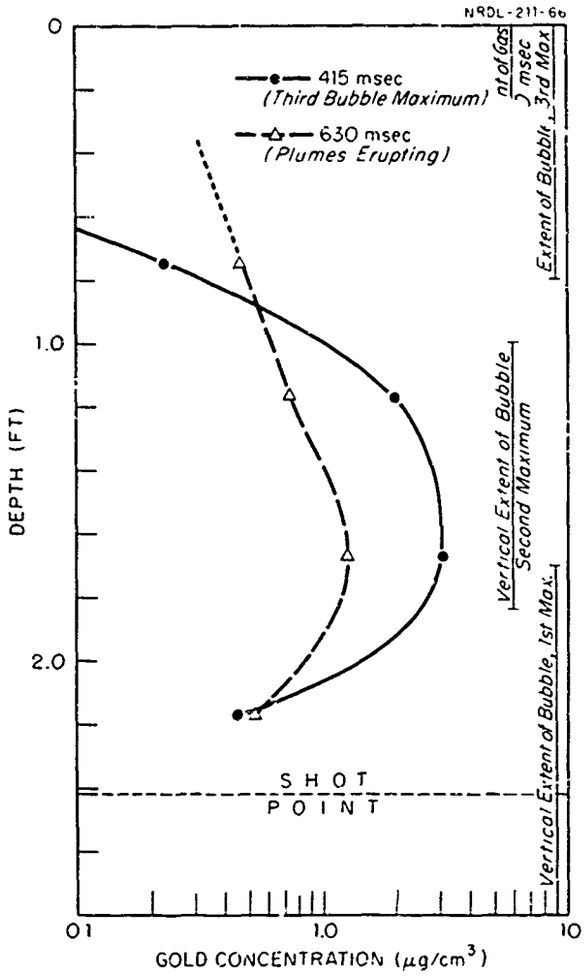

Fig. 5-29 The Explosion Product Concentration Along the Centerline Axis at Late Times - Condition C

REFERENCES

1. H. G. Snay, "The Hydrodynamic Background of the Radiological Effects of Underwater Nuclear Explosions (U)", in Proceedings of Tripartite Symposium on Technical Status of Radiological Defense in the Fleets, U.S. Naval Radiological Defense Laboratory, R & L-103, v2, 1960 (CLASSIFIED).

2. T. T. Folsom, J. D. Isaacs, "Operation WIGWAM, Project 2.6-1 Mechanism and Extent of the Early Dispersion of Radioactive Products in Water", Scripps Institution of Oceanography, ITR-1064, May 1955.

3. J. D. Isaacs, "Operation WIGWAM, Project 2.6-1 Mechanism and Extent of the Early Dispersion of Radioactive Products in Water", Scripps Institution of Oceanography, WT-1014, 28 March 1962.

4. T. R. Folsom, "Operation WIGWAM, Project 2.6-2 Mechanism and Extent of the Dispersion of Fission Products by Oceanographic Processes and Locating and Measuring Surface and Underwater Radioactive Contamination", Scripps Institution of Oceanography, WT-1015, 17 December 1956.

5. R. R. Buntzen, "The Underwater Distribution of Explosion Products from a Submerged Exploding Wire," USNRDL-TR-778, 31 July 1964.

6. F. H. Young, R. R. Hammond, "Hydra Program - A Non-Spherical Model Describing the Motion of a Shallow Underwater Explosion Bubble", USNRDL-TR-771, 23 June 1964.

7. H. G. Snay, "Underwater Exploding Phenomena: The Parameters of Migrating Bubbles", U.S. Naval Ordnance Laboratory, NAVORD 4185, 12 October 1962.

8. R. H. Cole, Underwater Explosions, Princeton, N.J.. Princeton University Press., 1948.

9. H. G. Snay, "Model Tests and Scaling (U)", U.S. Naval Ordnance Laboratory, DASA 1240-I (3), NOLTR 63-257, 1 December 1964, (CLASSIFIED).

10. R. R. Hammond, F. H. Young, E. A. Schuert, "Bubble Hydronamics of Shallow Underwater Explosions (U)", in The Sixth Navy Science Symposium, Weapons and Weapons Effects, Vol. II, ONR-12, 1962 (CLASSIFIED).

11. R. R. Hammond, "Hydra Program. Hydra IIB Series - An Investigation of Water Flow Adjacent to Shallow Underwater Explosion Bubbles Using Flourescent Dyes and Photographic Techniques", USNRDL-TR-968, 3 August 1965.

12. W. W. Perkins, "Hydra IIA Series - The Above-Surface Phenomena Created by 10,000-Pound Underwater Detonations (U)", USNRDL-TR-708, 28 October 1963 (CLASSIFIED).

13. R. R. Buntzen, "Hydra Program - The NRDL Low-Yield Underwater Explosion Tank and Associated Instrumentation", USNRDL-TR-623, 18 February 1963.

14. R. R. Buntzen, "The Use of Exploding Wires in the Study of Small-Scale Underwater Explosions", in Exploding Wires - Proceedings of The Second Conference on the Exploding Wire Phenomenon, Plenum Press, N. Y., 1962.

15. C. J. Aronson, et al., "Operation WIGWAM, Project 1.2 - Underwater Free-Field Pressures to Just Beyond Target Locations (U)", U.S. Naval Ordnance Laboratory, WT-1005, 27 May 1957 (CLASSIFIED).

16. E. F. Bryant, "Debris Distribution in Underwater Explosions", Malaker Laboratories Inc., High Bridge, N. J., CM-102-4, January 1964. (CLASSIFIED).

17. "Debris Distribution in Underwater Explosions", Malaker Laboratories Inc., High Bridge, N. J., CM-102-5, March 1965.

18. F. G. Karioris, B. R. Fish, G. W. Royster, Jr., "Aerosols From Exploding Wires", in Exploding Wires - Proceedings of the Second Conference on the Exploding Wire Phenomenon, Plenum Press, N. Y. 1962.

19. H. G. Snay, J. F. Goertner, R. S. Price, "Small Scale Experiments to Determine Migration of Explosion Gas Globes Towards Submarines (U)", U. S. Naval Ordnance Laboratory, NAVORD 2280, 1 July 1952 (CLASSIFIED).

20. C. O. J. G. Palmer, "Phenomena Associates with Small Underwater Explosions - An Investigation by Means of High Speed Photography (U)", Naval Construction Research Establishment, Rosyth (U.K.), URDEX-263, November 1950 (CLASSIFIED).

21. M. Shiffman, B. Friedman, "Studies on the Gas Bubble Resulting from Underwater Explosions - On the Best Location of a Mine Near the Sea Bed", Institute for Mathematics and Mechanics, New York University, May 1944.

APPENDIX A

THE SCALING OF BUBBLE BEHAVIOR

BASIC CONSIDERATIONS

In scaling the various aspects of underwater explosions, several types of scaling are of interest. It is, in practical terms, impossible to scale precisely all phases of the event simultaneously. What is done in practice is to confine attention to those aspects of the phenomenon which are relevant to the problem of interest, and then to scale these as closely as possible. For example, if we were interested in shock damage to underwater structures, we would attempt to scale shockwave phenomena, that is, to achieve Mach similitude.

The general scaling requirements which are applicable to underwater explosions are as follows:

Similitude of Gravitational Effects

If it is desired to scale properly the effects of gravity on the system, it is first necessary to define some 'characteristic force' for the model and the prototype. Then, similitude will be accomplished if the Froude number, or rather the ratio of the gravitational force to the characteristic force, is the same for both model and prototype. That is,

$$\left(\frac{F_{grav}}{F_{char}}\right)_m = \left(\frac{F_{grav}}{F_{char}}\right)_p$$

This may readily be reduced to the more familiar form:

$$\left(\frac{v^2}{gL}\right)_m = \left(\frac{v^2}{gL}\right)_p$$

Where

v = a characteristic velocity

g = acceleration of gravity

L = a characteristic length

m denotes the model

p denotes the prototype

Similitude of Effects Controlled by Evaporation and/or Condensation of Liquid

This requires that the Thomas number for model and prototype be the same, that is, that

$$\left(\frac{P}{P_{vapor}}\right)_m = \left(\frac{P}{P_{vapor}}\right)_p$$

where P is a characteristic pressure.

Similitude of Effects of Viscosity requires equal Reynolds numbers:

$$\left(\frac{vL}{\nu}\right)_m = \left(\frac{vL}{\nu}\right)_p$$

where ν is the kinematic viscosity.

Similitude of Compressibility (Shockwave) Effects requires equal Mach numbers:

$$\left(\frac{v}{c}\right)_m = \left(\frac{v}{c}\right)_p$$

where c is acoustic velocity

Other relationships of this sort may be fabricated as needed.

APPLICATIONS TO UNDERWATER EXPLOSIONS

In chapter 2, the relationships defining the parameters of underwater explosion bubbles were presented assuming standard environmental conditions, that is, air pressure = 1 atmosphere, the force of gravity = 1 g, the density of the liquid environment = 1 gram/cm^3, etc. In the present discussion, greater generality is required, but as will be seen, the expressions used here will reduce to more familiar forms if standard conditions hold.

Geometrical Scaling

As regards scaling of underwater explosions, it seems apparent that the first parameter which it is desirable to scale is the basic geometry characterizing the event, that is,

$$\left(\frac{L_i}{L_j}\right)_m = \left(\frac{L_i}{L_j}\right)_p \tag{A.1}$$

where L_i and L_j are lengths characterizing the shot. In particular, if we take the first maximum bubble radius, or rather α, and the shot depth, we can then require

$$\left(\frac{D}{\alpha}\right)_m = \left(\frac{D}{\alpha}\right)_p \tag{A.2}$$

or,

$$\beta_m = \beta_p$$

where

D is the shot depth in feet

$\alpha = (W/Z)^{1/3}$

$Z = \rho_f g D + 33 P_A$

ρ_f is the fluid density in grams/cm^3

g is the acceleration of the system in gravities

P_A is the air pressure over the water in atmosphere.

If the sea-bottom is near enough that it will affect the bubble motion, we must also keep this distance geometrically similar:

$$\left(\frac{D_w - D}{\alpha}\right)_m = \left(\frac{D_w - D}{\alpha}\right)_p \qquad (A.3)$$

where D_w = total water depth.

Gravitational Scaling

The driving force for the bubble migration is the buoyancy of the bubble. Hence, we must reproduce the gravitational effects upon the bubble to preserve similitude. Therefore we invoke the Froude criterion:

$$\left(\frac{F_{char}}{F_{grav}}\right)_m = \left(\frac{F_{char}}{F_{grav}}\right)_p \qquad (A.4)$$

Now $F_{char} = m_{char} L_{char}/(t_{char})^2$

and $L_{char} = \alpha$

$t_{char} = \tau$

$$m_{char} = \rho_f \alpha^3$$

so

$$F_{char} = \frac{\rho_f \alpha^4}{\tau^2} \tag{A.5}$$

The gravitational (buoyant) force is given by:

$$F_b = \rho_f g \, (\text{Volume}_{char}) = \rho_f g \alpha^3 \tag{A.6}$$

The Froude criterion becomes:

$$\left(\frac{\alpha}{g\tau^2}\right)_m = \left(\frac{\alpha}{g\tau^2}\right)_p \tag{A.7}$$

Expanding this expression in terms of more basic parameters,

$$\alpha = (W/Z)^{1/3}, \quad \tau = (W^{1/3}/Z^{5/6}) \, \rho_f^{1/2},$$

$$\frac{Z_m^{4/3}}{W_m^{1/3} g_m \rho_p} = \frac{Z_p^{4/3}}{W_m^{1/3} g_p \rho_p}, \text{ or} \tag{A.8}$$

$$\frac{W_p}{W_m} = \left(\frac{g_m}{g_p}\right)^3 \left(\frac{\rho_m}{\rho_p}\right)^3 \left(\frac{Z_p}{Z_m}\right)^4 \tag{A.9}$$

Invoking our geometrical scaling requirement, so as to reproduce the effect of the surface,

$$\beta_m = \beta_p$$

that is,

$$\frac{D_m Z_m^{1/3}}{W_m^{1/3}} = \frac{D_p Z_p^{1/3}}{W_p^{1/3}} \tag{A.10}$$

and, combining (9) and (10),

$$\frac{D_p^3 Z_p}{D_m^3 Z_m} = \left(\frac{g_m}{g_p}\right)^3 \left(\frac{\rho_m}{\rho_p}\right)^3 \left(\frac{Z_p}{Z_m}\right)^4, \text{ or rather } \frac{Z_p}{Z_m} = \frac{\rho_p g_p D_p}{\rho_m g_m D_m} \tag{A.11}$$

we obtain,

$$\frac{\rho_p g_p D_p}{\rho_m g_m D_m} = \frac{Z_p}{Z_m} = \frac{\rho_p g_p D_p + 33 P_{A_p}}{\rho_m g_m D_m + 33 P_{A_m}} \text{ by definition} \tag{A.12}$$

Therefore,

$$\frac{P_{A_p}}{P_{A_m}} = \frac{\rho_p g_p D_p}{\rho_m g_m D_m} = \frac{Z_m}{Z_m} \tag{A.13}$$

We may now rewrite (9) as:

$$\frac{W_p}{W_m} = \left(\frac{g_m}{g_p}\right)^3 \left(\frac{\rho_m}{\rho_p}\right)^3 \left(\frac{P_{A_p}}{P_{A_m}}\right)^4 \tag{A.14}$$

Also,

$$\frac{D_p}{D_m} = \left(\frac{P_{A_p}}{P_{A_m}}\right) \left(\frac{\rho_m}{\rho_p}\right) \left(\frac{g_m}{g_p}\right) \tag{A.15}$$

Thus, equations (A.14) and (A.15), if satisfied, will satisfy the basic scaling requirements (A.1) and (A.4). If we consider all prototype shots to be fired in water, at 1 atmosphere pressure, and in a gravity field of 1 g, we may drop subscripts and write:

$$\text{Yield scale factor} = \frac{W_p}{W_m} = \frac{(\rho g)^3}{P_A^4} \tag{A.16}$$

$$\text{Linear scale factor} = \frac{L_p}{L_m} = \frac{\rho g}{P_A} \tag{A.17}$$

$$\text{Time scale factor} = \frac{\tau_p}{\tau_m} = \left(\frac{\rho}{P_A}\right)^{1/2} g \tag{A.18}$$

Thus, the scaling of migration phenomena may be accomplished by varying the air pressure over the water, the density of the fluid and/or the force of gravity in the appropriate way.

The Effects of Vaporization and Condensation

In order to reproduce properly the effects of vaporization and condensation of the environmental fluid, it is clearly necessary to reproduce the composition of the bubble atmosphere - that is, if a point-source prototype is of interest, the model explosion must also be point-source, so that both model and prototype bubbles will contain steam.

If the effects of condensation and vaporization of the bubble atmosphere are considered to be important, the Thomas criterion must be adhered to, that is:

$$\left(\frac{P_{char}}{P_{vapor}}\right)_m = \left(\frac{P_{char}}{P_{vapor}}\right)_p \tag{A.19}$$

where P_{char} is a characteristic pressure relevant to the phase-change process.

If we take the pressure difference across the bubble interface as our P_{char}, we are left with two distinctly different situations. First, if we consider the bubble near one of its maxima, we recall that, near the bubble maximum, the internal pressure is a great deal

less than the hydrostatic head Z, so

$$P_{char}\ (max) = Z - P_i\ (max) \approx Z \qquad (A.20)$$

where P_i is the internal bubble pressure.

Near bubble minima, on the other hand, the reverse is true; that is, for reasonable shot depths, (less than 25,000 feet or so), the internal bubble pressure is a great deal higher than the hydrostatic pressure, so

$$P_{char}\ (min) = P_i\ (min) - Z \approx P_i\ (min) \qquad (A.21)$$

Considering first the situation near maxima, equation (A.19) and (A.20) require that

$$\frac{Z_m}{Z_p} = \frac{(P_{vapor})_m}{(P_{vapor})_p} = \frac{33\ P_A + \rho g\ D_m}{33 + D_p} \qquad (A.22)$$

That is, the situation must be arranged such that the hydrostatic pressures at the shot points for model and prototype must be in the same proportion as the vapor pressures of the environmental fluids. If the model explosion is fired in water, this means, essentially, that:

$$Z_m = Z_p \qquad (A.23)$$

if the water in the model and prototype situations is at the same temperature.

If we now must satisfy our most basic requirements of geometrical and gravitational scaling, we must then say:

$$P_{A_m} = 1 \text{ atmosphere}$$

$W_p = (g\rho)^3 = g^3$, since we are now dealing with water.

If this criterion is not satisfied, the results may be viewed as follows. Equation (A.22) implies that, if the pressure at the shot point is reduced, the prototype vapor pressure is increased - that is, near the bubble maximum, we are scaling a large explosion fired in a "warm' ocean. In particular, if the air pressure is reduced to the vapor pressure of the water, we are scaling a large explosion in a boiling ocean, and the pressure may be reduced no further. Physically, the significance of this is the observed boiling of the bubble interface near the bubble maximum for shots fired at hydrostatic pressures near the vapor pressure of water.[9,19] The effect of such boiling is not entirely clear.

The problem of reproducing vaporization and condensation phenomena near the bubble minimum is somewhat different. As we have seen (Eq. A.21).

$$P_{char} \text{ (min)} = P_i \text{ (min)}$$

where P_i (min) is the peak internal pressure attained by the bubble near its minimum size. The problem then becomes that of evaluating P_i (min). Ref. 9 presents the experimental result that for bubbles which do not migrate appreciably, the volume of the bubble minimum is approximately ten times that of the "initial bubble" (or, the "equivalent charge volume"), and that this volume, in contrast to the maximum bubble volume, is apparently independent of the local hydrostatic pressure.

Consequently, if the bubble atmospheres of model and prototype are composed of similar materials, such that the ratio of specific

heats (γ) is the same for both, then, since the expansion and contraction are adiabatic,

$$P_i(0)\ V_o^{\gamma} = P_i(\text{min})\ V_{min}^{\gamma} \qquad (A.24)$$

where,

$P_i(0)$ = pressure in initial bubble
V_o = volume of initial bubble
V_{min} = volume of bubble minimum

Hence, for the nonmigrating case,

$$P_i(\text{min}) \approx P_i(0)/10^{\gamma} \qquad (A.25)$$

Now, since

$$R_i \approx 0.135\ W^{1/3} \text{ feet} \qquad (A.26)$$

and the total internal energy in the initial bubble is just the bubble energy,

$P_i(0)$ = constant,

so that the internal pressure at the bubble minimum is independent of both yield and hydrostatic pressure for the non-migrating case.

For the migrating bubbles, the volume of gas in the bubble minimum is not well defined, since in all likelihood most of the "visible" volume of the minimum is occupied by the water in the underwater jet.[6,9] It is certainly not unreasonable to assume that:

$$E_{i(\text{min})}\ (M_s) = E_{i(\text{min})}\ (0) \times f'\ (M_s) \qquad (A.27)$$

where f' is an unspecified function of the specific migration, which is equal to 1 for non-migrating bubbles.[21] If this is the case, then the internal pressure at the minimum, $P_i(\text{min})$ is a function only of the strength of migration. Consequently, the Thomas criterion will

be satisfied, and evaporative and condensive phenomena will be scaled near the bubble minimum, if the requirements of gravitational and geometric scaling (which define the migration) are satisfied.

The Effect of Viscosity

The necessary criterion here is equality of Reynolds numbers:

$$\left(\frac{vL}{\nu}\right)_m = \left(\frac{vL}{\nu}\right)_p \tag{A.28}$$

where

$v = \alpha/\tau$ = a characteristic velocity

$L = \alpha$ = a characteristic length

ν = the kinematic viscosity of the fluid.

Substituting, this equation becomes:

$$\left(\frac{W_p}{W_m}\right)^{1/3} \left(\frac{Z_p}{Z_m}\right)^{1/6} = \frac{\nu_p}{\nu_m} \tag{A.29}$$

Now involing our gravity scaling criterion (Equation A.9),

$$\frac{W_p}{W_m} = \left(\frac{Z_p}{Z_m}\right)^4 \left(\frac{g_m}{g_p}\right)^3 \left(\frac{\rho_m}{\rho_p}\right)^3 = 1$$

we obtain:

$$\left(\frac{Z_m}{Z_p}\right)^{3/2} \left(\frac{g_p}{g_m}\right) \left(\frac{\rho_p}{\rho_m}\right) \left(\frac{\nu_p}{\nu_m}\right) = 1 \tag{A.30}$$

If $\nu_p = \nu_m$, $\rho_p = \rho_m$ (that is, both shots fired in water), we have

$$\frac{(Z_m/Z_p)^{3/2}}{(g_m/g_p)} = 1 \tag{A.31}$$

Multiplying equation (A.31) by 1 on either side (that is, by equation (A.30), we obtain,

$$\frac{W_p}{W_m} = P_A^{1/2} \tag{A.32}$$

For example, if $W_p = 10\ W_m$, then this means

$$P_A = 100 \text{ atmospheres}$$

Thus, to satisfy equation (A.9) for gravitational scaling,

$$g_m = 1000 \text{ gravities}$$

That is, we are actually requiring that the air pressure over the water be increased, leaving only g as an independent variable. Clearly, Reynold's similitude is not feasible.

It should be pointed out, however, that viscosity is not important for Reynold's numbers greater than about 100 or so - we then enter the regime of turbulent drag forces. Reynold's numbers are always very large during the bubble migration phase of an underwater explosion. The question is, then, how are turbulent drag forces reproduced? As was done previously, we set:

$$\left(\frac{F_{turb}}{F_{char}}\right)_m = \left(\frac{F_{turb}}{F_{char}}\right)_p \tag{A.33}$$

Now, the drag force may be characterized as follows:

$$F_{turb} = C_D \times A \times \rho_f \frac{v^2}{2} \tag{A.34}$$

where

A = cross sectional area
ρ_f = density of medium
v = velocity of body

C_D = drag coefficient

So, a characteristic drag force is as follows:

$$F_{turb} = C_D \frac{\rho_f}{2} \frac{\alpha^4}{2} \tag{A.35}$$

And, as before, our general characteristic force is:

$$F_{char} = \rho_f \frac{\alpha^4}{2} \tag{A.36}$$

Consequently, if the configuration of the bubble and the bubble migration is reproduced, turbulent drag forces will scale.

The Effects of Compressibility - Shock Effects

In order to scale the effects of the shockwave, we must set the Mach number for model and prototype equal, that is,

$$\left(\frac{v_{char}}{c}\right)_m = \left(\frac{v_{char}}{c}\right)_p \tag{A.37}$$

where

c = acoustic velocity in the medium

$v_{char} = \alpha/\tau = Z^{1/2}$

So the requirement becomes:

$$\frac{Z_p}{Z_m} = \left(\frac{c_p}{c_m}\right)^2 = \sim 1$$

If this criterion is to be satisfied, the air pressure in the model environment must remain at one atmosphere.

As we have seen, however, the interaction between the shockwave and the bubble ends at very early times in the first cycle, before any migration has occurred. Hence, for purposes of studying bubble behavior, Mach similitude is not required.

APPENDIX B

LIST OF SYMBOLS

A = Cross-sectional area

c = Acoustic velocity

C = Explosion product concentration

C_{BG} = Background explosion product concentration

C_D = Drag coefficient

$D = D_1$ = Shot depth

D_2 = Depth of second bubble maximum

D_w = Depth of water

E_s = Shockwave energy

E_T = Total energy

g = Acceleration of gravity

$k = W/W'$

$L = L_{char}$ = characteristic length

M_s = Specific migration = $(D_1 - D_2)/R_1$

Subscript m - Applies to model

Subscript p - Applies to prototype

p = Momentum

$P = P_{char}$ = Characteristic pressure

P_A = Air pressure in atmospheres

P_i = Internal bubble pressure

P_{vapor} = Vapor pressure

r = Radius of sample from explosion axis.

r_T = Period ratio = $T_{1/2}(\phi = 0)/T_{1/2}(\phi = 180')$

$R = R_1$ = First maximum bubble radius

R_i = Radius of initial bubble

$R_s = R(\pi/2)$ = First maximum side bubble radius

$R(t)$ = Bubble radius as a function of time

R_2 = Second cycle maximum bubble radius

$S = S(\beta)$ = Surface correction coefficient (a function of β)

T = First bubble cycle period

$T_{1/2}$ = First cycle "half period" (time to maximum expansion)

$T_s = T(\pi/2)$ = First side bubble cycle period

v = Characteristic velocity

W = TNT equivalent bubble yield

W' = Charge weight or total released energy.

z = Altitude of sample above explosion point

$Z = Z_1$ = Hydrostatic pressure at shot point in feet of water

α = Characteristic shot length = $(W/Z)^{1/3}$

β = Geometrically scaled depth = D/α

γ = Ratio of specific heat (C_p/C_v)

$\Delta D_{12} = D_1 - D_2$

$\epsilon = \varphi/\rho_e$

$\mu d/\alpha^3$ = Reduced unit of explosion product concentration - "micro-devices per cubic alpha"

ν = Kinematic viscosity

ρ_e = Mass density of explosive

$\rho = \rho_f$ = Density of fluid

τ = Characteristic shot time = $W^{1/3}\rho^{1/2}/Z^{5/6}$

ϕ = Bubble latitude

φ = Energy density of explosive

INITIAL DISTRIBUTION

Copies

NAVY

1 Chief of Naval Material (MAT 0331)
1 Chief of Naval Material (MAT 031)
2 Commander, Naval Ship Systems Command (SHIPS 2021)
1 Commander, Naval Ship Systems Command (SHIPS 03541)
1 Commander, Naval Ship Engineering Center (NAVSEC 6423)
1 Commander, Naval Ordnance Systems Command (ORD 03)
1 Chief of Naval Operations (Op-07T)
1 Chief of Naval Operations (Op 75)
1 Dir., Naval Research Laboratory
1 Chief of Naval Research (Code 418)
5 CO, Office of Naval Research, Branch Office, London
1 Supt., Naval Postgraduate School, Monterey
1 Commander, Naval Ordnance Laboratory, White Oak (Library)
1 Commander, Naval Oceanographic Office

ARMY

1 Chief of Research and Development (Atomic Office)
1 CG, Chemical Research and Development Laboratory, Maryland
1 Commander, Nuclear Defense Laboratory
1 Commandant, Army War College
1 Office of Civil Defense, Washington

AIR FORCE

1 Assistant Chief of Staff Intelligence (AFCIN-3B)
1 Dir., USAF Project RAND (WEAPD)
1 CO, Air Force Weapons Laboratory, Kirtland AFB (WLRB)
1 Dir., Air University Library, Maxwell AFB
1 Hq., Air Force Technical Applications Center

OTHER DOD ACTIVITIES

2 Dir., Nuclear Test Detection Office, Advanced Research Projects Agency
3 Dir., Defense Atomic Support Agency (Library)
3 Commander, FC/DASA, Sandia Base (FCTG5, Library)

20 Defense Documentation Center

AEC ACTIVITIES AND OTHERS

25 Division of Technical Extension, Oak Ridge

USNRDL

45 Technical Information Division

DISTRIBUTION DATE: 25 October 1966

UNCLASSIFIED
Security Classification

DOCUMENT CONTROL DATA - R&D

(Security classification of title body of abstract and indexing annotation must be entered when the overall report is classified)

1 ORIGINATING ACTIVITY (Corporate author)
U. S. Naval Radiological Defense Laboratory
San Francisco, California 94135

2a REPORT SECURITY CLASSIFICATION
UNCLASSIFIED

2b GROUP

3 REPORT TITLE
EXPLOSION PRODUCT REDISTRIBUTION MECHANISMS FOR SCALED MIGRATING UNDERWATER EXPLOSION BUBBLES

4 DESCRIPTIVE NOTES (Type of report and inclusive dates)

5 AUTHOR(S) (Last name, first name, initial)
Pritchett, John W.

6 REPORT DATE	7a TOTAL NO OF PAGES	7b NO OF REFS
25 October 1966	149	21

8a CONTRACT OR GRANT NO.

b PROJECT NO.
DASA NWER Program A-7, Subtask 10.061

c

d

9a ORIGINATOR'S REPORT NUMBER(S)
USNRDL-TR-1044

9b OTHER REPORT NO(S) (Any other numbers that may be assigned this report)

10 AVAILABILITY/LIMITATION NOTICES
Distribution of this document is unlimited.

11 SUPPLEMENTARY NOTES

12 SPONSORING MILITARY ACTIVITY
Defense Atomic Support Agency
Washington, D. C. 20301

13 ABSTRACT A submerged gold wire was electrically exploded to simulate a very deep underwater nuclear detonation. These small-scale tests were conducted in a test tank in which the air pressure may be varied to obtain various strenghts of buoyant bubble migration.

The mechanics of explosion bubble formation, pulsation, and migration are discussed, and relevant relationships are derived for scaling large-yield bubble behavior in the laboratory by variation of environmental parameters. The mechanisms by which the explosion products, initially at the bubble center during the first cycle, are redistributed by bubble bottom collapse, compression, re-expansion, and migration, are investigated.

The experimental technique involved physically sampling the bubble and its environment at the second bubble maximum to define the extent and nature of explosion product re-distribution. Three different shot conditions were investigated, corresponding to a "rest-point" condition, a condition characterized by slight upward migration, and one characterized by strong upward migration.

In all cases, it was found that most (77 to 94%) of the explosion products are lost to the environment by the time of the second bubble maximum. The probable mechanisms for this loss are discussed, and rules are derived for application of these results to full-scale underwater bursts.

DD FORM 1 JAN 64 1473

UNCLASSIFIED
Security Classification

14. KEY WORDS	LINK A		LINK B		LINK C	
	ROLE	WT	ROLE	WT	ROLE	WT
Underwater explosionn Weapons effects Hydrodynamics Explosion products						

INSTRUCTIONS

1. ORIGINATING ACTIVITY: Enter the name and address of the contractor, subcontractor, grantee, Department of Defense activity or other organization *(corporate author)* issuing the report.

2a. REPORT SECURITY CLASSIFICATION: Enter the overall security classification of the report. Indicate whether "Restricted Data" is included. Marking is to be in accordance with appropriate security regulations.

2b. GROUP: Automatic downgrading is specified in DoD Directive 5200.10 and Armed Forces Industrial Manual. Enter the group number. Also, when applicable, show that optional markings have been used for Group 3 and Group 4 as authorized.

3. REPORT TITLE: Enter the complete report title in all capital letters. Titles in all cases should be unclassified. If a meaningful title cannot be selected without classification, show title classification in all capitals in parenthesis immediately following the title.

4. DESCRIPTIVE NOTES: If appropriate, enter the type of report, e.g., interim, progress, summary, annual, or final. Give the inclusive dates when a specific reporting period is covered.

5. AUTHOR(S): Enter the name(s) of author(s) as shown on or in the report. Enter last name, first name, middle initial. If military, show rank and branch of service. The name of the principal author is an absolute minimum requirement.

6. REPORT DATE: Enter the date of the report as day, month, year; or month, year. If more than one date appears on the report, use date of publication.

7a. TOTAL NUMBER OF PAGES: The total page count should follow normal pagination procedures, i.e., enter the number of pages containing information.

7b. NUMBER OF REFERENCES: Enter the total number of references cited in the report.

8a. CONTRACT OR GRANT NUMBER: If appropriate, enter the applicable number of the contract or grant under which the report was written.

8b, 8c, & 8d. PROJECT NUMBER: Enter the appropriate military department identification, such as project number, subproject number, system numbers, task number, etc.

9a. ORIGINATOR'S REPORT NUMBER(S): Enter the official report number by which the document will be identified and controlled by the originating activity. This number must be unique to this report.

9b. OTHER REPORT NUMBER(S): If the report has been assigned any other report numbers *(either by the originator or by the sponsor)*, also enter this number(s).

10. AVAILABILITY/LIMITATION NOTICES: Enter any limitations on further dissemination of the report, other than those imposed by security classification, using standard statements such as:

(1) "Qualified requesters may obtain copies of this report from DDC."

(2) "Foreign announcement and dissemination of this report by DDC is not authorized."

(3) "U. S. Government agencies may obtain copies of this report directly from DDC. Other qualified DDC users shall request through _____."

(4) "U. S. military agencies may obtain copies of this report directly from DDC. Other qualified users shall request through _____."

(5) "All distribution of this report is controlled. Qualified DDC users shall request through _____."

If the report has been furnished to the Office of Technical Services, Department of Commerce, for sale to the public, indicate this fact and enter the price, if known.

11. SUPPLEMENTARY NOTES: Use for additional explanatory notes.

12. SPONSORING MILITARY ACTIVITY: Enter the name of the departmental project office or laboratory sponsoring *(paying for)* the research and development. Include address.

13. ABSTRACT: Enter an abstract giving a brief and factual summary of the document indicative of the report, even though it may also appear elsewhere in the body of the technical report. If additional space is required, a continuation sheet shall be attached.

It is highly desirable that the abstract of classified reports be unclassified. Each paragraph of the abstract shall end with an indication of the military security classification of the information in the paragraph, represented as *(TS), (S), (C), or (U)*

There is no limitation on the length of the abstract. However, the suggested length is from 150 to 225 words.

14. KEY WORDS: Key words are technically meaningful terms or short phrases that characterize a report and may be used as index entries for cataloging the report. Key words must be selected so that no security classification is required. Identifiers, such as equipment model designation, trade name, military project code name, geographic location, may be used as key words but will be followed by an indication of technical context. The assignment of links, roles, and weights is optional.